Strategies for Solid-State NMR Studies of Materials: From Diamagnetic to Paramagnetic Porous Solids

Vladimir I. Bakhmutov*

Department of Chemistry, Texas A&M University, P.O. Box 30012, Texas, 77842-3012

Received May 14, 2010

Contents

1. Introduction

The controlled design of porous and layered molecular systems with a three-dimensional porous network constitutes one of the most exciting directions of modern materials science. Numerous research papers and reviews have been published on the synthesis and applications of these materials. Ferey[1] has described details of so-called hybrid porous molecular systems obtained from the reactions of organic and inorganic species. A number of reports appeared on porous metal phosphates and phosphonates[2−7] with variations in the properties and structures depending on the nature of the metals used.[8] These materials can be used as ion-exchangers for processing of radioactive waste streams,[9] sorption,[10] and applications in catalysis,[11] sensor design,[12] and nonlinear optics.[13] Remarkable from the perspective of molecular magnetism,[14−16] porous supramolecular assemblies based on metal cyanides have been developed.[17−22] Consid-

* E-mail: bakhmoutov@mail.chem.tamu.edu.

10.1021/cr100144r
Published on Web 09/15/2010

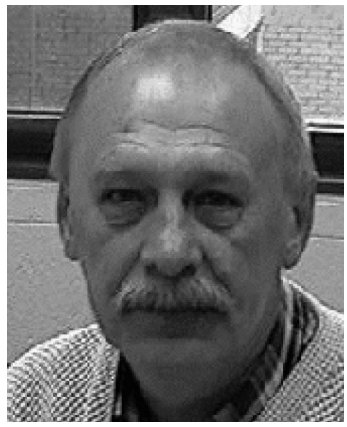

Vladimir I. Bakhmutov was born in Moscow, Russia. Having received his Ph.D. degree in Physical Inorganic Chemistry at the State University of Moscow in 1974, he moved to the Institute of Organo-Elements Compounds of the Russian Academy of Sciences. In 1984, he obtained his Doctor of Sciences degree in Chemical Physics, and in 1991−1995, he was Professor of Chemistry and Head of the NMR Department. His research interests are in the areas of chemical physics, weak organizing interactions, NMR in liquids and solids, and NMR relaxation. He is an author of more than 300 papers and three books: *Practical Nuclear Magnetic Resonance Relaxation for Chemists*, Wiley, 2005; *Applications of NMR in Chemistry*, CINVESTAV, Mexico, 2006; and *Dihydrogen Bonds: Principles, Experiments, and Applications*, Wiley, 2008. He has also contributed to three books: *The Encyclopedia of Applied Spectroscopy*, Wiley, 2009; *Unusual structures and physical properties in organometallic chemistry*, Editor M. Gielen, Wiley, 2002; and *Recent Advances on Hydride Chemistry*, Editor R. Poli, Elsevier, 2001. As a visiting Professor, he has worked at a number of universities in France, Spain, Switzerland, and Mexico. He is currently an NMR expert at Texas A&M University and a Blinn College Faculty member.

erable progress has been made in the synthesis of porous molecular sieves,[23] which show various framework structures and pore sizes. In addition to their traditional applications in the traditional areas of catalysis, ion-exchange, and separation, these systems have recently found use as contrast agents for diagnostic magnetic resonance imaging,[24] semiconductor nanowires,[25,26] and even as hosts for laser dyes.[27,28]

The area of applications of such porous systems depends on their physical and chemical properties[29] and structure, especially the morphology of the porous medium, which is critical to know in sufficient detail. Pore morphology determines dynamics of the pore-confined molecules[30−35] and is therefore critical for applications in membrane separation, lubrication, and oil recovery. This parameter can be probed by mercury intrusion, N_2 adsorption, neutron scattering, thermoporometry, NMR and NMR relaxation (see below), and a combination thereof.[29] The nature, concentration, and strength of the active sites that are important for catalysis, as well as the size of the channels, can be studied by X-ray and neutron scattering,[36,37] Fourier transform infrared (FTIR),[38−40] transmission electron microscopy (TEM),[41] calorimetry,[42,43] and solid-state NMR.[44,45] Computational methods (ab initio or Monte Carlo) can also be successfully applied for structural studies and understanding of the driving forces for the framework assemblies.[46,47]

Zeolites,[48−50] which are built of the corner-sharing SiO_4^{4-} and AlO_4^{5-} tetrahedral units, represent the most important class of known porous materials that are valuable as catalysts, sorbents, and ion-exchangers. These materials are more crystalline and commercially available. However, their pore size is relatively small and pore entrances are only ca. 10 Å in diameter,[51] which results in strong binding of the sorbed substrates to the cavities and tunnels. Although significant synthetic efforts have resulted in the synthesis of zeolites with larger pore sizes,[51,52] these materials have not found broad commercial utilization because of their lattice instability and the pore-blockage phenomenon. The development of new mesoporous phases such as FSM-16[53] and MCM-41[54] and their intense studies[55,56] have led to silica-based materials of high surface areas with the pore size ranging from 20 to 100 Å.[57,58] Similar nonsilica-based oxides are also known.[59]

The gap in pore sizes of 10−25 Å has been filled by the development of amorphous mixed oxides[60] made by sol−gel techniques[61] with various amines used as the templates. These materials can be generally formulated as systems with a matrix created by structure-directing reagents (SiO moieties or transition metal oxides in variable oxidation states[62,63]) and pores, channels, and cavities, with the pore sizes and shapes of the cavities depending on both the synthetic method used and postsynthesis treatment such as calcination at high temperatures. Besides the architecture, which can be fine-tuned for a particular application, the nature, concentration, and strength of the active sites that are important for catalysis can be modified by various transition and main-group metal ions added in high or low concentrations. Clearly, structural control of such systems requires reliable characterization methods. While zeolites and closely related systems are highly crystalline and hence their structure can be determined by diffraction techniques with reasonable accuracy, many porous composite systems exhibit low crystallinity, which complicates their structural characterization. In such cases, solid-state NMR studies[44] performed on static or spinning samples could provide critical structural information. However, for porous composites modified by paramagnetic ions, especially in high concentrations, the NMR method often loses its power.

The goal of this article is to overview the new NMR methodology for structural studies of *amorphous, paramagnetic solids*. As certain NMR approaches and interpretation of the experimental data are nontrivial, this article includes a brief introduction to the general principles of solid-state NMR and its parameters determined for diamagnetic molecular systems. The latter includes studies of the pore morphology by a combination of NMR cryoporometry and NMR relaxometry in section 3. There are a large number of reviews and research publications on the rapidly developing advanced solid-state NMR techniques. This article will first provide a brief survey of these techniques to illustrate the spectroscopic problems appearing in the studies of paramagnetic materials (section 4). Then we will focus on the nature and magnitudes of chemical shifts measured in solids containing unpaired electrons, as well as on the influence of paramagnetic centers on NMR relaxation and relaxation times. Finally, in sections 5 and 6, we will review particular NMR experiments performed on static and spinning samples and T_1 and T_2 NMR relaxation measurements, showing the scope and limitations of the method. These sections are aimed at shaping the general NMR strategy for the structural studies of paramagnetic solids with the main focus on the most challenging area of NMR studies of amorphous porous materials doped by paramagnetic metal ions.

2. General Problems in Structural Studies of Amorphous Porous Materials

Characterization of porous materials can be carried out by various physical methods and theoretical approaches. The

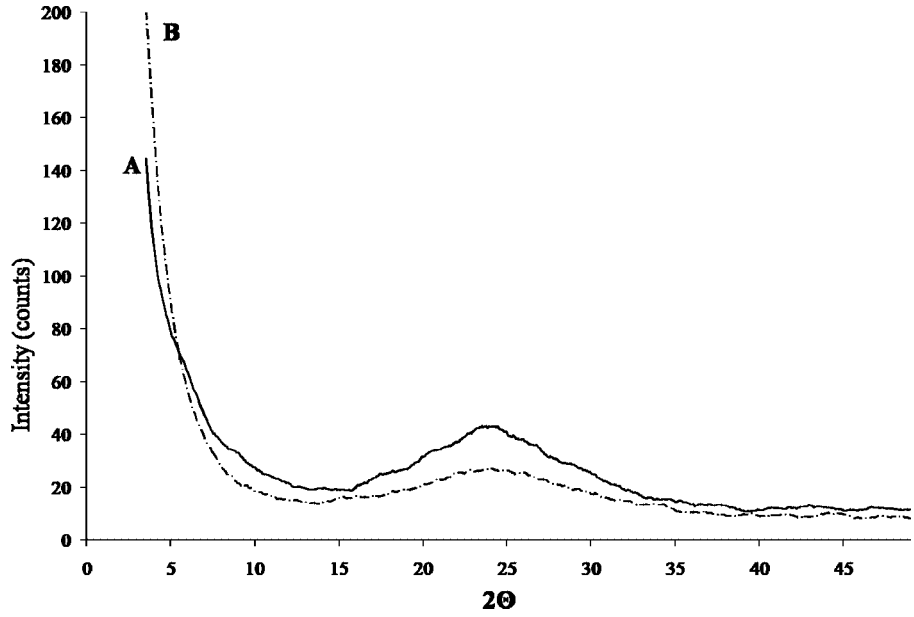

Figure 1. X-ray powder diffraction patterns typical of manganese−alumina−silica composites obtained by the sol−gel method: (A) the material as made and (B) the material calcined in air at 450 °C. Reprinted with permission from ref 78. Copyright 2010 Elsevier B.V.

nature of the material dictates the choice of the corresponding adequate methods or combinations thereof. For example, *tin*-containing materials can be characterized by UV and Mossbauer spectra,[63] and their porosity can be measured by N_2 absorption−desorption isotherms. Probing the microstructures and/or the morphology of microporous Mg/Al/Si systems or the hybrid mesoporous organo−Al−silicates can be successful by transmission electron microscopy (TEM) and scanning electron microscopy (SEM).[64,66] Some publications[63,65] report applications of FTIR and UV spectroscopy. A recent review[61] describes advanced solid-state NMR techniques for studies of various materials prepared by the sol/gel method. Clearfield and co-workers[67] have characterized catalysts of the $NiO/SiO_2/Al_2O_3$ family by X-ray photoelectron spectroscopy (XPS). Both the Raman and extended X-ray absorption fine structure (EXAFS) methods have been used to study hybrid aluminum and gallium systems.[68−70] Electron nuclear double resonance (ENDOR)[71] and the temperature-programming reduction method[67] are also available for studies of porous molecular systems.

In spite of the large arsenal of modern physical methods, single-crystal X-ray diffraction still remains the most popular direct method for accurate determination of molecular structures of solids. However, large enough, high-quality single crystals required for this method are extremely difficult to obtain for many porous composite materials, including the well-known silica zeolites and their derivatives that are widely used in catalysis.[72,73] Therefore, characterization of such solids can be based only on powder X-ray diffraction (XRD). Three main steps are involved in these studies.[74] First, unit cell parameters and the space group are determined from the XRD patterns. Note that this step often requires independent supporting data from another method, e.g., solid-state NMR.[75] Next, an initial structural model is proposed, which should be consistent with general chemical concepts while being in agreement with available experimental data. This step is most critical because of the well-known phase problems. Finally, the structural analysis is completed by location of the missing atoms in structural model refinement against the diffraction data. However, in spite of the impressive developments of this approach and data treatment, determination of the structure directly from the powder XRD pattern is often difficult or even impossible, particularly for complex heterogeneous materials.[74] Thus, the sol−gel techniques, with appropriate organic template molecules providing regulations of the pore sizes and entrances and even lengths and shapes of the pore channels, nonetheless produce amorphous materials.[76] Whereas zeolites (e.g., of the MCM-41 family) exhibit informative XRD patterns, typically with an intense diffraction peak, three higher-order peaks, and a diffuse peak,[77] XRD data collected for silica-based materials prepared by the sol/gel method are of insufficient quality for interpretation. As seen in Figure 1, no additional peaks $2\Theta < 2°$ are observed at measurements with small angles,[78] and thus no valuable structural conclusions can be drawn. Such XRD patterns only confirm the amorphous nature of the systems and keep aiming at applications of other more adequate physical methods.

2.1. Key Structural Issues in Characterization of Materials Modified by Metal Ions and Methods for Structure Solution

Insertion of the transition or main-group metal ions into the zeolite frameworks to tune their catalytic properties is one of the main directions of heterogeneous catalytic research. Such materials can be prepared directly in the presence of the metal ions, for example, by the sol/gel method,[50] including applications of surfactants, by ion exchange,[79] or even by simple impregnation[80] of the premade materials in the corresponding solutions. It is obvious that interpretation of the catalytic behavior of the systems requires knowledge of the metal-ion distribution (homogeneous or nonhomogeneous), interactions between the metal ions and the matrix of the materials, and their interactions with the absorbed molecules.

A priori, the metal atoms can be uniformly incorporated into the silica matrix, be situated within the cavities, or form separate phases. This is a key structural issue in studies of these materials. In addition, the final products are generally calcined at high temperatures in the presence of air. Under these conditions, oxidation states of the metal ions can

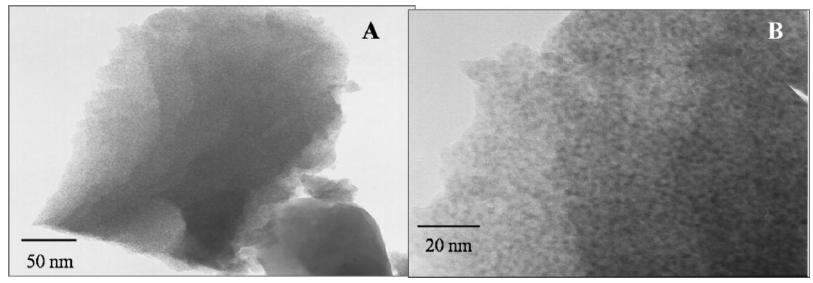

Figure 2. Electron micrographs of the porous material $MnO/Al_2O_3/SiO_2$ (19.8% Mn, 2.2% Al, 26.9% Si) preheated to 540 °C (A) and 650 °C (B). Reprinted with permission from ref 78. Copyright 2010 Elsevier B.V.

change. Because the materials are often amorphous, application of X-ray powder diffraction techniques is useless (Figure 1), particularly at low concentrations of the doped ions. Even the formation of a second phase can be often below the level of X-ray detection. For example, separate phases of supermicroporous mixed oxides of the $NiO/SiO_2/Al_2O_3$ family remain "invisible" in most of their powder X-ray diffraction patterns even at relatively high nickel loadings.[81] Only in some cases can the Ni^0 and NiO clusters be observed. Some information about metal-ion distributions throughout the sample bulk could be obtained by the TEM technique. However, the TEM patterns, as illustrated in Figure 2 for a typical porous material $MnO/Al_2O_3/SiO_2$, are not valuable in the above structural context.

It is shown in sections 3.5 and 3.6 how the key structure determination problem can be solved even for strongly amorphous porous materials by applications of advanced solid-state NMR techniques providing detailed localizations of the doped metal atoms and also their oxidation states and coordination numbers. It is obvious that this method is particularly powerful when the materials are mostly diamagnetic or if they contain paramagnetic centers as impurities that do not distort the NMR parameters. Moreover, such centers can even be added to materials as paramagnetic probes.[80] At the same time, the design of many catalytically active porous systems requires the significant presence of paramagnetic metal ions, leading to the materials Ni-MCM-41,[82−84] MnSBA-15,[85] silica xerogels,[86] Co-MCM-41,[87,88] Cr-MCM-41,[89] Fe-MCM-58,[90] and Fe-ZSM-5.[91] The zeolites containing paramagnetic ions of Nd, Sm, and Gd[79] and porous aluminophosphates doped with manganese and cobalt[71,92−96] also have been reported. NMR studies of such paramagnetic systems are not simple, and they will be discussed below in the methodical context along with paramagnetic alumina-supported nickel catalysts[97] and mesoporous niobium oxides.[98]

When the doping metal ions are active in the Mossbauer spectra, e.g., ^{119}Sn and ^{57}Fe,[91] this method is probably one of the best for structure determination of such amorphous molecular systems. In fact, chemical isomer shifts and quadrupole splitting observed for the nuclei of such atoms in the Mossbauer spectra result in accurate determination of their oxidation states and coordination numbers and geometries (tetrahedral, octahedral, etc.). Moreover, the Mossbauer spectra provide discrimination between the framework and extraframework species, as has been well demonstrated for porous materials of the Sn-SBA-15 family.[63,99] It is clear, however, that these studies are limited to only Mossbauer-active ions.

The X-ray absorption techniques EXAFS and XANES are currently viewed as one of the most promising methods to structurally probe porous molecular systems.[100] EXAFS can give detailed information about coordination numbers of metal ions and local environments, including the bond lengths. These techniques, when applied to structural analysis of the mesoporous materials Ni-MCM-41,[82] have indicated that the Ni ions are tetrahedral, with the surrounding oxygen atoms being incorporated into the material matrix. Applications of X-ray absorption techniques for the systems of the Co-MCM-41 and Cr-MCM-41 family have been reported.[87,89] Characterization of the Ni-MCM-41 systems used in the synthesis of carbon nanotubes have also been recently communicated. It has been established, however, that the size of the Ni−O clusters can be measured from the coordination numbers determined by EXAFS only for particles <3−5 nm.[84] Finally, when applied for manganese aluminophosphates, this technique has shown that the Mn^{2+} ions are surrounded by four oxygen atoms and incorporated into the AlPO framework.[92]

X-ray photoelectron spectroscopy, XPS,[101] is an important alternative approach to evaluation of different sites and oxidation states for metal ions used in the design of heterogeneous systems. This technique does not require high crystallinity (unlike XRD) or a minimal particle size (unlike TEM). Nonetheless, analysis of some alumina-supported nickel catalysts[97] has demonstrated that the results obtained by this spectroscopy can depend on the repartition of the catalyst components, and therefore, independent data and measurements are often required for correct interpretation.

Figure 3 illustrates an additional, rather intrinsic problem that often emerges in the studies of porous systems such as supermicroporous materials of the $SiO_2-Al_2O_3-NiO$ family.

These systems are very amorphous, according to X-ray powder diffraction measurements.[81] Figure 3 shows a typical XPS pattern for the material $SiO_2-Al_2O_3-NiO$ containing 13.4% Ni (by weight) with a peak centered at 854 eV and a satellite at 860 eV, corresponding to the NiO particles. However, because the observed lines are very broad, the presence of more than one type of nickel species cannot be ruled out. Moreover, even the standard deconvolution procedures for such XPS patterns seem to be doubtful because the two broad bands might fit two peaks at 854.2 and 859.8 eV from "free" NiO, or three peaks at 854.3, 857.8, and 859.9 eV as a combination of free and silica-bound NiO, or even four peaks at 854.3, 855.9, 858.3, and 860.6 eV. Clearly, such XPS data are not particularly insightful.

The UV, IR, and Raman methods are commonly applied to probe the behavior of molecules absorbed within pores[64,65,98,102] or to characterize transformations of the porous systems during the synthesis and specific treatments.[96] Nevertheless, some structural conclusions can be drawn. For instance, functionalization of the MCM-41 surface to create active titanium sites can be monitored by IR spectra,[103] which show bands that are characteristic of silica lattice vibrations.

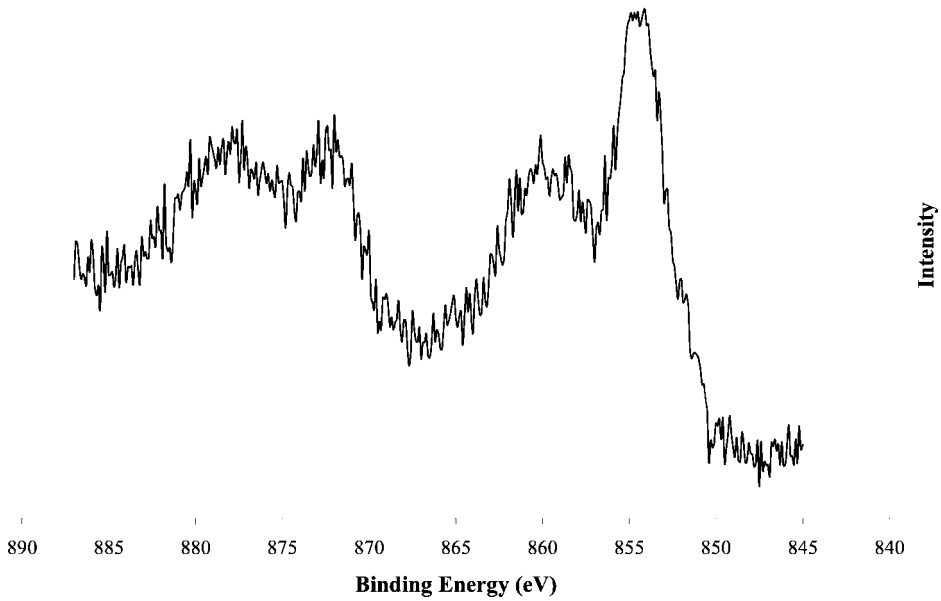

Figure 3. XPS Ni 2p3/2 spectrum of material $SiO_2-Al_2O_3-NiO$ with 13.4 wt % of Ni calcined at 540 °C. Reprinted with permission from ref 81. Copyright 2009 Elsevier B.V.

It has been found that the intensity of the Si−O band at 960 cm^{-1} increases considerably upon replacement of the proton in the Si−O−H moieties with the metal atoms (Ti). Generally, the presence of bands around 960 cm^{-1} is considered as evidence for the presence of Ti, V, or Fe atoms in the zeolite frameworks.[104]

Electron paramagnetic resonance (EPR) spectroscopy is a direct method for determination of the nature and location of paramagnetic metal ions in porous materials, as long as electron relaxation times allow for observations of EPR lines. However, use of EPR also deals with a number of intrinsic problems, mainly dealing with interpretation and assignment of the EPR patterns. For example, Calis and co-workers[91] have studied by EPR ZSM-5 zeolites doped with Fe^{3+} at different concentrations. The isotropic signal observed at $g = 4.3$ (characteristic of Fe^{3+} in the $^6S(5/2)$ spin state) was attributed to tetrahedral Fe sites incorporated into the zeolite lattice, and the signals at $g = 2.6$ and 2.0 were assigned to Fe^{3+} located in the pores and the channels.

More recently, however, materials of the Fe(III)MCM-58 family were studied by EPR again to exhibit signals at $g = 4.49$ with shoulders at $g = 9.05$ and 2.30 along with intense broad signals at $g = 2.00$, typical of Fe(III) in zeolites.[90] In this fundamental work, it is emphasized that assignments of the Fe^{3+} EPR signals "*to various iron species in zeolites were controversially discussed in numerous papers and are still a matter of debate*". In general, EPR data do not provide an opportunity to distinguish accurately between the Fe(III) ions in the framework and in the ion-exchange sites. Similar problems appear in the EPR data for MnAlPO-5, MnAlPO-18, and their cobalt analogues.[92] For example, the spectra of the Mn systems show a resonance at $g = 2.00$ with six resolved hyperfine lines that can be interpreted as evidence for *either tetrahedral or octahedral Mn(II) or Mn(IV) located in the framework or for the presence of extraframework Mn(II) species*. Such uncertainties obviously require independent additional information, such as XANES and EXAFS data.

Mesoporous sieves of the MnSBA-15 family have also displayed six EPR lines at $g = 2.00$ that have been assigned, for not obvious reasons, to Mn^{2+} incorporated in the silica pore walls.[85] The CoAlPO-5 and CoAlPO-18 analogues have exhibited resonances at $g = 5.8$ and 2.00.[92] The former was assigned to tetrahedral Co(II) incorporated in the framework of the material. Another publication,[96] however, suggests that Co(II) sites incorporated in the framework of CoAPO-5 show the signal at $g = 2.03$. The calcined and oxidized porous Ni-MCM-41[83] did not show any EPR signals at 77 K. In spite of the lack of observable signals expected from Ni^{2+}, the EPR study of the material after H_2 reduction pointed to isolated Ni(I) species ($g = 2.09$).

Some of the above problems complicating the use of EPR can be avoided by the pulsed electron nuclear double resonance (ENDOR) technique.[71,105,106] For example, Goldfarb and co-workers[71] have reported the ENDOR studies of aluminophosphate materials $AlPO_4$-20 and analogues, where the field-sweep-echo-detected spectrum revealed the presence of a single type of Mn(II) ions with a ^{55} Mn hyperfine coupling constant of 8.7 mT. Moreover, the ENDOR spectra, obtained with Mims and Davies sequences, displayed a ^{27}Al signal at the Larmor frequency and *a ^{31}P doublet corresponding to a hyperfine coupling of 8 MHz*. The relatively large ^{31}P hyperfine coupling and the weak ^{27}Al coupling provide unique and direct evidence for Mn(II) substitution of the Al framework.

The nature of paramagnetic centers located on nickel or manganese atoms of porous systems may be revealed by variable-temperature magnetic susceptibility experiments.[81] Data treatment in terms of the Curie and the Curie−Weiss law has allowed for the determination of the spin states and also for observation of both magnetically isolated and coupled centers. However, this method cannot discriminate the incorporated and extraframework metal ions.

Clearly, the large arsenal of physical methods still does not solve the key problem of structural determination of amorphous, porous, metal ion-containing materials. Obtaining structural information is particularly problematic at low concentrations of the metal ion dopant. Obviously, new methods are needed to extract structural information on such

materials. As will be shown below, solid-state NMR and NMR relaxation can be most useful for this purpose.

3. Solid-State NMR in Materials Chemistry: Diamagnetic Molecular Systems

Solid-state NMR is an extraordinarily powerful physical method that is widely applied in different fields of chemistry. It is particularly valuable at probing complex molecular systems such as composites and other heterogeneous materials, representing an ideal tool for characterizations of materials with dimensions on a nanoscale. This method is also capable of solving various dynamic tasks directed to understanding of the local molecular mobility. A recent search,[107] performed by Dybovsky and Bai, has demonstrated that, only between 2005 and 2009, the solid-state NMR literature increased by >3300 original articles. A number of excellent reviews exist in the literature, focusing on applications of NMR for supramolecular systems,[109] molecular sieves catalysts,[111] and zeolite structures[110] and on new solid-state NMR techniques.[108,112] For materials chemists, one article[108] is of greatest interest. This work describes the technique providing precise characterizations of interfaces in sol/gel-materials and hybrid interfaces where the experimentalist can use the NMR parameters from isotropic chemical shifts to quadrupolar and dipolar interactions.

Because the physical basis of NMR is well-known to chemists, in this section it will be pertinent to briefly consider some parameters and principles that are important for NMR applications to studies of diamagnetic solids. This, in turn, is expected to provide a better clarification of paramagnetic spectroscopic effects.

3.1. Isotropic Chemical Shifts and Magnetic Shielding Tensors in Diamagnetic Solids

Nuclear spins in molecules are not isolated, which gives rise to the phenomena of chemical shift and relaxation, directly related to chemical structures.[113] According to Abragam,[114] three principal terms contribute to total chemical shifts δ (or total shielding constants σ): diamagnetic term, as a function of the unperturbed electronic density, paramagnetic term, as a function of the average energy of the electron excitation and the nucleus−electron distance, and a less significant term emerging from electrons situated at neighboring groups. Combinations of these terms lead to large δ (or σ) variations dependent on the nature of the nuclei. The shifts, named *isotropic* (δ(iso)), are registered by the NMR experiments in solutions and liquids due to high-amplitude fast molecular motions. For the same molecular structure in solution and in the solid state, the isotropic chemical shifts of the target nuclei would be identical. However, because of the closer proximity of molecules in solids, their mutual influence can result in a δ(iso) difference on going from solutions to the solid state that can reach 10 ppm and even more. In addition, for the same reason, the nuclei can become crystallographically different, which would result in an increase in the number of observed resonances in the solid state.

Theoretically, δ and σ are three-dimensional and can be described as tensor magnitudes[115] with components σ_{XX}, σ_{YY}, and σ_{ZZ}, which are also associated with chemical structures. These components are generally different, giving rise to chemical shift anisotropy, $\Delta\sigma$, defined as: $\Delta\sigma = \{2\sigma_{ZZ} - (\sigma_{XX} + \sigma_{YY})\}/3$. In turn, isotropic chemical shifts δ(iso) or isotropic screening constants σ(iso) are determined as $\sigma(\text{iso}) = (1/3)(\sigma_{XX} + \sigma_{YY} + \sigma_{ZZ})$.

Table 1. Chemical Shift Anisotropy, $\Delta\sigma$ (in ppm), Measured for Some Heavy Important Nuclei in Diamagnetic Complexes

complex/nucleus	$\Delta\sigma$ (ppm)
$Sn_2P_2O_7$/^{31}P	−81, −74[116]
$Sn_2P_2O_7$/^{119}Sn	694, 660[116]
bis(2-carbomethoxyethyl)−bis(*N*,*N*-dimethyldithiocarbamato)tin(IV)/^{119}Sn	1015[117]
Pt(en)Cl_2/^{195}Pt	−8100[118]
$Mg_3(VO_4)_2$/^{51}V	31[119]
V_2O_5−WO_3 TiO_2/^{51}V	636[120]
Co(TPP)Py_2/^{59}Co	1650[121]
bis(pentamethylcyclopentadienyl)lead/^{207}Pb	1900[122]
Ag_2CO_3/^{109}Ag	711[123]
cadmium glycinate/^{113}Cd	401[124]

In solids, because of the absence of high-amplitude molecular motions, resonance shapes, detected in static samples, will strongly depend on the symmetry of tensors σ (or δ) and chemical shift anisotropies. Table 1 shows the chemical shift anisotropies expected for some heavy nuclei (often used as target nuclei in probing different materials), which can reach very large values. In contrast to solutions, detections of such nuclei in the solid-state static NMR spectra will be difficult, particularly at their relatively low natural abundance (8.6% for ^{119}Sn, 12.2% for ^{113}Cd, and 33.8% for ^{195}Pt) and low contents in investigated subjects. It is also obvious that the registration remains difficult even in the magic-angle spinning (MAS) solid-state NMR spectra where the wide static signals transform to the sideband patterns (see below). Significantly smaller anisotropies can be observed for nuclei ^{1}H, ^{13}C, ^{27}Al, and ^{29}Si, which are also used as target nuclei in studies of different materials. However, even in the case of these nuclei, the situation changes in going to paramagnetic systems.

3.2. Nuclei With a Spin of 1/2

Solid-state NMR experiments at MAS, performed for nuclei ^{1}H, ^{13}C, ^{15}N, ^{31}P, ^{29}Si, and ^{129}Xe, play a central role in various investigations of structures and dynamics in catalysts, polymers, glasses, zeolites, batteries, liquid crystals, natural products, pharmaceutical compounds, membrane proteins, and amyloid fibrils. Because of the advanced techniques, the solid-state MAS NMR spectra of such nuclei can be well resolved for diamagnetic solids, thus providing detailed structural information.[112]

Nuclei with spins of 1/2 undergo homonuclear or heteronuclear (proton−proton or proton−carbon, for example) dipolar interaction, and their resonance frequencies depend on the dipolar coupling constants. This coupling describes how the magnetic field, created by neighboring spins, changes due to varying orientations of interspin vectors in the external field.[44] For example, the resonance of static ice is broadened to $\sim 10^5$ Hz due to strongest H−H couplings, whereas ^{29}Si−^{29}Si dipolar coupling produces line widths of only 2−3 kHz.[113] Fast, high-amplitude molecular motions in solutions average to zero this dipolar coupling, resulting in relatively sharp resonances in the NMR spectra. In rigid solids, however, the dipolar coupling, governed by term ($3\cos^2\theta - 1$) with an angle, θ, between the interspin vectors and the external magnetic field, cannot be averaged, and as a result, resonances observed in static samples are very broad proportionally to the dipolar coupling constants and as a function of internuclear distances and orientations of the

above vectors. Because at the angle θ of 54.4°, named "magic" by Andrew,[113] the factor $(3\cos^2\theta - 1)/r^3$ transforms to 0, use of the magic-angle spinning (MAS) technique eliminates, or at least reduces, orientation-dependent effects in the solid-state NMR spectra.

Complete elimination of the dipolar coupling can be obviously reached at spinning rates that are significantly larger than the line-widths of resonances detected in the corresponding static samples. This is technically possible because modern commercial NMR spectrometers can be equipped with MAS probes with the spinning rates of 30−50 kHz,[113] providing high-resolution NMR spectra even for ^{1}H nuclei with the highest dipolar coupling constants. When the homonuclear dipolar coupling dominates and spinning rates are smaller with respect to line-widths of resonances in static samples, the lines detected in the MAS NMR spectra are still broadened due to the remaining time-dependent terms.[44] In contrast, MAS NMR spectra of molecular systems with dominant heterodipolar and chemical-shift-anisotropy interactions will show sharp lines even at intermediate spinning rates. According to Strub, Grant, and co-workers,[125] distributions of sidebands in such cases can be used to determine magnetic screening tensors. It should be emphasized that, in paramagnetic solids, where the dominating dipolar electron−nucleus interactions have a "hetero" nature, lines in the sideband patterns can still be broadened for relaxation reasons.

In general, high-resolution MAS NMR spectra can be easily obtained even in heterogeneous materials for rare nuclei, such as ^{13}C or ^{15}N, particularly when suppressing the very strong dipolar interactions at short bond distances ^{1}H−^{13}C or ^{1}H−^{15}N. It can be realized by the high-power decoupling technique producing ^{1}H irradiation, when the ^{13}C or ^{15}N NMR free induction decays (FIDs) are recorded.[44] The decoupling can be realized by continuous irradiation at a power of 100−1000 W or by special pulse sequences operating at proton frequency. Among them, sequences *TPPM* (heteronuclear X-{^{1}H} decoupling), *WAHUHA*, and *MREV-8* (homonuclear, for example, proton−proton decoupling) are most applicable. It should be noted that, in contrast to diamagnetic solids, the high-power ^{1}H irradiation applied for paramagnetic systems can produce negative effects, recently analyzed by Wasylishen and co-workers.[126] The authors have carefully investigated different methods of proton decoupling for observation of nuclei ^{13}C in paramagnetic complexes of amino acids and demonstrated the approaches that were most effective.

3.3. Quadrupolar Nuclei in Solids

Most of the nuclei of interest to materials science have spins more than 1/2: ^{2}H, ^{7}Li, ^{11}B, ^{17}O, ^{23}Na, ^{27}Al, ^{47}Ti, ^{51}V, ^{93}Nb, etc. Such nuclei, named quadrupolar, are characterized by nonspherical electrical charge distributions and nuclear quadrupole moments Q, respectively. Therefore, their spins can interact with not only the external and local magnetic fields (the Zeeman interactions) but also with electric field gradients (EFG) at these nuclei, resulting in a splitting of the nuclear energy levels.[127] The energy of quadrupole interactions is expressed through nuclear quadrupole coupling constant: NQCC $= e^2q_{ZZ}Q/h$ where eq_{ZZ} is the principal component of the EFG tensor with the asymmetry parameter η_q. Theoretically, the quadrupole interactions, perturbing the Zeeman energy, are considered as the first- and second-order energy corrections, where the first-order term includes an angular dependence, which is similar to that in dipolar interactions.[44] In contrast, the second-order correction represents an isotropic term, which is dependent, however, on the Larmor frequency: *this term decreases with increasing external magnetic field strength*. The last two statements are particularly important in practice when target nuclei of studied materials are quadrupolar. In fact, the aforementioned quadrupole effects in solids can become very significant, and the first-order broadening can spread the signal intensity over a very large frequency range.[127] Under this circumstance, even registration of the resonances in static powder samples will be difficult. In addition, powerful and relatively long (90°) radio frequency pulses used for direct excitation of spins in solids often lead to resonances coming from both the central (+1/2 - −1/2) and noncentral or satellite transitions of the quadrupolar nuclei. In this connection, it should be emphasized that solid-state NMR experiments with quadrupolar nuclei at highest magnetic field strengths can provide significant advantages, recently illustrated by Wasylishen and co-workers.[128]

Quadrupolar nuclei can be divided into two categories: the ones with integer spins (for example, ^{2}H) and those with noninteger spins, for example, ^{27}Al, ^{47}Ti, ^{51}V, ^{93}Nb, etc. The nuclei from the last group, while playing an important role in the chemistry of materials, do not undergo first-order broadenings for their central transitions, which are generally observed as most intense resonances in static powder samples (the satellite transitions are spread over a frequency range of many MHz and their detection is difficult by regular pulse techniques[127]). At the same time, in solids, the central transitions of these nuclei can be remarkably broadened by tens of kHz due to the strong second-order quadrupolar effects. As a result, static powder samples display NMR spectra where any different resonances present can overlap.

The MAS experiments generally increase the resolution in NMR spectra of solid materials. Since the first-order terms are angular dependent, these quadrupole effects can actually be eliminated by the MAS technique. In contrast, the second-order quadrupole broadenings are reduced only partially under these conditions, and hence resonances from the central transitions remain broadened. A higher resolution in such MAS NMR spectra can be reached by alternative approaches that are based on two-dimensional (2D) experiments, complex sample reorientations during the experiments, and excitation of multiple quantum transitions. Applications of these techniques and also multiple resonance experiments including cross-polarization and indirect detection (TRAPDOR) and nutation can be found in a review.[127]

Finally, it should be emphasized that interactions of nuclear spins with electric field gradients (EFG) at these nuclei are strongest, and therefore, the nuclear quadrupole coupling constants and the asymmetry parameters, η_q, dictate the line shapes of the central and satellite transitions in the static and MAS NMR spectra. This statement remains valid even for paramagnetic systems, particularly at relatively small concentrations of paramagnetic centers. The simplest line shapes are generally observed for the axially symmetric electric field gradients ($\eta_q = 0$) typical of ^{2}H nuclei, which are often used for probing different materials.

3.4. Detection of NMR Signals in Solids: Common Aspects

Methods of signal detection and radio frequency pulse sequences used for NMR data collection develop constantly

to meet the needs to characterize new materials containing the target nuclei.

Reviews[127,129] on diamagnetic amorphous materials cover quadrupolar nuclei, whereas nuclei with spins of 1/2 are considered in another review.[112] In spite of the large variety of the NMR techniques, applied for solids, these well-known principles can be divided into two major parts: direct and nondirect excitation, which are considered here in the context of their possible applications for probing paramagnetic systems.

3.4.1. Direct Excitation

Such simple NMR experiments include three time sections: (i) relaxation delay, providing complete nuclear relaxation important for quantitative analysis; (ii) action of radio frequency pulse (RFP); and (iii) recording the NMR data as free induction decays followed by Fourier transformation. According to Ernst and Anderson,[130] the pulse angle α is defined as $\alpha = \gamma B_1 t_P$, where B_1 is the power of the pulse and t_p is its duration. Modern solid-state NMR spectrometers can produce RFP with amplitudes on the order of 50−100 kHz, sufficient to observe resonances for most diamagnetic materials with nuclei with spins of 1/2 even at their strong dipolar coupling or chemical-shift-anisotropy magnitudes. The situation changes for quadrupolar nuclei, where dominating quadrupolar interactions can be too strong to produce inhomogeneous broadenings on the order of MHz. When the REF is applied at the Larmor frequency, only central transitions are effectively irradiated and the satellite transitions are off resonance. The effects lead to significant distortions of the resonance shapes that can be avoided by decreasing the RFP lengths and increasing the pulse power or by selective irradiations.[44,127] For example, ^{27}Al-containing materials are often studied with short RF pulses or by using frequency-stepped adiabatic half passage (FSAHP). Kentgens et al. emphasize that this technique has an advantage over short-pulse experiments because it leads to NMR spectra with increased peak intensities and less dependent on the RF field strength.[131]

Registration of the quadrupolar nuclei, excited directly by a single-pulse sequence, can be complicated by the so-called dead time of NMR spectrometers. When a magnetization, created by a radio frequency pulse, decays rapidly with respect to the spectrometer dead time, Fourier transformation converts the FIDs into NMR spectra where signal intensities are strongly reduced and a baseline shows strong distortions. Generally, this technical problem is minimized by experiments with pulse sequences Hahn-echo ($90°_X-\tau-180°_Y-\tau$−FID) or solid echo ($90°_X-\tau-90°_Y-\tau$−FID), where τ is echo-delay time and the FIDs can be collected immediately after 180° pulses. It should be noted that such experiments in spinning samples require echo-delays synchronized with rotor periods.[44,113]

As will be shown below, strong paramagnetic effects can lead to extremely wide spreads of resonances for target nuclei in static and spinning samples, giving rise to problems similar to those observed for quadrupolar nuclei. Moreover, the resonances can be invisible in regular NMR experiments with direct excitation.

3.4.2. Cross-Polarization

Following Kolodzieski and Klinowski,[132] cross-polarization (CP) from abundant spins (^{1}H, ^{19}F) to dilute spins (^{13}C, ^{15}N, or ^{29}Si) solves two important problems of NMR in solids. First, the CP improves a signal/noise ratio in NMR spectra of nuclei with a low natural abundance and low γ values. The second problem connects with spin−lattice relaxation times of dilute spins, which are very long in diamagnetic solids. For example, they can vary from tens of seconds for ^{13}C or ^{15}N to several minutes for ^{29}Si in silicates. It means that long relaxation delays should be used at direct excitations, leading to very long experimental times at collections of NMR data.

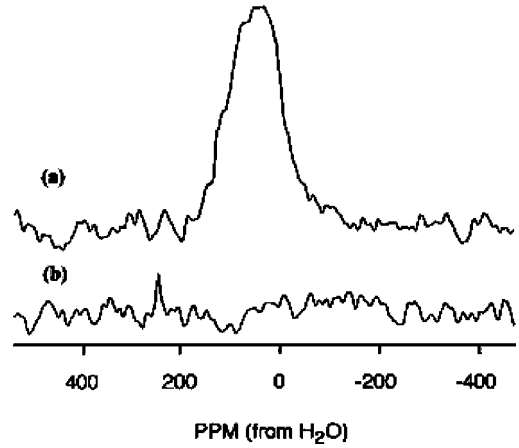

Figure 4. ^{27}Al−^{17}O cross-polarization NMR spectrum recorded in a static sample of α-alumina (a) and the NMR spectrum obtained by ^{17}O direct excitation (b). Reprinted with permission from ref 127. Copyright 1999 Elsevier B.V.

The CP, for example, from ^{1}H to ^{13}C, based on close proximity of the dilute and abundant nuclei, exploits a pulse sequence, where the main task is magnetization transfer from the ^{1}H spins with a high natural abundance to the ^{13}C spins via dipolar coupling between them. The amplitudes of two contact pulses, operating at the proton and carbon frequencies, should be adjusted to achieve the Hartmann−Hahn conditions:[133] $\gamma_H B_1(^1H) = \gamma_C B_1(^{13}C)$. Under these conditions, the energy gaps between the ^{1}H and ^{13}C rotating-frame spin states become equal, and a transition requiring energy on a ^{1}H spin can be exactly compensated by a transition releasing energy on a ^{13}C spin. The CP pulse sequence, besides increasing the signal intensity, obviously leads to more rapid accumulations of the ^{13}C NMR spectra because the relaxation delay is decided by the ^{1}H (but not ^{13}C) relaxation. Finally, since the polarization transfer goes via heteronuclear dipolar interactions, the CP is sensitive to internuclear distances and the mobility of molecules or functional groups involved, thus providing structural information and dynamics in solids.[132]

The CP can also be performed even for quadrupolar nuclei, requiring, however, the corresponding Hartmann−Hahn matching conditions.[127] These conditions can be realized when the energy of splitting in the rotating frame of both nuclei is the same. For this reason, only a small fraction of the quadrupolar nuclei will have a Hartmann−Hahn match with the other nuclei, and therefore the signal-to-noise ratio in such NMR spectra will be poor. These results are often observed for CP(^{1}H−^{27}Al) experiments, for example. In spite of this limitation, the cross-polarization can be still successful in some cases important for materials science. Figure 4 compares the ^{27}Al−^{17}O cross-polarization NMR spectrum recorded in a static sample of α-alumina and the NMR spectrum obtained by ^{17}O direct excitation. Here only very weak radio frequency fields have been used and the RF field strengths have been the same (≈10 kHz) for both nuclei.

As seen, the CP experiment illustrates a very large increase in a signal/noise ratio.

Kinetics of the CP shows that its effectiveness strongly depends on molecular mobility in diamagnetic solids: increasing the mobility remarkably reduces signal/noise ratios.[132] In this context, one can expect that strong shortening of the ^1H T_1 times can violate the conditions of polarization transfers. Therefore, *because of the fast relaxation in paramagnetic materials, the efficiency of the CP experiments is dramatically reduced*. Nevertheless, as will be shown below, sensitivity enhancement is still possible in the ^{13}C solid-state NMR spectroscopy in some paramagnetic systems.

3.5. Increasing the Structural Information for Diamagnetic Materials by Solid-State NMR

Generally, chemists describing structures of materials by solid-state NMR focus on determining the number of structurally different species and their relative contents involving multinuclear NMR experiments. This aim can be reached by increasing the spectral resolution and developing new NMR techniques. Both of the aspects have been considered in two recent works reviewing the high-resolution solid-state NMR experiments performed for nuclei with spins of 1/2[112] and quadrupolar nuclei.[129] The first group of the nuclei, especially ^1H, can be detected at ultrafast magic-angle spinning rates with the frequency of up to 65 kHz. Because in rigid solids the homonuclear dipolar interaction $^1H-^1H$ is particularly strong, lines in the ^1H MAS NMR spectra, recorded even at high spinning rates, are still broadened due to remaining dipolar interaction. However, such broadenings can be weakened or completely removed at ultrafast spinning in a combination with homonuclear dipolar decoupling techniques CRAMPS (combined rotation and multiple pulse spectroscopy), pioneered by Gerstein.[134] The technique, improving the resolution, involves also new pulse sequences, such as DUMBO or PMLG, and the 2D $^1H-^1H$ double-quantum (DQ) MAS experiments.

Finally, the ^1H signals can be narrowed by isotopic dilution with deuterium. It should be noted that all these ^1H NMR approaches provide the best results for crystalline samples but not for strongly amorphous systems where line broadenings have a slightly different nature.

For nuclei, other than ^1H, with spins of 1/2, for example, ^{13}C, good results can be reached by the homonuclear correlation spectroscopy, where the NMR data are collected either by dipolar-based transfers or via J-based techniques. Double-quantum (or zero-quantum) homonuclear dipolar recoupling MAS techniques have been also developed to probe the $^{29}Si-^{29}Si$ (or $^{31}P-^{31}P$) dipolar interaction, as an important part of structural information in solids.[112] For example, the structure of zeolites can be accurately solved by the ^{29}Si DQ dipolar recoupling NMR experiments, resulting in internuclear silicon distances. Some structural details of inorganic and hybrid systems can be obtained by multidimensional and multinuclear MAS NMR correlation experiments. For example, the 2D ^{29}Si DQ technique is very suitable for zeolites and mesoporous silica-based materials. The 2D ^{29}Si INADEQUATE experiments are widely applied to determine unambiguously interconnectivities between the silicon atoms. Finally, the accurate structure of frameworks in many materials can be obtained by a combination of the solid-state NMR data with X-ray diffraction data and first principle calculations.

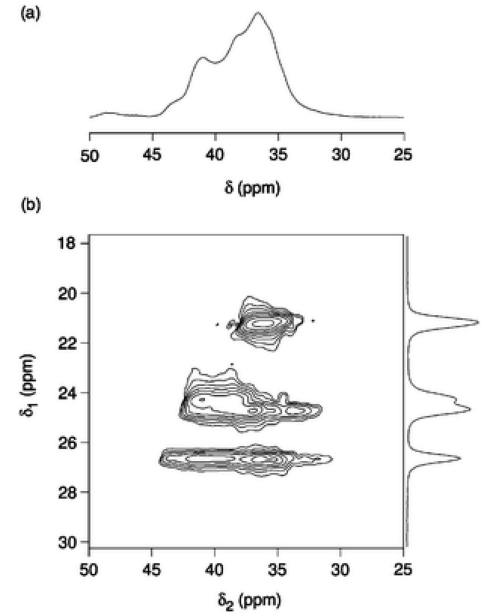

Figure 5. ^{27}Al (a) MAS and (b) two-dimensional triple-quantum MAS NMR spectrum and corresponding isotropic projection recorded in material $AlPO_4$-14. Reprinted with permission from ref 129. Copyright 2009 Royal Society of Chemistry.

The main problem with NMR spectra of quadrupolar nuclei is the second-order quadrupolar broadening, which cannot be completely removed by simple MAS techniques even at high spinning rates.[44] This effect that masks structurally different sites can be strongly reduced by sample rotations around two different angles or by the so-called double rotation (DOR). However, Ashbrook[129] emphasizes that, in spite of the large advantage of the DOR technique resulting in the high-resolution NMR spectra obtained in real time in a one-dimensional experiment, it requires a special design of NMR probes.

The 2D MQMAS experiments can be performed with regular NMR probes, and they are more popular. Representing a combination of regular sample MAS rotations and manipulations with the nuclear spins, these experiments also reach a high resolution, as is illustrated in Figure 5. As seen, the regular ^{27}Al MAS NMR spectrum obtained in the material $AlPO_4$-14 shows a very poor spectral resolution due to the second-order quadrupolar broadening. This effect is suppressed completely in the two-dimensional triple-quantum MAS NMR spectrum, providing a detailed structural study.

Alternative approaches to increasing the spectral resolution in solid-state NMR spectra of quadrupolar nuclei are based on the satellite-transition MAS experiments at a very precise magic angle setting.[129] The advantages of experiments with quadrupolar nuclei at highest magnetic field strengths can be found in ref 135, where lanthanum halides have been probed at fields of 7.0, 9.4, 11.7, and 17.6 T.

Finally, to enhance resolution of chemically nonequivalent sites in the NMR spectra of powdered or disordered solids, Frydman and co-workers[136] have suggested the relaxation-based strategies.[136] In combination with signal-enhancement methodologies, such as the quadrupolar Carr-Purcell Meiboom-Gill (CPMG) pulse trains, the relaxation-assisted separations can be very successful for the high-resolution NMR characterizations of materials having insensitive low-γ nuclei. The authors have also demonstrated the limitations of these 2D NMR approaches and their potential.

3.6. Practical Aspects in a Structural Analysis of Porous Diamagnetic Materials by Solid-State NMR

Commonly, structural investigations of porous molecular systems imply the multinuclear solid-state (MAS or static) NMR experiments directed to characterizations of the matrix of materials: its surface, including behavior of surfactant molecules, to description of molecules, located in pores, and their dynamics, the nature and locations of doping metal ions, and their coordination numbers and oxidation states. This section shows typical examples of such studies and their strategy, illustrating mainly porous diamagnetic silica-based materials important in the context of understanding the NMR behavior of relative paramagnetic solids.

3.6.1. Structural Features of the Silica Lattice by Solid-State ^{29}Si and ^{27}Al NMR Spectra

Simonutti and co-workers[137] have performed multinuclear MAS NMR experiments on mesoporous silica materials of the MCM-41 family prepared in the presence of cetyltrimethylammonium chloride as a surfactant. These studies represent good practical examples of structural characterization of the matrix of the materials. Figure 6 shows the ^{29}Si $\{^1$H$\}$ MAS NMR spectra recorded by a single-pulse sequence for noncalcined and calcined MCM-41 systems with very long relaxation delays (100 s) to ensure complete relaxation of the silicon nuclei. Since ^{29}Si$-^{29}$Si dipolar coupling is relatively weak, the MAS NMR spectra *did not show spinning sideband patterns*. The spectrum of the noncalcined material exhibits two intense peaks at -99 and -109 ppm, which are generally attributed to group $(Si-O)_3Si-OH$, named as Q^3, and group $Si(Si-O)_4$ (Q^4).[44] A weaker peak at -89 ppm is from geminal silanol groups $(Si-O)_2Si-(OH)_2$ (Q^2). On calcination, the resonances broaden, partially overlapping, and the Q^4 signal becomes more intense. The Q^3 and Q^2 species are present at the surface of the silica matrix, and the intensity ratio $(Q^3 + Q^2)/Q^4$ is associated with the surface area. Then, a decrease in this ratio, as observed on calcination, corresponds to partial condensation of the silanolic groups and the shrinkage of the channels. In addition, the line-broadening effect in the calcined material can also be related to the shrinkage due to a distortion of the siloxanic tetrahedrons and an inhomogeneous broadening. Finally, quantitative information can be obtained by deconvolution in the above spectra.

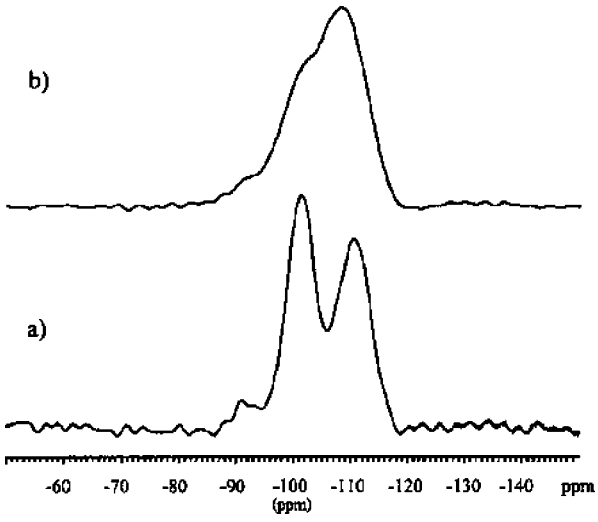

Figure 6. Single-pulse ^{29}Si $\{^1$H$\}$ MAS NMR spectra of noncalcined (a) and calcined (b) material MCM-41. Reprinted with permission from ref 137. Copyright 2001 American Chemical Society.

Recently, Davis and co-workers[138] have suggested a technique that operates on a different principle for analysis of Si(Q) distributions based on 2D magic-angle-flipping experiments applied for potassium disilicates enriched by ^{29}Si. It is remarkable that the 1D spectra of these glasses are completely unresolved.

In the ^{29}Si MAS NMR spectra of aluminosilicates and zeolites containing Al atoms, line assignments and deconvolution procedures can be very problematic because the resonances of ^{29}Si nuclei in the (3Si, 1Al) and (3Si, OH) structural units often overlap. Moreover it is difficult to discriminate one group from another. The latter is particularly important because the Si[3Si, 1Al] units are generally associated with the acidic SiOHAl groups, while the Si[3Si, 1OH] units correspond to nonacidic silanol groups in zeolite defects. Luo and co-workers[139] have shown how to apply the triple-resonance techniques based on the ^{1}H/^{27}Al/^{29}Si TRAPDOR-CP and ^{1}H/^{27}Al TRAPDOR pulse sequences. For example, the different peaks, observed in the ^{29}Si CP NMR spectra of materials MCM, can be distinguished and assigned by this triple-resonance NMR approach. Combination of the ^{1}H/^{27}Al double-resonance NMR experiments with the ^{1}H/^{27}Al/^{29}Si triple-resonance spectra reveals the presence of two different acidic sites.

Sometimes even the regular ^{1}H MAS NMR experiments can be sufficient to distinguish the different OH groups located in the surface of silica-based materials. In particular, the isolated Si$-$OH groups show a ^{1}H signal at 1.3$-$2.2 ppm, whereas resonances from the hydrogen-bonded SiOH groups are shifted to 3.9$-$4.0 ppm and appear generally as broadened resonances due to a distribution of the hydrogen bond strength.[137] Finally, the structure of the matrix can be accurately solved by a combination of solid-state NMR with the powder XRD data when they are informative. This approach has been recently applied for the determination of zeolite structures, where the important step of structure solution includes the solid-state ^{29}Si double-quantum dipolar recoupling NMR experiments, sensitive to the distance-dependent dipolar interactions between naturally abundant ^{29}Si nuclei in the zeolite framework.[75]

3.6.2. Distribution of Diamagnetic Metal Ions by Solid-State NMR

Because diapasons of chemical shifts for heavy nuclei, such as ^{51}V, ^{47,49}Ti, ^{117,119}Sn, etc., are very large and their resonance frequencies depend strongly on atomic coordination numbers and oxidation states and also on types of chemical bonding, direct observations of these nuclei in the solid-state NMR spectra can lead to reliable conclusions on the locations of the diamagnetic metal ions inside or outside the matrix. In the case of Al ions and diamagnetic silica-based materials, this key problem can be solved relatively easily: if the ^{27}Al MAS NMR spectra show resonances with isotropic chemical shifts around 54$-$62 ppm, then they say that aluminum atoms are incorporated into the silica matrix as four-coordinated species.[44] The presence of lines at 0 to -6 ppm points to extraframework aluminum. More accurate and complete characterizations of different Al moieties require a better spectral resolution (see the second-order quadrupolar broadening), which can be reached by the 2D

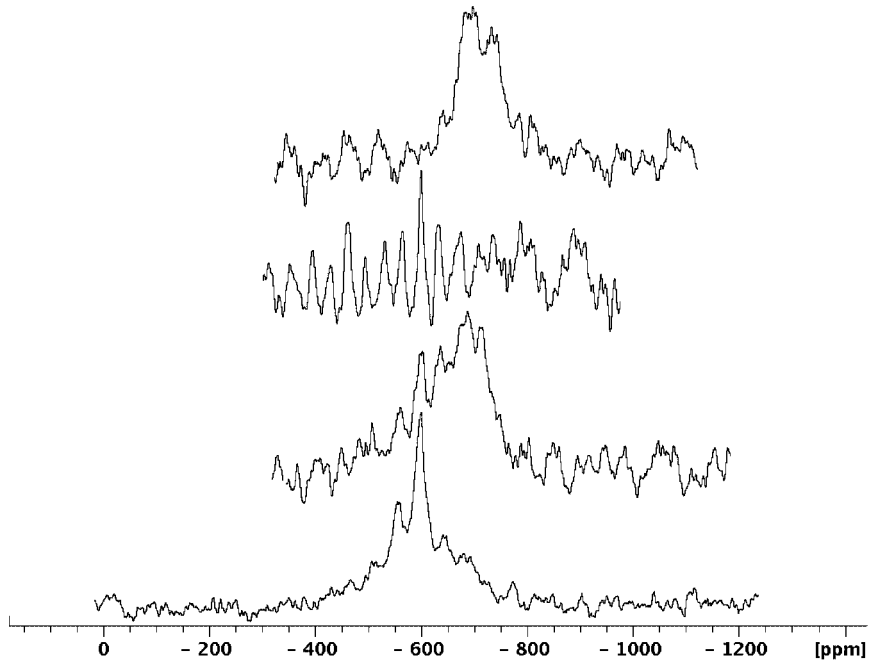

Figure 7. ^{119}Sn Hahn-echo MAS (6 kHz) NMR spectra from top to bottom: material SiO_2-SnO_2, containing 2 wt % of tin; dehydrated material SiO_2-SnO_2 containing 3 wt % of tin; the same material obtained in an air/water atmosphere; and material SiO_2-SnO_2, containing 14 wt % of tin. Reprinted with permission from ref 78. Copyright 2010 Elsevier B.V.

^{27}Al 3Q-MAS approach, as applied for some titanium-substituted zeolites. Here, the Al species represent four-, five-, and six-coordinated Al atoms.[140] Moreover, two different tetrahedral and octahedral Al environments atoms have been observed. It should be emphasized that ^{27}Al is a very convenient target nucleus for the above studies even at low Al concentrations due to the 100% natural abundance and short relaxation times.

In contrast to quadrupolar and fast-relaxing ^{27}Al nuclei, ^{119}Sn T_1 relaxation times in diamagnetic solids are very long and the natural abundance is relatively low. These circumstances obviously complicate ^{119}Sn NMR data collections particularly at low tin concentrations. Such materials are conventionally characterized by experiments with ^{119}Sn-*enriched* samples. Thus, Renz and co-workers[102] have characterized catalytic sites in some tin-containing amorphous materials, by directly measuring isotropic ^{119}Sn chemical shifts. It is known that ^{119}Sn chemical shifts between −670 and −740 ppm can be attributed to framework Sn^{IV} sites with octahedral or tetrahedral coordination. For example, the ^{119}Sn resonance at $\delta = -688$ ppm, observed in the MAS NMR spectra of dehydrated zeolite Sn−MFI, can be assigned to octahedral Sn^{IV} units, whereas the shoulder at −439 ppm can be attributed to framework tetrahedral tin sites. The authors have shown that the shoulder shifts to −579 ppm, due to the formation of five-coordinate Sn species upon hydration. Similarly, the ^{119}Sn MAS NMR spectrum of hydrated zeolite Sn-β-2 exhibits two signals at −690 and −740 ppm, which transform to a resonance at −445 ppm in the dehydrated sample. This signal was attributed to tetrahedral Sn^{IV} framework sites where the coordination number increases by bonding to extra water molecules.

Figure 7 shows the series of the ^{119}Sn MAS NMR spectra, recorded at the ^{119}Sn natural abundance for supermicroporous materials SiO_2-SnO_2, synthesized at different Sn contents.[78]

The spectrum of the material with 14 wt % of tin exhibits a sideband pattern with an isotropic resonance observed at −600 ppm, typical of bulk SnO_2 with six-coordinated tin(IV) atoms. In addition to this signal, the spectrum of the material with 3 wt % of tin displays another line, which is upfield shifted. Furthermore, the material with 2 wt % of tin exhibits only this upfield resonance (−697 ppm). This evolution of the NMR spectra proposed to indicate that only ∼2 wt % of tin can be incorporated into the silica surface, likely forming catalytic centers. In full agreement with these assignments, the ^{119}Sn MAS NMR spectrum of the *dehydrated* material doped with 3 wt % of tin exhibits a low-field sideband pattern with an isotropic chemical shift of −460 ppm, corresponding to four-coordinated Sn sites situated in the silica matrix surface. Again, this transformation is reversible. It should be noted that such spectra require a large number of accumulations and a long experimental time.

Ganapathy and co-workers[140] have reported some titanium-substituted zeolites studied by solid-state NMR. In contrast to the ^{27}Al nuclei, the ^{47,49}Ti nuclei show strong quadrupolar coupling. Therefore the ^{47,49}Ti NMR experiments were performed in static samples. These experimental and computer-simulated spectra revealed a ^{49}Ti resonance at −850 ppm with a quadrupole constant of 5 MHz, which can be used as a test for the octahedral Ti atoms incorporated into the matrix of zeolites. Applications of other targeted quadrupolar nuclei such as ^{71}Ga[141] and ^{51}V[119,120] have been reported. In these papers, the NMR spectra obtained for different materials in static and spinning samples were used to determine the magnitudes of the quadrupole and shielding anisotropy tensors as a function of the nuclear environments.

Finally, it should be emphasized that direct NMR detection of nuclei in metal atoms and investigation of their spectral parameters are probably the best approach to localizing metal ions and determining their distributions in various materials. This approach is obviously impossible in the case of materials doped with paramagnetic metal ions.

3.6.3. Internuclear Distances from Solid-State NMR

It is probable that determination of internuclear distances is one of the best approaches to structural descriptions of solids. The principles of high-precision measurements of internuclear distances by solid-state NMR techniques have been recently reviewed by Lee and Khitrin.[142] Usually, the distance measurements come from the magnitudes of long-range dipole−dipole interactions that give rise to the so-called Pake signal shapes in static samples. The modern NMR technique applied in this context is based on 2D single-echo experiments enhanced with adiabatic cross-polarization. It is important that the 2D NMR experiments resulting in unperturbed dipolar powder spectra can be performed on even diluted (1% and lower) nuclear spins to resolve structures of amorphous or disordered systems. At the same time, these measurements are more effective for crystalline molecular systems. For example, C−N distances can be determined with the accuracy comparable with the X-ray technique.[142]

Recent developments of new solid-state MAS NMR techniques have created an opportunity for 3-D structure determinations in microporous materials, where the main attention is focused on structural characterizations of molecular complexes with absorbed organic molecules. Fyfe and co-workers[143] have demonstrated usefulness of the $^{19}F-^{29}Si$ CP, REDOR, and TEDOR NMR experiments and localized the F anions within the three-dimensional framework of the silicate octadecasil. The accurate Si−F distances have been measured via the $^{19}F/^{29}Si$ dipolar couplings and their nonlinear least-squares fittings, providing good agreements with the single-crystal X-ray data. The authors emphasize that these NMR experiments can be applied for other materials to determine, for example, $^{19}F-^{31}P$ interatomic distances in aluminophosphate molecular sieves ($AlPO_4$'s) with fluorine-containing guests and to other framework/sorbate host−guest complexes.

3.6.4. Molecular Mobility in Diamagnetic Systems from Solid-State NMR Spectra

Studies of molecular mobility in porous materials result in better understanding their catalytic properties. Ashbrook[129] has emphasized that solution and solid-state NMR is very sensitive to molecular mobility and molecular motions on a very large time scale: from very fast motions, effecting on nuclear relaxation, to very slow motions, detected by two-dimensional exchange NMR experiments. Molecular motions on an intermediate time scale can be observed in solid-state NMR due to anisotropic interactions, which can be reduced by molecular reorientations. These reorientations affect line shapes and/or line widths that can be directly observed by variable-temperature NMR spectra. Since the dynamic effects are more evident for line shapes of quadrupolar nuclei, they are more preferable in such studies than nuclei with spins of 1/2. If lines are broadened by the first-order quadrupolar interactions, then molecular motions are on a time scale of 100 ns−10 μs. In turn, when central-transition line shapes are affected by the second-order quadrupolar broadenings, the molecular reorientations are between 100 μs and 1 ms. In general, MAS NMR spectra are sensitive to molecular mobility on a time scale of 10 μs −100 μs.

Sometimes even the "simple" variable-temperature NMR spectra can provide useful information on molecular mobility. For example, mesoporous materials MCM-41, synthesized in the presence of cationic surfactants, show a remarkable temperature dependence of the ^{13}C MAS NMR spectra, illustrating, thus, intense motions of the surfactant aggregated into a gel-like state.[137]

Variable-temperature NMR spectra describe successfully behavior of small molecules that are absorbed by porous materials and situated in pores. Theoretically, liquids within small pores freeze or melt at lower temperatures than regular liquids. The temperature depression of the melting point is described by the Gibbs-Thompson equation[145] and depends on pore sizes.[144] In turn, pore-size distribution, evidently resulting in distribution of the melting-point temperatures, can be estimated by measurements of the liquid fraction at different temperatures by regular ^1H NMR, for example. This liquid-state ^1H NMR technique characterizes, for example, pore-size distribution and pore-wall thickness in the mesoporous materials FSM-16 after their saturations with water or benzene.

Behavior of olefin molecules, 1-butene or 1-pentene, absorbed by zeolites can be successfully described by the high-resolution ^1H and ^1H NOESY MAS NMR techniques on the basis of ^1H chemical shifts measured for the adsorbed olefins as a function of pore fillings.[146] It has been found that, at lower pore fillings, the chemical shifts of olefins are very close to those observed in the gas phase, whereas at higher pore fillings, the chemical shift values approach those in the bulk liquids. More detailed descriptions of the adsorbed molecules in terms of their fast librations and overall reorientation−translation motions are also available.

Because deuterium line shapes are very sensitive to the translational, librational, and rotational motions with the activation energies associated with thermally activated jumps between structurally different sites,[46] the solid-state ^2H NMR technique is often applied for characterizations of materials. Even the coking phenomena in zeolites[147] can be monitored by ^2H NMR. In general, the ^2H NMR method, directed to probing mobility of absorbed molecules in porous systems, consists of recording the variable-temperature ^2H NMR spectra of deuterated objects (for example, benzene, ethanol, etc.) to document their temperature evolution from an isotropic resonance, due to fast reorientations, to the shape with a quadruple splitting,[147,148] observed at slow motions. Brown and co-workers[149] have shown the theory and the practice of deuterium line-shape analysis performed for solid dimethyl sulfone-d_6.

As mentioned above, polarization transfer via heteronuclear dipolar interactions is sensitive to the molecular mobility or mobility of functional groups involved. Therefore the cross-polarization NMR experiments can also give some information on molecular dynamics in solids. The strategy of these studies is based on analysis of the cross-polarization kinetics at variations in magnitudes of contact times.[132,150] For example, the ^{13}C CP(C−H) NMR kinetic approach has recently been used for mesoporous silica materials, containing cationic surfactant molecules. The data obtained and particularly the carbon cross-polarization times (T_{CH}) have shown that the surfactant, located in the pores, can be characterized by anisotropic motions, which reduce from the chain end toward the polar head.[137] In addition, NMR experiments involving magnetization transfer from surfactant protons to silicon atoms located on the surface of pores have illustrated relatively strong interaction between ammonium groups of the surfactant and the silica surface.

3.6.5. Mobility from NMR Relaxation in Diamagnetic Solids

Molecular reorientations in solids can be better characterized by nuclear spin relaxation experiments because the frequency domain in condensed phases studied by a spectroscopist is very large from slow motions around 10 Hz to fast motions of up to 10^{12} Hz. The theory of nuclear spin−lattice and spin−spin relaxation in solids, analysis of second moments, basic relaxation experiments, and their interpretations, including solids with very mobile fragments like the quantum tunneling methyl groups, can be found in reviews.[151−153] Klinowski[111] gives a summary of the relaxation data, which are very useful for studies performed in diamagnetic porous silica-based materials and zeolites. (a) ^{29}S Spin−lattice relaxation times, T_1, are *relatively* short and typically measured as 5−30 s (in some systems, however, they can reach 100 s or more). (b) ^{29}Si Relaxation is not affected by the presence of ^{27}Al in the matrix. (c) Generally, nuclear spin−lattice relaxation in solids is controlled by spin diffusion via paramagnetic centers. However, in zeolites this mechanism is inefficient because of the large distance between neighboring silicon atoms and the relatively low natural abundance of ^{29}Si nuclei. (d) Nevertheless, the ^{29}Si T_1 effects of molecular oxygen are dramatic, whereas other paramagnetic impurities or water play a secondary relaxation role. (e) Relaxation times of crystallographically different Si atoms are different, and the ^{29}Si T_1 times increase in amorphous zeolites because many Si atoms in these samples are inaccessible to oxygen. (f) Spin−lattice relaxation times of ^{27}Al nuclei in zeolites are between 0.3 and 70 ms and depend on the temperature. Their relaxation is governed by the electric quadrupole interactions with the crystal electric field gradients, which are modulated by translational motions of polar sorbate molecules.

In practice, NMR relaxation studies in materials science are generally focused on the mobility of absorbed molecules often with applications of the ^{1}H−^{13}C cross-relaxation time measurements,[146] organic template molecules by measurements of ^{1}H T_1 and $T_{1\rho}$ times,[154] or on dynamics of liquids in porous media by ^{1}H relaxation imaging.[154−156] The pore morphology can be investigated by ^{1}H T_2[29] or ^{2}H T_1 relaxation times.[144,145] The corresponding relaxation models and interpretations can also be found in the above publications. Other NMR approaches, developed recently, are based on relaxation behavior of gases when they saturate pores of materials. For example, the ^{19}F T_1 times of CF_4 gas, typically measured as 0.2 to 5−6 ms and dominated by spin-rotation interaction, have been applied for pore-size measuring.[157] The relaxation measurements have shown that the gas, condensed on the pore walls and in a region near the wall, is denser than the bulk gas.

Stupic and coauthors[158] have reported on quadrupolar relaxation of hyperpolarized ^{83}Kr nuclei, which can be used as a probe for surfaces of porous polymeric systems: the ^{83}Kr T_1 times (measured between 2 and 7 s) depend strongly on the chemical composition of the surfaces in the vicinity of the gas, as well as on the chemical treatment of the glass surfaces. Recently, it also has been demonstrated that porosity of materials can be characterized by NMR imaging of C_2F_6 gas:[159] the C_2F_6 relaxation time is longer in pores than in bulk gas and increases with the pore-size decrease.

Except spin diffusion and other specific mechanisms in diamagnetic solids, nuclei relax commonly via dipole−dipole, quadrupole, spin-rotation, scalar, and chemical shift anisotropy interactions. According to the theory of Bloembergen, Purcell, and Pound, relaxation rates can be written as $1/T_{1,2} = CJ(\omega_0,\tau)$, where C is the coupling strength and $J(\omega_0,\tau)$ is the spectral density function.[113] In turn, the $J(\omega_0,\tau)$ corresponds to fluctuations of magnetic fields directly associated with thermal molecular motions characterized in turn by molecular motion correlation times τ. Thus, relaxation time measurements provide determinations of correlation times and activation energies of molecular motions. The situation changes in paramagnetic solids, where fluctuations of magnetic fields are governed by electron spin flips and, thus, the τ time reflects electron relaxation.

4. Paramagnetic Effects in Solid-State NMR: Theoretical Aspects

Unpaired electrons in paramagnetic centers give rise to strong local magnetic fields that mask original spectroscopic properties of objects investigated, such as chemical shift values, line shapes of resonances, and their T_1, T_2 relaxation times.[160] Thus, generally, the presence of paramagnetic centers in solids (molecular oxygen, paramagnetic impurities, etc.) is not desirable, particularly at accurate structural studies of materials by NMR or at probing their dynamic behavior. On the other hand, influence of paramagnetic centers will obviously depend on their concentrations and electron relaxation times. Therefore, their optimal combinations can lead to a number of "positive" effects. These effects significantly shorten relaxation delays in long-term solid-state NMR experiments and increase NMR sensitivity by optimizing ^{1}H T_1 relaxation,[161,162] by dynamic nuclear polarization,[163,164] or by applications of the so-called contrast media in the magnetic resonance imaging experiments.[165]

However, generally, the significant presence of paramagnetic centers requires development of new NMR approaches and new strategies for structural characterizations of solids. For example, the ^{13}C MAS NMR experiments, including very-fast magic-angle spinning (≥20 kHz) and recoupling-based polarization transfer, are recently reported by Wickramasinghe and Ishii.[166] It has been shown that these experiments, performed in paramagnetic complexes, such as Cu(DL-Ala)$_2$, discriminate groups ^{13}CH, ^{13}CH$_2$, ^{13}CH$_3$, and ^{13}CO$_2$ in the 1D NMR spectra, simplifying the spectral assignments, or even provide determination of distances between nonbonded C−H pairs by quantitative analysis of cross-peak intensities in the 2D NMR spectra.

The strong dipolar interactions between target nuclei and the electronic magnetic moments produce the chemical shift anisotropy (see below), which can be significantly larger than those shown in Table 1. The anisotropy can be larger than the radio frequency amplitudes, giving rise to technical problems for signal registrations. Kervern and co-workers have successfully solved this problem by applications of short high-power adiabatic RF pulses for population inversion in paramagnetic complexes of Fe(II), Yb(III), and Tb(III).[167] The application of very fast spinning, a wideband sensitivity enhancement, and simultaneous adiabatic spin-locking cross-polarization have been demonstrated by Peng and coauthors in NMR studies of some Cu(II) paramagnetic complexes.[168] However, these methods, being rather specific, cannot be applies for strongly paramagnetic and amorphous materials, which are considered in detail in the next sections.

4.1. Chemical Shifts and Magnetic Shielding Tensors in the Presence of Unpaired Electrons

A very high magnetic moment of an unpaired electron, located on a paramagnetic center, affects a resonance frequency of target nuclei via effective magnetic field B_{EF}:

$$B_{EF} = 2\pi A\mu_B g B_0 S(S+1)/3\gamma_N kT + \mu_0\mu_B{}^2 g^2 B_0 S(S+1)(3\cos^2\theta - 1)/3kTr^3 + B_{BMS} \quad (1)$$

where A is the isotropic electron/nucleus hyperfine coupling constant,[169] μ_B is the Bohr magneton (9.2741×10^{-24} J T^{-1}), r is the electron/nucleus distance, θ is the angle between the electron−nucleus vector and the external magnetic field B_0, and g is the electron g factor. The first term in eq 1 produces the so-called Fermi-contact (FC) chemical shifts.[170] Because of direct delocalization of the unpaired electron density on the nuclei, the Fermi-contact shifts are dependent on hyperfine coupling constant A and can reach 3000 ppm or even higher as a function of nuclei and paramagnetic centers. The magnetic shielding tensors in paramagnetic solids are often axially symmetric. They can have very large anisotropies covering ranges up to 3500−4000 ppm. It is obvious that this situation takes place when atoms, containing target nuclei, are chemically binding to paramagnetic ions, creating technical difficulties for detection of such nuclei.

It should be emphasized that there is a fundamental difference between the FC shifts, observed in nonmetallic molecular complexes, and the so-called Knight shifts, detected in metallic systems. The Knight shifts, for example, for ^{27}Al or ^{29}Si nuclei can be found in systems URu_2Si_2[171] or UNiAl.[172] According to Abragam,[114] in contrast to nonmetallic systems, the conducting electrons in metals are not localized, and thus, each nuclear spin "sees" a magnetic field from all the electrons.

The second field, created in the presence of an unpaired electron, corresponds to dipolar electron/nucleus interaction. Equation 1 shows that this interaction strongly depends on distance r and is angle-dependent, as $3\cos^2\theta - 1$, where θ is defined as an angle formed by the **r** vector and the external magnetic field.[114] In powder solids, because of the absence of fast high-amplitude molecular reorientations, the spectral effect of this field is obvious: a resonance of target nuclei undergoes strong broadening in a static sample similarly to dipole−dipole internuclear interactions.

The last term, B_{BMS}, represents a demagnetization field that appears in a sample due to bulk magnetic susceptibility (BMS). In general, this effect is insignificant for diamagnetic solids, but it can play a very important role in paramagnetic systems. In spite of this, it is often ignored in practice. Kubo et al.[173] have investigated BMS effects experimentally and theoretically by calculations on a model basis with random orientations and distributions of crystallites in powder. It has been found that the BMS shifts, resulting in the BMS broadenings in static samples, can be very large and even dependent on the shape of NMR containers. For example, the demagnetization field is uniform at all the points on the axis of a cylinder container, situated at magic angle with respect to the external magnetic field, but it changes strongly toward walls and ends of the cylinder.[173,174] The theory agrees well with the ^{1}H and ^{13}C NMR experiments performed for paramagnetic Ln, Pr, and Yb complexes.

Since dipolar coupling and term BMS are orientation-dependent, they produce strong broadenings of resonance lines in static paramagnetic samples. In turn, by analogy with dipole−dipole internuclear interactions or chemical shift anisotropy effects,[44] these broadenings transform to intense sideband patterns in the MAS NMR spectra,[175] when spinning rates are comparable or larger than line-widths in static samples. However, it is difficult to estimate, a priori, relative contributions of both effects to these sideband patterns.

Finally, unpaired electrons can strongly shorten nuclear spin−lattice and spin−spin relaxation times, T_1 and T_2. The latter is particularly remarkable for nuclei undergoing the significant Fermi-contact interactions. As a result, the line broadenings can be so strong that the resonances can become even spectrally "invisible".

4.2. Nuclear Relaxation in the Presence of Unpaired Electrons

Nuclei in diamagnetic solids can relax by different mechanisms. For example, nuclear relaxation due to dipolar interaction between two identical nuclei is expressed as[176]

$$1/T^{DD}{}_1 = (2/5)\gamma^4\hbar^2 r^{-6} I(I+1)\{\tau/(1+\omega_I{}^2\tau^2) + 4\tau/(1+4\omega_I{}^2\tau^2)\} \quad (2)$$

$$1/T^{DD}{}_2 = (1/5)\gamma^4\hbar^2 r^{-6} I(I+1)\{3\tau + 5\tau/(1+\omega_I{}^2\tau^2) + 2\tau/(1+4\omega_I{}^2\tau^2)\} \quad (3)$$

where ω_I is the resonance frequency. This mechanism is particularly powerful at strong dipolar coupling, $\gamma^4\hbar^2 r^{-6} I(I+1)$, short internuclear distances r, and molecular motional frequencies ($1/\tau$) close to ω_I. If molecular motions in solids are quite intense, nuclear relaxation can be relatively fast like in liquids. We must emphasize, however, that in contrast to liquids reorientations of molecules or functional groups in solids cannot be characterized by a single molecular correlation time. Generally, various correlation time distributions, Cole−Cole and Davidson−Cole, for example, or a Havriliak−Negami's model,[177] can be used for quantitative interpretations of relaxation data. Forte and co-workers[177] have illustrated application of this Havriliak−Negami's model for probing dynamics in amorphous polymer systems. Fittings of the variable-temperature ^{1}H and ^{13}C T_1 data collected at different frequencies have provided the ability to recognize and characterize segmental main-chain motions, rotations of the methyl groups, and even librations of C−H bonds. Finally, nuclear relaxation in solids can be nonexponential, particularly in the absence of the spin-diffusion (see below), and the relaxation process can follow a stretched exponential law, $\exp(-(\tau/T_1)^\beta)$. Tse and Hartmann[178] have shown that β of 0.5−0.6 is typical of powder samples.

In rigid solids, motions are strongly restricted and nuclear relaxation becomes extremely slow. For example, ^{29}Si T_1 relaxation times in silica-based materials and glasses can be more than 100 s, when paramagnetic impurities are absent or minimal. In their presence, however, even at small concentrations, the relaxation rates ($1/T_1$ and $1/T_2$) can increase due to the so-called spin diffusion, suggested by Bloembergen in 1949.[179] Because of mutual flips of spins, belonging to dipolar-coupled nuclei, leading to energy-conserving spin transitions, a target spin is "transferred" to a paramagnetic center, where it relaxes very rapidly by electron−nuclear dipolar interaction. Under these conditions,

the observed relaxation T_1^{SD} times are controlled by spin-diffusion coefficients D:

$$1/T_1^{SD} = (1/3)8\pi N_p C^{1/4} D^{3/4} \quad (4)$$

$$C = (2/5)\gamma_I^2\gamma_S^2\hbar^2 S(S+1)$$

These coefficients are defined as $D = (M^{1/2}/30)a^2$, where N_p is the paramagnetic center density, M is a second moment of the dipolar internuclear interaction, and a is the internuclear distance. Equation 4 shows that effectiveness of the spin-diffusion mechanism is dictated by internuclear dipolar coupling and depends on values γ and the natural abundance of target nuclei. That is why the spin-diffusion mechanism is practically negligible for NMR relaxation of ^{13}C nuclei in polymer systems[177] or for the ^{29}Si NMR relaxation in kaollnite.[180] In contrast, this mechanism can dominate in the ^{1}H or ^{27}Al relaxation.[180]

Phenomenologically, there are two cases to be distinguished: rapid spin diffusion and diffusion-limited relaxation. Relaxation via fast spin-diffusion (T_1^{SD}) is always *exponential*, whereas a diffusion-limited relaxation is *nonexponential* but can be treated by a stretched exponential function at $0.5 < \beta < 1$, as was mentioned previously.

Fluctuating magnetic fields created by a large magnetic moment of an unpaired electron, $\mu_S = -g_e\beta eS$, can affect nuclear relaxation via direct dipolar and/or contact interactions between target nuclei and electrons in paramagnetic centers. The dipolar mechanism, controlled by reorientations of electron−nucleus vectors **r**, has been formulated by Solomon[181] and can be written for $S = 1/2$ as

$$1/T_1^{DD} = 0.1\gamma_I^2\gamma_S^2\hbar^2 r^{-6}\{\tau_e/(1+(\omega_I-\omega_S)^2\tau_e^2) + \tau_e/(1+\omega_I^2\tau_e^2) + \tau_e/(1+(\omega_I+\omega_S)^2\tau_e^2)\} \quad (5)$$

$$1/T_2^{DD} = (1/20)\gamma_I^2\gamma_S^2\hbar^2 r^{-6}\{4\tau_e + \tau_e/(1+(\omega_I-\omega_S)^2\tau_e^2) + 3\tau_e/(1+\omega_I^2\tau_e^2) + 6\tau_e/(1+\omega_S^2\tau_e^2) + 6\tau_e/(1+(\omega_I+\omega_S)^2\tau_e^2)\} \quad (6)$$

In contrast to liquids, here τ_e is an electron relaxation time, if molecular reorientations are slow. It is seen that different electron relaxation times can cause different NMR effects. Because the nuclei, situated closer to paramagnetic centers, relax much faster (see the r^{-6} factor), the dipolar $T_{1,2}$ times can be rationalized in structural terms.

According to Bloembergen,[182] strong Fermi-contact electron−nucleus coupling can lead to a situation where electron-spin flips are directly accompanied by nuclear-spin flips. This mechanism, arising because of delocalization of the unpaired spin density in a nucleus, is given by

$$1/T_1^{CON} = (2/3)S(S+1)(A/\hbar)^2(\tau_{E2}/(1+\omega_I^2\tau_{E2}^2)) \quad (7)$$

$$1/T_2^{CON} = (1/3)S(S+1)(A/\hbar)^2(\tau_{E1} + (\tau_{E2}/(1+\omega_I^2\tau_{E2}^2))) \quad (8)$$

where τ_{E1} and τ_{E2} are the longitudinal and transverse electron spin relaxation times, respectively. Again, the nuclear relaxation times are remarkably dependent on electron relaxation times. In general, the Fermi-contact mechanism can dominate at $\omega_S\tau > 1 > \omega_I\tau$ and lead to T_2 times that are much shorter than T_1, as well as strong broadenings of resonance lines.

5. Practical Consequences from the Theory of the Paramagnetic Effects

5.1. ^{1}H, ^{31}P, ^{13}C, ^{2}H, ^{29}Si, ^{7}Li, and ^{6}Li NMR Spectra of Paramagnetic Solids

Fermi-contact and dipole−dipole coupling, and also BMS effects, can lead to resonances with exclusively large frequency shifts, chemical shift anisotropies, and short spin−spin and spin−lattice relaxation times. In practice, the nuclei in static samples of paramagnetic solids are detected as strongly broadened signals that transform to very wide and intense sideband envelopes in MAS NMR spectra comparable with area of spectral excitation. All of these factors decrease signal/noise ratios in the NMR spectra, requiring, thus, remarkably larger numbers of scans.[183]

In addition, the contact or pseudo-contact chemical shifts exhibit temperature dependences (proportionally to T^{-1} and T^{-2}, respectively) that can be well observed by NMR experiments, for example, in solids containing paramagnetic lanthanide ions with relatively short electron relaxation times. In the presence of such paramagnetic centers, resonances of target nuclei are generally sharp. Gray and co-workers[183] have illustrated the temperature dependences of ^{89}Y chemical shifts in MAS NMR spectra of some mixed oxides and emphasized, thus, that comparing the spectral parameters of different paramagnetic compounds can be correct only at the same temperature.

Finally, target nuclei can become "invisible" in regular solid-state NMR spectra when the electron−nucleus distances are very short and paramagnetic effects are too strong. In this situation, the NMR spectra can show a remarkable loss in sensitivity observed even for nuclei with high natural abundances such as ^{1}H or ^{31}P. Peeters and co-workers[95] have reported on the significant intensity loss in the ^{31}P MAS NMR spectra of aluminophosphates, doped with ions of cobalt. They have found that amounts of undetectable phosphorus can reach 30% determined in the presence of an internal standard. This intensity-loss effect has been attributed to locations of the paramagnetic centers in the first and second coordination phosphorus spheres.[93,95] Similar effects in the ^{31}P NMR spectra of aluminophosphate materials, modified by ions of Ni, Co, Fe, and Mn, have been reported by Mali and co-workers.[184]

In contrast, the ^{31}P resonances in cobalt polyoxometalates can be observed in ^{31}P MAS NMR spectra. Flambard and co-workers[185] have shown that these nuclei are characterized by the large paramagnetic shifts of the Fermi-contact nature, where resonances of ^{31}P nuclei, situated closely to the cobalt centers, exhibit the chemical shift anisotropy (CSA) values up to 3300 ppm versus 500−700 ppm for ^{31}P nuclei, which are remote from the paramagnetic centers.

The large CSA magnitudes give rise to ineffective excitation of the large Larmor-frequency diapasons by the so-called single-pulse NMR experiments, additionally resulting in significant baseline distortions.[44] Generally, the spin−echo pulse sequences (180°−τ−90°) can be more effective under these conditions. Figure 8 shows the ^{31}P spin−echo MAS NMR spectra, recorded at a spinning rate between 30 and 35 kHz. As seen, even at the very high spinning rates, the spectra exhibit the intense sideband patterns that cover the

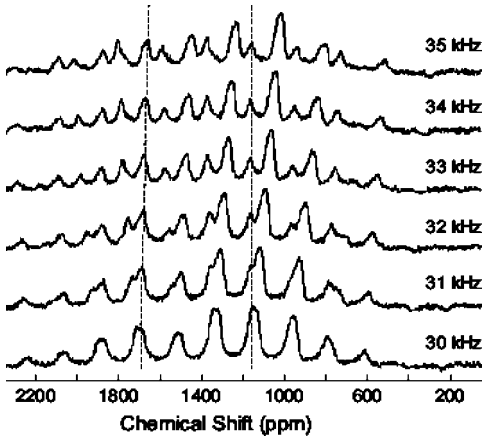

Figure 8. ^{31}P spin−echo MAS NMR spectra of paramagnetic complex $\alpha\beta$-$[Co_3Na(H_2O)_2(P_2W_{15}O_{56})_2]^{17-}$ recorded at high spinning rates. The dotted lines show the positions of two different isotropic resonances. Reprinted with permission from ref 185. Copyright 2008 Elsevier Masson.

diapason of 1700 ppm. The ^{31}P MAS NMR experiments in Figure 8 again illustrate the temperature-dependent Fermi-contact chemical shifts of ^{31}P nuclei. However, here this effect appears even at "a constant temperature": the isotropic chemical shifts, attributed to two different phosphorus sites (see the dotted lines), change with the spinning rates. The reason is the rise in temperature when increasing the spinning rates from 30 to 35 kHz.

Similarly, an isotropic ^{13}C chemical shift measured by Blumel and co-workers[186] in the MAS NMR of solid Cp_2Cr changes from −258 to −231 ppm, when a spinning rate increases from 3 to 15 kHz. ^{13}C MAS NMR parameters of other paramagnetic metallocenes Cp_2V, Cp_2Co, and Cp_2Ni can be found in the work,[187] where the ^{13}C isotropic chemical shifts change from −398 to +1594 ppm, as a function of the metal center, and chemical shift anisotropy varies between 828 and 2640 ppm.

It should be emphasized that, because of fast proton relaxation, the cross-polarization ^{13}C NMR experiments performed in the above metallocenes were not efficient, and the lines observed were remarkably broadened.[186] In contrast, as expected, paramagnetic lanthanide complexes have shown the relatively sharp ^{13}C resonances (due to fast electron relaxation), which have been accompanied by very wide sideband patterns.[188,189] Some line broadening was explained in terms of the BMS effects.[185] Brough and coauthors[189] have emphasized that the ^{13}C MAS NMR spectra and ^{13}C chemical shifts in crystalline lanthanide acetates can be quantitatively analyzed or even predicted by considering the interactions between the nuclei and the single nearest paramagnetic ion.

Because the ^{2}H NMR powder line shapes are very sensitive to local structure and/or molecular dynamics, ^{2}H NMR is often applied for studies of static diamagnetic solids. Here ^{2}H spectra, dominated by quadrupole interactions, are generally recorded with the ordinary quadrupole-echo pulse sequence.[44] These experiments, however, are focused on only the dephasing of the quadrupole interactions, and their applications for paramagnetic solids are not effective because of distortions in the line shapes, caused by large paramagnetic shifts and their anisotropies. To avoid such spectral distortions, Siminovitch and co-workers[190] have suggested the so-called shift-compensated quadrupole echo. This method works particularly effectively when electron relaxation times are relatively short. For long electron relaxation times,

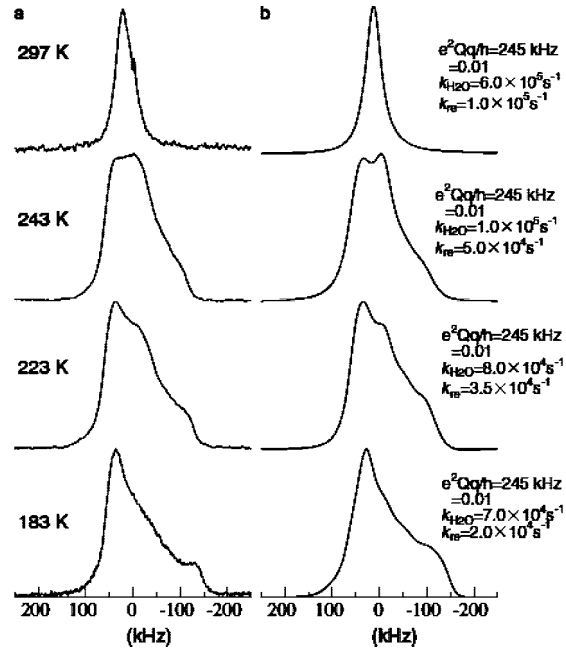

Figure 9. Temperature dependences of the ^{2}H NMR spectra of complex $[Mn(H_2O)_6][SiF_6]$ observed experimentally (a) and calculated (b) with the corresponding parameters. Reprinted with permission from ref 191. Copyright 2005 Elsevier B.V.

observed, for example, for ions Mn^{2+} in the crystal complex $[Mn(^2H_2O)_6][SiF_6]$ (or ions Gd^{3+}), Mizuno et al.[191] have performed the NMR experiments, based on the exorcycled quadrupole-echo sequence (EQES). The authors have shown that these EQES experiments and the spectral simulations in the frameworks of the developed theory can be very powerful for analysis of dynamics in strong paramagnetic molecular systems. The effectiveness of this approach is illustrated in Figure 9, where the agreements between experimental and calculated ^{2}H NMR spectra are reached assuming 180° flips of water molecules in a combination with the site jumps of the $[Mn(H_2O)_6][SiF_6]$ complex around the C_3 axis.

The quadrupolar moments of ^{7}Li and ^{6}Li nuclei are small, their natural abundance is high, and therefore they are often applied as targets for characterizations of zeolites. These nuclei show sharp lines in MAS NMR spectra, and their signal intensities correlate with crystallographic site populations in low-silica zeolite phases.[192] The magnetic properties of ^{7}Li nuclei are also useful in the context of probing paramagnetic systems. For example, the resonances in ^{7}Li MAS NMR spectra, belonging to extraframework lithium cations,[193,194] are very sensitive to the presence of paramagnetic gas species in samples: the NMR signals of the nuclei, located closely to paramagnetic centers, undergo broadenings and show shorter relaxation times and remarkable paramagnetic shifts. The ^{7}Li MAS NMR spectra of the zeolite Al-ZSM-5 (Figure 10) illustrate the influence of oxygen.[194] It is clear that such effects can be used to characterize accessibility of lithium cations in high-silica zeolites, where the Li cations, interacting with oxygen molecules, exhibit paramagnetic shifts that are more pronounced at low temperatures. In turn, the paramagnetic shifts clarify the Li coordination environments. The recent Chazel's ^{6}Li, ^{7}Li static and MAS NMR experiments[195] performed for systems (LiNiO) with different component ratios have resulted in data that are important for materials chemists. It has been shown that Fermi-contact and dipolar interactions with the electron

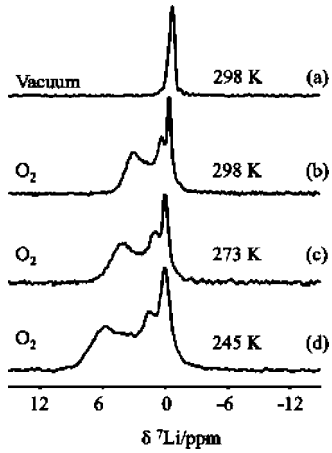

Figure 10. ^{7}Li MAS NMR spectra for zeolite Al-ZSM-5: (a) oxygen-free dehydrated sample (300 K), (b) spectra of the oxygen-containing sample at 300 K, (c) at 273 K, and (d) at 245 K. Reprinted with permission from ref 194. Copyright 2004 American Chemical Society.

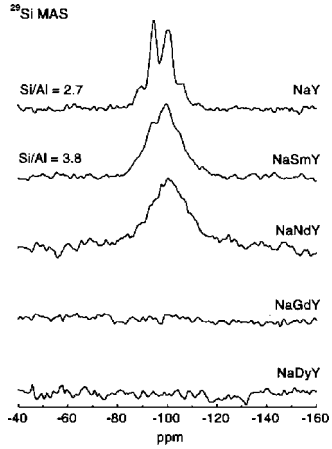

Figure 11. ^{29}Si MAS NMR spectra of zeolites, marked as Na−Y, NaSmY, NaNdY, NaGdY, and NaDyY, prepared by exchange with the corresponding lanthanide ions at similar concentrations. Reprinted with permission from ref 79. Copyright 2000 Elsevier B. V.

spins on the Ni centers can cause isotropic Li chemical shifts more than +700 ppm.[195] The ^{6}Li, ^{7}Li resonances with the strongly asymmetric shapes due to anisotropy have been observed in the static experiments.

The well-established ^{29}Si, ^{27}Al MAS NMR structural criteria, discriminating different Si and Al sites in diamagnetic zeolites, are described in the Duer's book.[44] However many zeolite relatives have been prepared as solids exchanged with paramagnetic lanthanide cations. These systems are often catalytically active, and therefore, paramagnetic effects for resonances of ^{29}Si, ^{27}Al nuclei require detailed studies. Unfortunately, the zeolites, exchanged with cations Nd^{3+}, Sm^{3+}, Gd^{3+}, and Dy^{3+}, show the ^{29}Si, ^{27}Al MAS NMR spectra, which are poorly informative in the structural context and dependent on the nature cations.[79] Figure 11 illustrates this influence, where the ^{29}Si resonances broaden in going from the diamagnetic zeolite to Sm- and Nd-systems and completely disappear for ions of Gd and Dy. Similar effects are reported for ^{27}Al MAS NMR. The ^{29}Si MAS NMR studies of the fully exchanged rare-earth zeolites, containing ions Ce^{3+}, Pr^{3+}, Nd^{3+}, Sm^{3+}, and Eu^{3+},[196] were more successful: isotropic high-field chemical shifts (up to −146 ppm) of the Fermi-contact nature have been measured for the Nd-zeolite, whereas a small low-field shift of +6 ppm has been obtained in the Eu zeolite. Recently, Stebbinds and co-workers[197] have measured the ^{29}Si shifts in complex ($[Mg,Fe]_3Al_2Si_3O_{12}$), containing 3.5 wt % of FeO. They have suggested that these resonances, shifted by 25 to 200 ppm from "normal" ranges, correspond to pseudocontact interaction with the unpaired electron spin.

5.2. Special NMR Techniques for Observations of "Invisible" Target Nuclei

One of the important consequences from the theory is the fact that nuclei, located in closest environments of unpaired electrons, are difficult for direct observation in the conventional NMR spectra due to strong paramagnetic effects. This situation is typical of the $CoAPO_4$-*n* molecular sieves,[198] where ^{31}P NMR spectra of static samples show low-intense broadened lines and demonstrate the strong intensity loss even at relatively low cobalt contents. The ^{31}P MAS NMR spectra of such systems exhibit the wide sideband patterns due to strong dipolar interactions, which, however, are not sufficient to make a conclusion about the nature of the frameworks of the materials.[93] Canesson and Tuel[198] have emphasized that the presence of the sidebands in the MAS spectra can be *incorrectly* used as proof for incorporation of paramagnetic ions into the matrix of materials.

The groups of Tuel[93,198,199] and Mali[184] have suggested and applied a spin−echo mapping technique, involving the Hahn-echo ^{31}P static NMR spectra recorded at different carrier frequencies to observe finally the NMR lines within broad spectral regions. Figure 12 shows a schematic of the experiment, where a whole echo is acquired. The resonance lines are expected to be very broad, and echo delays applied should obviously be short. Technically, this condition can be easily realized in the static NMR experiments, while any MAS NMR experiments, being synchronized with spinning rates, automatically increase the echo delays.

It has been demonstrated that this Hahn-echo technique leads to observation of ^{31}P resonances of nuclei in the closest environments of paramagnetic ions Co^{3+} in the $CoAPO_4$-*n* molecular systems. The resonances can be observed even in the case of high Co contents, and the detected lines are exclusively broad and cover a range between about −500 and 10 000 ppm.[93] In addition, the authors have shown that ^{31}P T_2 times decrease when changing the ^{31}P chemical shifts from a few ms around 0 ppm to 30−40 μs around 8 000 ppm. Moreover, a fast T_2 time decrease has been noted between 0 and 1500 ppm, whereas a slow decrease was observed for higher shift values.[93] Thus, the presence of ^{31}P resonances with $\delta > 500$ ppm can be considered as direct proof for Co incorporations into the framework of the materials.

Interesting features in ^{7}Li static spin−echo NMR experiments performed for the LiNiO materials have been reported

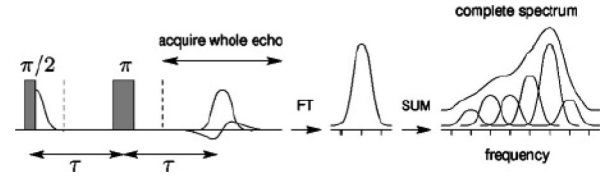

Figure 12. Schematic representation of the spin−echo mapping experiment used for recording broad ^{31}P NMR spectra. Vertical dashed lines show dead time after radio frequency pulse. Reprinted with permission from ref 184. Copyright 2005 American Chemical Society.

by Chazel and co-workers.[195] The authors have observed "a hole" appearing exactly at the carrier frequency. The phenomenon has been explained in terms of a saturation resulting from the longer second pulse in the echo pulse sequence. It has been established that this undesirable effect can be reduced by decreasing the pulse lengths. In addition, shorter pulses improve the detection of broader signals.

Wilke and coworkers[200] have suggested another technique based on the so-called stochastic pulse sequences combined with high magic-angle spinning rates to observe the broad and largely shifted resonances. They have used low power, approximately 1° pulses acting stochastically 0° and 180° out of phase relative to one another, and measured the shift of ^{31}P nuclei in paramagnetic solid $LiNiPO_4$ equal to 1726 ppm.

5.3. Relaxation Measurements in Paramagnetic Solids

The nuclear spins, excited by a radio frequency irradiation, reach an initial equilibrium state by two relaxation mechanisms that differ in their operating principle: spin−lattice and spin−spin relaxation,[114] where the behavior of macroscopic magnetization measured experimentally is given by the Bloch's equations:

$$dM_Z/dt = -(M_Z - M_Z^0)/T_1$$
$$dM_{X,Y}/dt = -M_{X,Y}/T_2 \quad (9)$$

The time constants T_1, T_2 can be obtained by the well-known methods: the inversion-recovery, saturation-recovery, or progressive saturation experiments (to measure T_1), where radio frequency pulses can be simple or composite; the Hahn-echo or Carr-Purcell pulse sequences (measuring T_2); and the spin-locking experiments in a rotating coordinate system (to measure $T_{1\rho}$).[201]

Equation 9 describes evidently exponential relaxation processes that are typical of isolated (or weakly coupled) spins in isotropic liquids with a single correlation time of molecular reorientations. However, even in diamagnetic solids, numerous structurally nonequivalent sites can have different motions and will show different nuclear relaxation. Similarly, in paramagnetic materials, where each site has its own relaxation via dipolar interaction with unpaired electrons (see eqs 5 and 6), the relaxation curves do not follow the exponential law, generally leading to a multiexponential process. In a common case, the relaxation behavior, dependent on the nature of target nuclei, their coupling, and also structural features of objects, can be determined, in practice, by fittings of magnetization decays to the corresponding functions. Even conditions of NMR experiments can affect the observed relaxation process. For example, Zhou and coworkers[202] have observed the ^{13}C T_1 NMR relaxation in organic solids as a triple-exponential process at ^{1}H radio frequency irradiation of a medium power. At the same time, under stronger ^{1}H field irradiation or in its absence, the process can be reduced to a simple exponential function.

When target nuclei in solids can be characterized by only two distinct environments (or only two distinct motions), then the relaxation process can become biexponential. This case has been well documented in the careful ^{1}H, ^{19}F T_1 relaxation study of solid hexafluoroacetylacetone,[203] where the intramolecular ^{19}F−^{1}H dipolar interactions dominated and the biexponential T_1 relaxation showed two physically distinguishable CF_3 rotors with different energy activations. The presence of both crystalline and amorphous regions within the bulk of silica gel systems[204] was probably responsible for the biexponential NMR decays collected by the ^{29}Si T_1 NMR experiments.

As noted above, nuclear relaxation can be monoexponential even in solids, when it is dominated by spin-diffusion. In such a case, a single T_1 value characterizes all of the nuclei, situated within the barrier radius effective for spin-diffusion to paramagnetic centers.[205,206] However, Roberts and co-workers[205] have emphasized that, commonly, nuclear relaxation in materials follows a stretched exponential, $\exp(-(\tau/T_1)^\beta)$, where the β-parameter, measured experimentally, can vary between 0 and 1 from a highly nonexponential relaxation to a monoexponential relaxation behavior.

A stretched exponential with the β-value of 0.5 corresponds to nuclear spin−lattice relaxation occurring via paramagnetic centers without spin-diffusion,[176] while intermediate values between 0.5 and 1.0 can be attributed to a "diffusion-limited" mechanism of relaxation via random paramagnetic impurities.[207] On the other hand, it seems to be reasonable that a stretched exponential function can approximate a superposition of monoexponential decays in the presence of smooth relaxation-time distributions. For example, a Gaussian T_1 distribution will correspond to the β-parameter of 0.67.

Thus, relaxation measurements and their interpretations for paramagnetic materials are not simple for the following reasons. First, the β-parameter should be determined reliably on the basis of a large number of delay times in the relaxation experiments, performed with the carefully adjusted radio frequency pulses.[201] As has been shown in practice, incorrect pulse adjustments in experiments with silica-based materials, doped with the paramagnetic metal ions, can lead to changes in the ^{29}Si T_1 times and the β-parameters by >30%.[208] Second, even at the well-determined β-parameters, discrimination in the different relaxation mechanisms is still problematic. For example, an exponential relaxation, which could be an evidence for dominating the spin-diffusion mechanism, is often observed for ^{29}Si nuclei (as will be shown below) that are coupled weakly, and therefore, probability of their mutual spin flops is very low. In contrast, a stretched-exponential relaxation with $\beta > 0.5$ can be caused by the dipolar mechanism or the so-called diffusion-limited mechanism. Third, if T_1 or T_2 values are reliably determined and the spin-diffusion mechanism completely dominates, these relaxation times characterize NMR properties of solids but not their chemical structure. Fourth, when the dipolar mechanism dominates, eqs 5 and 6 describe the relaxation rates due to one of the nucleus−electron dipolar contacts. Commonly, however, in the absence of independent data, the number of these contacts remains unknown. Finally, spin diffusion and dipole−dipole relaxation differently depend on concentrations of paramagnetic centers. Therefore, their relative contributions to $T_{1,2}$ times measured experimentally can change at variations in concentrations of paramagnetic ions. In other words, experimentalists need criteria discriminating the relaxation mechanisms.

Kessemeier and Norberg[209] have carefully investigated static and spinning samples containing paramagnetic centers and shown that the spin-diffusion coefficient $D(\omega_R)$ decreases in spinning samples, and thus, the T_1^{SD} times in eq 10 depend on MAS rates ω_R.

$$1/T_1^{SD} = (1/3)8\pi N_p C^{1/4} D^{3/4}(\omega_R) \quad (10)$$

In turn, the T_2^{SD} times increase in spinning samples as

$$T_2^{SD} = (4/3)(\omega_R)^2\tau^2/\Delta\nu^2\tau \quad (11a)$$

$$\text{or } T_2^{SD} = (4/3)(\omega_R)\psi/\Delta\nu^2 \quad (11b)$$

It should be noted that these expressions are valid at $\nu_R/\Delta\nu \geq 1$, where spinning rates ν_R and line widths $\Delta\nu$ are measured in Hz.

Because the dipolar spin−lattice relaxation times T_1^{DD} are independent of magic-angle spinning, the variable spinning rate experiments performed in solids can potentially recognize the relaxation mechanisms. Gil and Alberti[210] have reported on remarkable spinning effects on ^{1}H T_1 values measured in solid organic compounds, for example, in adamantane and glycine. The data have been interpreted in terms of decreasing the spin diffusion efficiency at faster rotations. Similarly, reducing the ^{1}H spin diffusion by 65% has been found for the high-density polyethylene, when the MAS rate has been increased from 2 to 12 kHz.[211] In addition, the authors have predicted a decrease in the effective spin diffusivity by >90% at spinning rates of 30 kHz and more. Hayashi[212] has measured the room-temperature ^{1}H and ^{29}Si T_1 times in talk where paramagnetic impurities work as relaxation centers. Since spin-diffusion plays an important role in ^{1}H relaxation, the ^{1}H T_1 times remarkably increase in spinning samples (Figure 13). In contrast, the ^{29}Si T_1 times did not change practically in going from static to spinning samples (46 and 47 s, respectively), showing that spin-diffusion is negligible and relaxation occurs via direct ^{29}Si−^{29}Si dipolar interactions.

Interpretation of spinning effects on T_2 measurements in solids is more complex especially for systems with relatively high molecular mobility.[210] In fact, even in the absence of spin diffusion, the dipolar spin−spin relaxation can depend on spinning rates ω_R:

$$1/T_2^{DD} = (1/5)\gamma^4\hbar 2r^{-6}I(I+1)\{2\tau/(1+\omega_R{}^2\tau^2) + \tau/(1+4\omega_R{}^2\tau^2)\} \quad (12)$$

According to Haeberlen and Waugh,[213] the dipolar T_2^{DD} time becomes spinning-dependent, if $\omega_R{}^2\tau^2 > 1$. This condition is valid at the relatively long correlation time, τ, calculated via eq 12 as $>2 \times 10^{-5}$ s at a spinning rate of 10 kHz. Then, like in the case of the spin-diffusion T_2^{SD} times in eq 11a, the dipolar T_2^{DD} time will be proportional to $\omega_R{}^2$.

5.3.1. Solid-State T_1 Measurements

Spin−lattice relaxation time measurements by the inversion-recovery, saturation-recovery, or progressive saturation methods are experimentally simple even for paramagnetic amorphous materials, where T_1 times are relatively short. They require only accurate pulse calibrations particularly in the case of a nonexponential relaxation behavior. Because generally nonlinear regression fittings to stretched exponentials, dependent on the β-parameter, are more complicated than those to an exponential function, the relaxation data would be collected at high enough signal-to-noise ratios and treated statistically. Roberts and co-workers have investigated silica gels with the surface covered by copper ions and demonstrated that the β-values, obtained in triplicate measurements with >20% errors, are statistically unreliable and should be ruled out. Only the β-values, obtained with smaller errors (Figure 14), can be truly analyzed in terms of relaxation mechanism and distributions of paramagnetic centers.[205] It is obvious that the T_1 times, resulting from treatments of relaxation data with stretched exponentials, should be also statistically reliable.

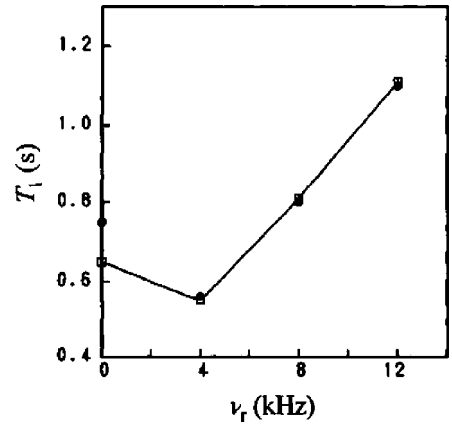

Figure 13. Spinning-rate dependence of the ^{1}H T_1 time in talk, measured at room temperature. Reprinted with permission from ref 212. Copyright 1994 Elsevier Inc.

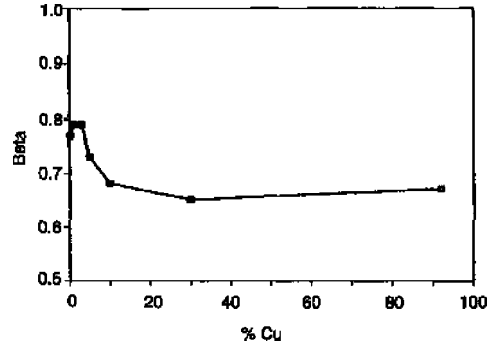

Figure 14. β-parameters, obtained by triplicate measurements with <20% errors in the ^{29}Si T_1 relaxation studies of silica gels with the surface covered by copper ions at their different concentrations. Reprinted with permission from ref 205. Copyright 1997 Elsevier Inc.

5.3.2. Spin−Spin Relaxation Times and Anomalies in Solid-State T_2 Measurements

In general, the spin−spin relaxation times T_2 of different nuclei in solids are strongly shorter than the T_1 times and their accurate determinations are more difficult. In spite of this problem, the T_2 times are often applied for structural studies or probing dynamics in diamagnetic and paramagnetic systems. Oldfield and co-workers[214] have demonstrated how ^{27}Al T_2 times can be applied for characterizations of the complex commercial zeolite catalysts. The authors have reported on the ^{27}Al T_2 times of 1.1−4.6 ms in diamagnetic zeolites and amorphous silica−aluminas extracted from practically exponential NMR decays and demonstrated their dependence on hydration of the samples. ^{1}H T_2 NMR decays also have been exponential in silicate fiberglass supports and resulted in the ^{1}H T_2 times of 0.2−6.8 ms characterizing the surface silanol groups.[215]

More complex ^{1}H NMR decays, showing several relaxation components in the Hahn-echo and CPMG experiments, have been observed in diamagnetic elastic polymers by Hayashi and Komori.[216] The authors have improved the

formula expressing a proton transverse magnetization decay together with distributed residual dipolar couplings, and they have shown that T_2 times extracted from spin−lattice relaxation experiments in the rotating frame can be successfully used for characterization of the cross-link density in these systems. A biexponential ^{31}P T_2 relaxation has been observed for the NMR-detectable phosphorus nuclei in the materials AlPO-5.[95] This relaxation is very sensitive to incorporation of paramagnetic ions into the matrix of the materials. For example, the material CoAlPO has shown ^{31}P spin−spin relaxation, which consists of slow and fast T_2 components (269 and 0.4 ms, respectively) as characteristics of close and remote cobalt environments. Finally, the effects of anisotropic deuterium spin−spin relaxation on line shapes in ^2H NMR spectra of paramagnetic complex $[Mn(H_2O)_6][SiF_6]$ have been analyzed by Mizuno and co-workers.[191]

Electron relaxation times in eqs 5 and 6 can produce nuclear T_2 times that are too short, and their accurate determination can be difficult in practice. Potentially, such a situation can be expected for materials doped with ions Mn^{2+}, Ni^{2+}, or Cu^{2+}. Therefore, the Hahn-echo ^{29}Si T_2 experiments in supermicroporous materials SiO_2−MnO and SiO_2−Al_2O_3−MnO have recently been performed with τ echo delays, varying from very short magnitudes of 10 μs.[217] These methodically important experiments have been carried out in static samples because the Hahn-echo MAS NMR requires synchronization with spinning rates,[44] limiting, thus, applications of shortest delays. Figure 15 shows that already at τ of 2 ms the ^{29}Si line intensity is going to zero.

According to the principles of signal registration in solid-state NMR,[44] shortest echo delays and an instrumental dead time can distort the collected FIDs. Because the effect is difficult to predict theoretically and real instrumental dead time is generally unknown, the distorted FIDs, in practice, will complicate T_2 determinations. The patterns "intensity-τ" for materials SiO_2−MnO and SiO_2−Al_2O_3−MnO, doped with different Mn concentrations, are shown in Figure 16, where the echo-intensity initially increases with increasing τ values and then it "normally" reduces because of spin−spin relaxation. These normal τ zones can be well fitted to an exponential function, $I(\tau) = I_0 \exp(-\tau/T_2)$ (dashed lines in Figure 16), to give the ^{29}Si T_2 times between 1.7 and 0.2 ms for the diamagnetic system SiO_2−Al_2O_3 and the material SiO_2−MnO with 13 wt % of Mn, for example.

Menetrier and co-workers[195] have shown that echo-intensities in paramagnetic solids can be decreased due to saturation at a carrier frequency, which can be minimized by reducing pulse lengths. However, the character of the curves (for example, in Figure 16) has been practically independent of pulse lengths, and thus, the abnormal points can be definitely connected with the instrumental dead time comparable with the shortest τ magnitudes. Thus, the "abnormal" zones can reflect recovery of the receiver.

The author[217] has formally described the behavior of the echo-intensity assuming that the current intensity can be represented as magnitude, relaxing exponentially, but reduced by intensity loss, which, in turn, also decreases exponentially with time constant T^R:

$$I(\tau) = I_0[a \exp(-\tau/T_2) - (1 - a) \exp(-\tau/T^R)] \quad (13)$$

The solid lines in Figure 16 correspond to this *formal* description, where at $\tau = 0$ the intensity loss is very large.

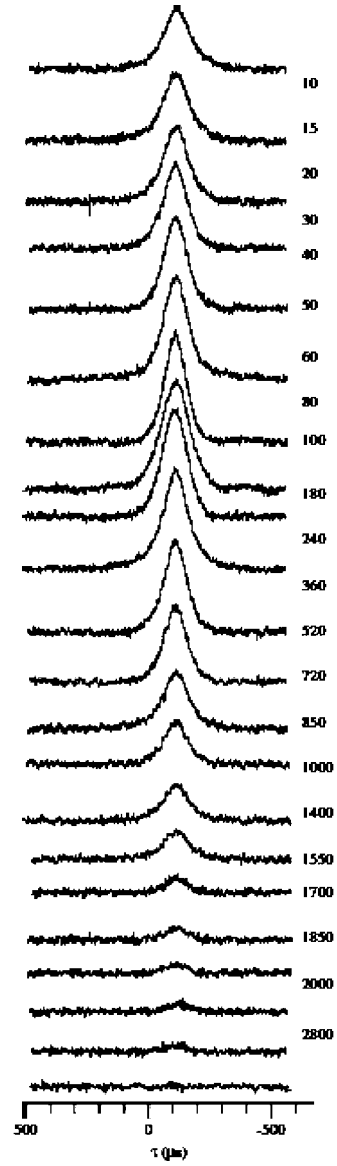

Figure 15. ^{29}Si Hahn-echo NMR spectra (chemical shifts in ppm) recorded for a static material SiO_2−MnO (15 wt % of Mn) at echo delays from 10 (top) to 2800 (bottom) μs. Reprinted with permission from ref 217. Copyright 2009 Elsevier Inc.

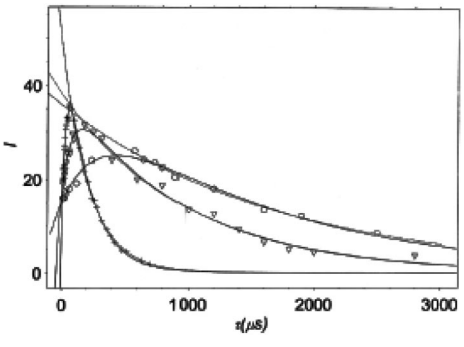

Figure 16. ^{29}Si Hahn-echo curves in coordinates "intensity (au)−echo delay (μs)"obtained in materials SiO_2−MnO with 0 (o), 2 (▽), and 12 (+) wt % of manganese. Reprinted with permission from ref 217. Copyright 2009 Elsevier Inc.

It has been emphasized that the dashed and solid lines are very similar in the normal τ zones, and thus, if the first abnormal points are ruled out, the calculated ^{29}Si T_2 times change insignificantly. The latter is very important because the MAS experiments synchronized with spinning rates will

be performed in these τ zones. Finally, the T^R constants, obtained as fitting parameters, correlated well with the T^*_2 values measured experimentally from the line widths at half-height as $T^*_2 = 1/\Delta\nu$.[217]

Some solids, containing ^{29}Si nuclei at their natural abundance, also show an unusual behavior in ^{29}Si T_2 experiments.[218,219] However, here, the anomalies are connected with the appearance of long-lived spin-echoes detected as long magnetization tails. Franzoni and Levstein[219] have explained the nature of this phenomenon in the limits of two conditions: inhomogeneity of the applied radio frequency field and the absence of spin diffusion, when flip−flop interactions are not effective.

In summary, it should be noted again that high concentrations of paramagnetic centers generally complicate NMR studies of solids and prevent applications of various advanced techniques developed for diamagnetic systems. Even the CP NMR experiments providing great advantage in observations of nuclei at their small natural abundance are not effective due to "negative" paramagnetic effects. Finally, the NMR technique based on dynamic nuclear polarization leading to sensitivity enhancement cannot be applied for paramagnetic materials according to the dynamic nuclear polarization (DNP) principles, which can be found in the review of Wind et al.[220]

6. Strategy in NMR Studies of Amorphous Porous Paramagnetic Materials

The previous sections have shown how unpaired electrons affect chemical shifts of target nuclei, their line shapes in static and spinning regimes, and also spin−lattice and spin−spin relaxation times. This section reviews the available literature focused on distributions of paramagnetic ions through the volume of a material and on incorporation of the ions into the matrix of the material based on (i) interpretation of sideband patterns, observed in MAS NMR of paramagnetic solids; (ii) direct spectral NMR observation of atoms, binding to paramagnetic ions; and (iii) relaxation times, dependent on concentrations of paramagnetic ions and relaxation models providing reliable structural conclusions.

6.1. Analyzing the Intense Sideband Patterns in MAS NMR Spectra of Paramagnetic Amorphous Materials

When the supermicroporous silica-based materials[221] or the aluminophosphates[198] are doped with paramagnetic metal ions (Mn^{2+} or Co^{2+}), then their single-pulse ^{27}Al, ^{29}Si, or ^{31}P MAS NMR spectra exhibit broadened resonances, accompanied by numerous intense sidebands similarly to those shown in Figure 8. This is in full contrast to the well-resolved MAS NMR spectra of diamagnetic materials that do not exhibit sidebands (for example, Figure 6). Such intense sidebands in the ^{31}P MAS NMR spectra of cobalt−aluminophosphates have initially been considered as a proof for incorporations of cobalt atoms into the framework of the materials. However, later Tuel and co-workers[198,199] have observed similar spectral behavior in the Co-*impregnated* aluminophosphates and concluded that the phenomenon cannot generally make the discrimination between the framework and nonframework cobalt atoms. Moreover, the intense sidebands can appear in ^{29}Si MAS NMR spectra of silica-based materials even at their mechanical mixing with paramagnetic Mn or Ni salts due to large BMS effects (as will be shown below). Intuitively, it is clear that, in the absence of quantitative analysis of the observed effects, reliable structural conclusions are impossible.

NMR sideband patterns can be quantitatively analyzed, for example, in solid complexes containing paramagnetic lanthanide ions, which do not lead to remarkable line broadenings due to relatively short electron relaxation times. Recently, it has been demonstrated that local geometry of the lanthanide ions in a series of oxo-tungstates can be accurately solved by analysis of anisotropic electron−nuclear dipolar interactions that completely dominate in the observed ^{31}P MAS NMR spectra.[225] The anisotropy of these interactions for ^{31}P nuclei is determined directly from NMR spectra and calculated theoretically on the basis of a point−dipole approximation. In this model, the electron−nuclear dipolar coupling tensor is expressed in a matrix representation: $\mathbf{D}_{en} = r^{-3}(\delta_{\alpha\beta} - 3e_\alpha e_\beta)$ where r is the electron−nuclear distance, $\delta_{\alpha\beta}$ is the Kronecker delta function, and e_α and e_β are the (x, y, z) components of the electron−nuclear dipolar vector. The calculations of the anisotropy have been carried out in account for the paramagnetic centers located within 100 Å relative to phosphorus atoms to provide good agreement with experimental magnitudes. For objective reasons, the phosphorus−ion distances obtained by NMR have been slightly elongated versus those determined by the X-ray data.

This approach, applicable to nuclei other than ^{31}P and for other noncrystalline inorganic solids, is principally limited by features of lanthanide ions: because of very large magnetic moments of Gd, Dy, and Tb, they complicate observations of ^{31}P resonances due to very short ^{31}P T_2 times.[225] Similarly, Goldfarb[226] has analyzed the intense sideband patterns observed in the ^{27}Al and ^{31}P MAS NMR spectra of the paramagnetic materials $MnAlPO_5$ prepared at different concentrations of manganese, which has been identified as Mn^{2+} by EPR. Again, the anisotropic dipolar electron−nucleus interactions have been calculated and fitted to the experiments. It has been demonstrated that the Mn^{2+} cations occupy framework sites as well as extraframework positions.

One of the main points in applications of the above calculations is *the complete dominance of dipolar electron−nucleus interaction* in the observed sideband patterns. However, in general, validity of this domination is not always obvious and requires independent experimental proofs. More complex behavior of the sidebands has recently been illustrated by the single-pulse ^{27}Al and ^{29}Si MAS NMR spectra of supermicroporous silica-based Si/Al/Mn materials obtained at various Si/Mn ratios.[221] Figure 17 (bottom) shows the single-pulse ^{29}Si MAS NMR spectrum of the calcined Si/Al/Mn porous system, prepared at a Si/Mn ratio of 8. The spectrum shows that distribution of the sideband intensities is virtually symmetrical versus an axial symmetry, expected for Fermi-contact interaction at the Mn−O−Si sites, or a strong asymmetry reported for dipolar interaction in paramagnetic lanthanide materials.[225] The isotropic chemical shifts of ^{27}Al and ^{29}Si nuclei, determined in this Si/Al/Mn system (and its numerous relatives), are very similar to those observed usually for calcined diamagnetic Si/Al materials.[222−224] The shifts correspond to the silica framework with 4-coordinated Al atoms incorporated into the silica matrix in accord with the well-known criteria.[44] Thus, the target ^{27}Al and ^{29}Si nuclei of the silica matrix are remote from the paramagnetic centers, and intensities of the spinning sidebands can be increased by the BMS effects.[173] Abidi and co-workers[227] have also discussed the BMS influence on the solid-state

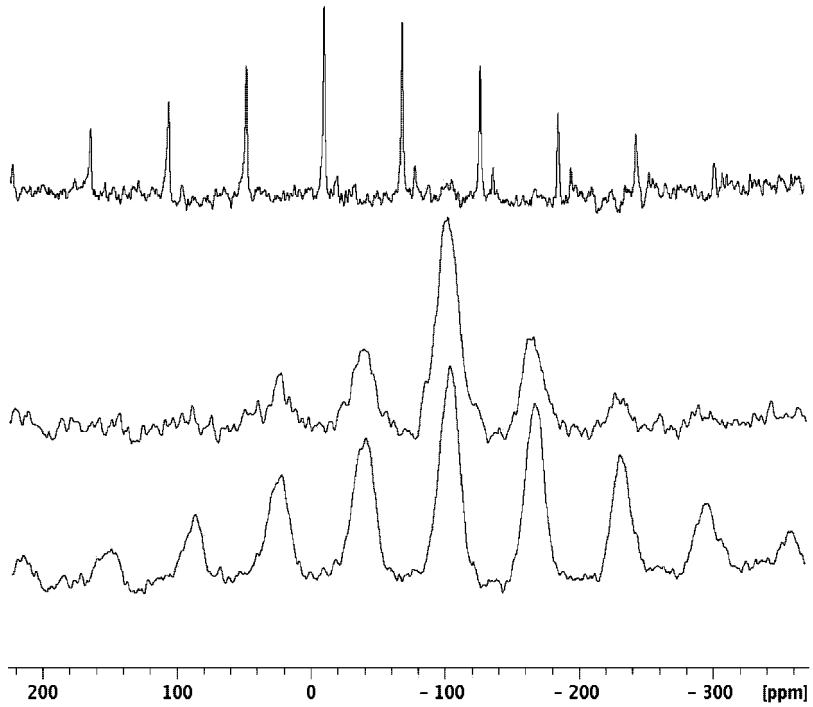

Figure 17. Single-pulse ^{29}Si MAS NMR spectra, recorded at spinning rates of 5 kHz: (top) tetrakis(trimethylsilyl)silane, mixed with 50 wt % of $Mn(CH_3COO)_2 \cdot 4H_2O$, where lines at −10.3 and −135.9 ppm correspond to isotropic chemical shifts; (middle) a diamagnetic Si/Al sample mixed mechanically with 30 wt % of $Mn(CH_3COO)_2 \cdot 4H_2O$; (bottom) a calcined Si/Al/Mn sample prepared at Si/Mn = 8. Reprinted with permission from ref 221. Copyright 2006 John Wiley & Sons.

NMR spectra of silica xerogels doped with low Mn^{2+} concentrations. A direct proof follows from the medium ^{29}Si MAS NMR spectrum in Figure 17: the intense sidebands are observed in a mechanical mixture of the diamagnetic silica-based Si/Al material with $Mn(CH_3COO)_2 \cdot 4H_2O$, where close Fermi-contacts and dipolar contacts ^{29}Si−Mn are excluded, and thus, the BMS is completely responsible for the appearance of sidebands.

According to the model of Kubo et al.,[173] the BMS effect in powder samples is governed by distances between paramagnetic ions and "*centers of crystallites*". In full agreement with this model, the ^{29}Si and ^{27}Al MAS NMR spectra of the mixture, recorded at the same spinning rates and plotted *on frequency scales*, have shown identical distributions of sidebands,[221] in spite of remarkable differences in the γ values of ^{29}Si and ^{27}Al nuclei. Finally, the model agrees with the ^{29}Si MAS NMR spectrum in Figure 17 (top) reported for a 1:1 solid mixture (by weight) of tetrakis(trimethylsilyl)silane and $Mn(CH_3COO)_2 \cdot 4H_2O$, where the ^{29}Si sideband patterns are very similar for two ^{29}Si nuclei, one of which is peripheral. Again, the sideband intensities are distributed identically for ^{29}Si and ^{13}C nuclei of the mixed tetrakis(trimethylsilyl)silane, when the spectra are plotted on frequency scales. It is interesting that the BMS does not change remarkably the ^{29}Si T_1 times that remain in the mixture as long as in the individual tetrakis(trimethylsylil)-silane.

In addition, as noted earlier, the demagnetizing BMS field and its effects on NMR frequencies of target nuclei depend on even shapes of NMR containers and their orientations in the external magnetic field.[173,228] Barbara[174] has demonstrated theoretically that the BMS field is uniform at all the points on the axis of a cylinder container, situated at magic angle with respect to the external magnetic field, but it changes strongly toward walls and ends of the cylinder. For example, in a water-containing cylinder, placed in a magnetic field of a 500 MHz NMR spectrometer, the ^{1}H resonance can be broadened by 1.8 kHz. However, in practice, the sideband BMS effects are generally ignored in structural NMR studies of materials.

Unfortunately, separations of dipolar and BMS contributions to sideband patterns and their calculations are impossible in the absence of the accurately determined coordinates of the corresponding paramagnetic centers. The sideband analysis in paramagnetic systems will therefore usually be difficult and unreliable because of superposition of both contributions. For example, Si/Al/Mn materials, doped with Mn^{2+} ions incorporated into the silica matrix,[78,221] show the ^{29}Si and ^{27}Al sideband patterns in the MAS NMR spectra, plotted *on frequency scales*, which depend on the nature of the nuclei. The widths of the sideband patterns and the sideband intensities in Figure 18 reduce significantly with decreasing γ_N magnitudes from ^{27}Al to ^{29}Si, proving the presence of the electron−nucleus dipolar contribution to the spinning sidebands.

6.2. Direct Detecting the Nuclei Closest to Paramagnetic Ions in Porous Materials by the Hahn-Echo Mapping Experiments

Evidencing the incorporation of metal paramagnetic ions into the matrix of porous materials is one of the important steps in their structural studies. The proof can be provided by direct spectral observation of nuclei that are the closest neighbors of paramagnetic centers. It is obvious that target nuclei with a low natural abundance, for example,^{13}C or ^{29}Si, and paramagnetic ions Mn^{2+} or Ni^{2+}, having relatively long electron relaxation times in contrast to paramagnetic lanthanide ions,[229] represent a most difficult case, especially at high contents of paramagnetic centers.

The supermicroporous silica-based materials, synthesized and studied by Clearfield, Shpeizer, and co-workers,[78] have

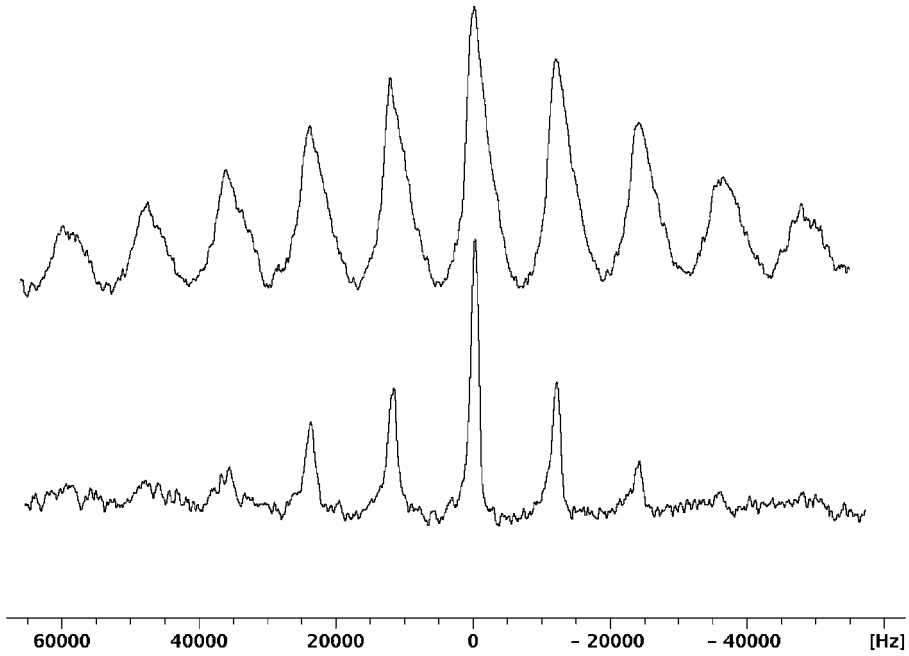

Figure 18. Single-pulse ^{27}Al (top) and ^{29}Si (bottom) MAS NMR spectra, recorded for a calcined Si/Al/Mn material (wt % of Mn ≈ 4) at a spinning rate of 12 kHz. The spectra are depicted on the frequency scale where the lines, corresponding to isotropic ^{27}Al and ^{29}Si chemical shifts, are taken as 0 Hz. Reprinted with permission from ref 221. Copyright 2006 John Wiley & Sons.

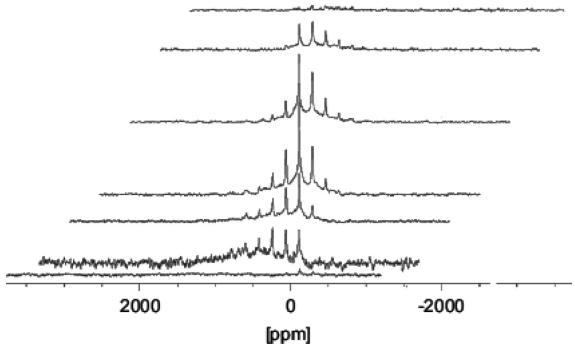

Figure 19. ^{29}Si Hahn-echo MAS NMR spectra of silica-based material $SiO_2-Al_2O_3-MnO$ (Si/Mn = 3.5, Si/Al = 21) spinning at 14 kHz, recorded with the echo-delay corresponding to a single rotational cycle at a carrier frequency centered at (from top to bottom): −1200, −800, −400, 0, 400, 800 (scaled by a factor of 4), and 1200 ppm from TMS. Reprinted with permission from ref 208. Copyright 2008 Elsevier Inc.

shown single-pulse ^{29}Si MAS NMR spectra similar to those in Figure 18, where intense ^{29}Si sideband patterns are caused by combinations of the BMS and dipolar effects. The spin-echo mapping technique, generally applied for static samples,[93,184,198,199] has resulted in the Hahn-echo NMR spectra exhibiting the very broadened and practically symmetric ^{29}Si resonances with line widths reaching up to 40 kHz.[208] The static resonances have transformed to combinations of broad lines and isotropic resonances with $\delta \approx -110$ ppm, accompanied by intense sideband patterns in the ^{29}Si Hahn-echo MAS NMR spectra, recorded at various carrier frequencies. One of the experiments is illustrated for the system $SiO_2-Al_2O_3-MnO$ (Si/Mn = 3.5, Si/Al = 21) in Figure 19. The spectral assignment is obvious: the sideband pattern, typical of paramagnetic systems,[226,228] can be attributed to ^{29}Si nuclei situated in the silica matrix and remote from the manganese, while the wide line belongs to the nuclei located in closest environments of paramagnetic centers.[230,231] A number of interesting and useful factors for performances of such experiments has been emphasized.[231] First, there is an insignificant temperature dependence of the spectra collected, where sideband intensities slightly increase from 50 to −70 °C due to electron relaxation. Second, the broad resonance is observed much better at a carrier frequency, shifted by 600−800 ppm from tetramethylsilane (TMS) as is shown in Figure 20. Here, the wide component looks asymmetric and stretches from +1400 (taken as δ_{11}) to −400 ppm (δ_{33}) and shows a maximum at ∼100 ppm (δ_{22}), roughly corresponding to an isotropic chemical shift of 300 ppm. This value is not large relatively to magnitudes observed for nuclei ^{31}P and ^{13}C in paramagnetic systems, containing Mn, Co, Fe, and Ni,[184,188,198] but it is remarkably larger than paramagnetic shifts of ^{29}Si nuclei, measured in zeolites, containing paramagnetic lanthanide ions.[196] Third, the broad resonance can be completely "filtered" by increasing the echo-delays in the ^{29}Si Hahn-echo MAS NMR spectra (Figure 21). Because the Hahn-echo MAS experiments, synchronized with spinning rates, are phase-sensitive,[44] the above factors confirm a nonartifact nature of the wide resonances.

Similarly to the spin−echo ^{27}Al MAS NMR and static ^{27}Al NMR experiments performed by Schmitt and co-workers[232] at probing the framework/extraframework ^{27}Al sites in zeolite catalysts, the above filtration of wide lines by the ^{29}Si Hahn-echo MAS experiments was very effective even at small spinning rates as shown in Figure 21. As a result, the sideband patterns are ready to be analyzed quantitatively in terms of section 6.1.

The single-pulse ^{27}Al MAS NMR spectra of the numerous porous silica-based Al-containing materials doped with high concentrations of ions Mn^{2+}, Ni^{2+}, or Co^{2+}[230,231] show the framework Al atoms, observed as signals accompanied by intense sidebands with δ(iso) ≈ 50−60 ppm,[44] while the extraframework ^{27}Al signals are unobservable. Generally, these spectra reveal a remarkable intensity loss with respect to diamagnetic Si/Al materials. Again, the Hahn-echo ^{27}Al MAS NMR spectra obtained at different carrier frequencies operating, for example, between 2400 and −2400 ppm have

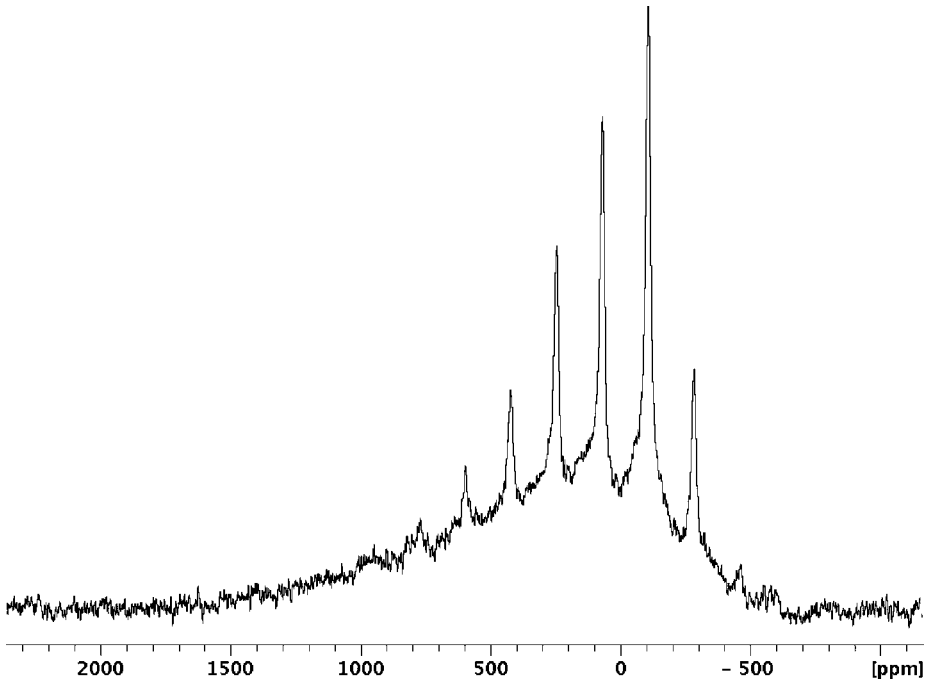

Figure 20. ^{29}Si Hahn-echo MAS NMR spectrum recorded for sample $SiO_2-Al_2O_3-MnO$ (Si/Mn = 2.6) with carrier frequency at 600 ppm, a spinning rate of 14 kHz, a number of accumulations of 500 000, and a total relaxation delay of 0.01 s. Reprinted with permission from ref 231. Copyright 2007 John Wiley & Sons.

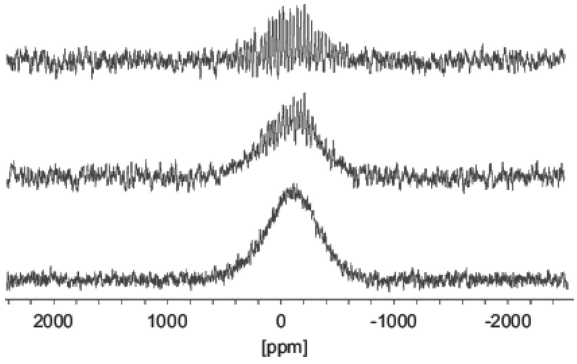

Figure 21. ^{29}Si Hahn-echo MAS NMR spectra of silica-based material $SiO_2-Al_2O_3-MnO$ (Si/Mn = 3.5, Si/Al = 21) recorded at a spinning rate of 2.5 kHz with the echo-delay corresponding to three rotational cycles (top), at a spinning rate of 2.5 kHz with the echo-delay corresponding to one cycle (middle) and in static sample (bottom). Reprinted with permission from ref 208. Copyright 2008 Elsevier Inc.

provided direct observation of the extraframework Al species as extremely wide lines.[231] Thus, the paramagnetic ions are located mainly in pores of materials, and they are chemically binding to Al−O units of the extraframework Al atoms.

Finally, it is pertinent to formulate the obvious limitations in application of the Hahn-echo MAS NMR mapping for characterizations of paramagnetic materials. First, echo signals, corresponding to very broad lines with short T_1 and T_2 times, should be collected properly at the shortest echo delays. Because synchronization with spinning rates, required in the MAS experiments, automatically increases the τ values, there are evident difficulties in quantitative determinations of relative integral intensities corresponding to the broad line and sideband pattern, shown, for example, in Figure 20. Second, detection of wide signals in the mapping Hahn-echo MAS NMR experiments is directly connected with absolute amounts of the nuclei, closely situated relatively to paramagnetic ions: *incorporation of paramagnetic ions into the matrix of the materials is difficult to observe, when the ions can be incorporated only at small concentrations (2−5 wt %) and target nuclei have a low natural abundance (^{13}C or ^{29}Si)*. Therefore, the absence of wide resonances, for example, in the mapping Hahn-echo ^{29}Si MAS NMR spectra of paramagnetic microporous materials $SiO_2-Al_2O_3-NiO$ or $SiO_2-Al_2O_3-CuO$[81] is not valuable in a chemical sense, and investigations of such paramagnetic systems require independent data that can be obtained by FTIR[233] and EPR[234] techniques or by NMR relaxation measurements.

6.3. NMR Relaxation Approaches to Porous Amorphous Paramagnetic Silica-Based Materials: From Experiments to Interpretations

The chemistry of porous materials, prepared by the sol/gel method in the presence of transition or main-group metal ions, shows that, due to high-temperature calcinations, the amount of ions incorporated into the matrix cannot often reach more than 2−5 wt %.[235−237] In addition, organic templates, applied in the sol/gel synthesis, can reduce metal ions under high-temperature calcinations.[238]

The mapping Hahn-echo MAS ^{29}Si NMR experiments, performed for one of these systems, $SiO_2-Al_2O_3-MnO$ (2.5 wt % of Mn^{2+}), are shown in Figure 22, where the sideband patterns belong to ^{29}Si nuclei remote from paramagnetic ions and no evidence indicating the presence of fragments Si−O−Mn is observed in spite of the actual incorporation of these ions into the silica matrix.[78] Because this structural situation is not rare in the chemistry of porous systems, it is necessary to show how the incorporation can be determined by relaxation studies performed for the nuclei observed directly but remote from paramagnetic ions. It should be emphasized that NMR spectra of paramagnetic materials were constantly in focus of investigators while accurate relaxation measurements and their interpretations were relatively limited. However, recently a series of works

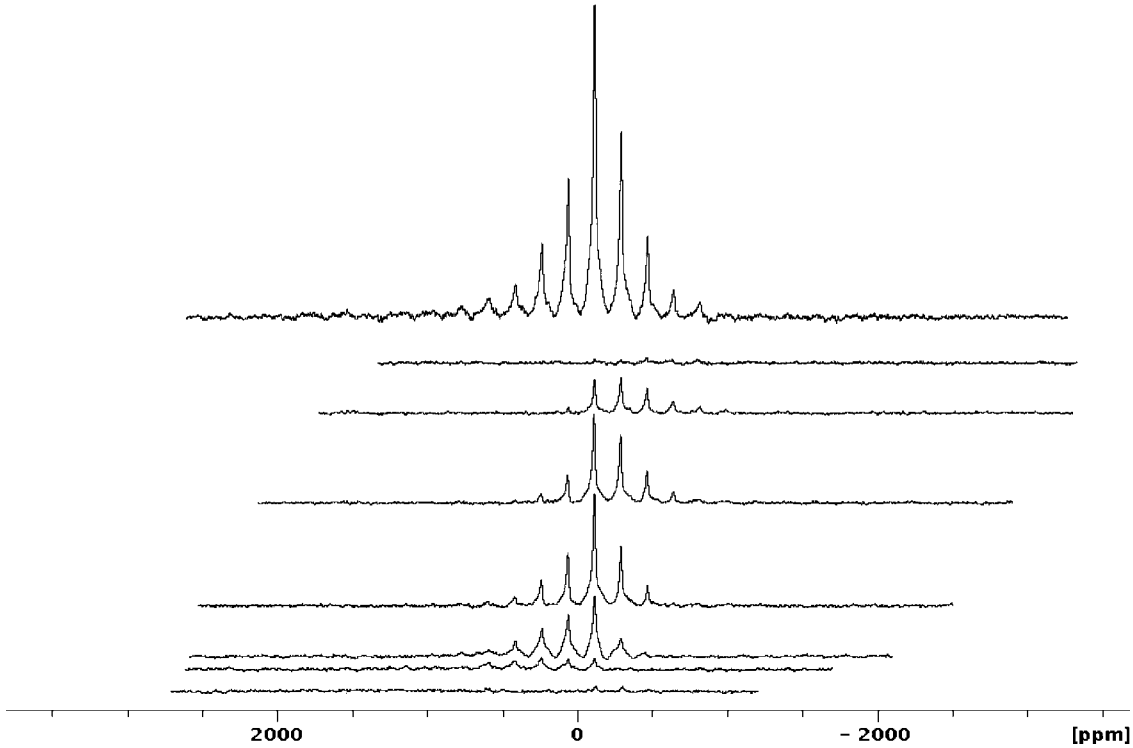

Figure 22. ^{29}Si Hahn-echo MAS NMR spectra of material $SiO_2-Al_2O_3-MnO$ containing 2.5 wt % of Mn^{2+}, recorded at different carrier frequencies similar to those in Figure 19. Reprinted with permission from ref 231. Copyright 2007 John Wiley & Sons.

directed to probing the long-range electron−nucleus interactions in amorphous solids has resulted in formulation of true NMR relaxation criteria based on T_1, T_2 measurements for isotropic resonances and their sidebands that better describe objects under investigation.

6.3.1. Factors Affecting Relaxation Times in Porous Solids

Theoretically, nuclear relaxation in solids is extremely sensitive to the presence of paramagnetic centers and relaxation times depend on concentrations and the nature of paramagnetic ions, as well as on their distributions through the volume of samples and electron relaxation times. In practice, however, some additional relaxation effects can be expected because of the structurally inhomogeneous nature of amorphous solids and their chemical prehistory.

Scholz and Thomas[239] have shown that the ^{29}Si spin−lattice times in silicate glasses are very long, can reach several minutes, and reduce dramatically in the presence of MnO. The authors have noted that the ^{29}Si relaxation rates $1/T_1$ have been proportional to the MnO contents at homogeneous distributions of paramagnetic ions. Sen and Stebbins[240] have revealed the influence of phase separations on the ^{29}Si spin−lattice relaxation observed in silicate glasses and induced by direct dipolar interactions with paramagnetic ions. Relaxation time effects connected with migrations of paramagnetic centers have been demonstrated by McHenry and co-workers.[241]

Influence of chemical prehistory on the ^{29}Si T_1 times has been well illustrated by measurements in the supermicroporous materials $SiO_2Al_2O_3NiO$.[81] It has been found that ^{29}Si T_1 times in the *freshly prepared* materials with 4.8 wt % of the nickel but calcined at 450 and 540 °C are different and measured as 1.0 and 0.64 s, respectively. However, after one month, the T_1 times reduce to the same values (0.24 s) for both systems, and then, after two and three months, the ^{29}Si T_1 values do not change in the 10% limit. The effects have been interpreted by slow migrations of the nickel centers along pores, resulting in their more homogeneous redistributions through the *volumes* of the samples and providing, thus, a larger number of close contacts Ni···Si. Similarly, the porous systems $SiO_2Al_2O_3MnO$ also demonstrate influence of the prehistory: the materials calcined at 130 and 650 °C have shown reducing ^{29}Si T_1 times by a factor of 4.[230] Thus, comparing the relaxation data, available in the literature, can be correct only when accounting for the above effects. It should be added that the prehistory does not affect the ^{29}Si MAS NMR spectra.

6.3.2. Concentrations of Paramagnetic Ions and T_1 Relaxation Times in Porous Silica-Based Materials

Because spin-diffusion and dipolar relaxation depend on a number of paramagnetic centers, consequent variations in their concentrations could be one of the simplest tools in studies of paramagnetic materials. In fact, the formalism of eqs 4 and 14,[242] corresponding to spin diffusion and dipolar relaxation, respectively, describes increasing the relaxation rates ($1/T_1$) proportionally to N_p or N_p^2, where N_p is the number of paramagnetic centers.

$$1/T_1 = (16/9)\pi^3 N_p^2 (2/5)\gamma_I^2 \gamma_S^2 \hbar^2 S(S+1) r^{-6} \tau_e/(1+\omega_I^2 \tau_e^2) \quad (14)$$

As mentioned above, Scholz and Thomas[239] have interpreted increasing the ^{29}Si $1/T_1$ rates in silicate glasses proportionally to [MnO] in terms of homogeneous distributions of ions Mn^{2+}. None were observed in the supermicroporous silica-based materials $SiO_2Al_2O_3NiO$,[81] where ^{29}Si spin−lattice relaxation, dominated by dipolar electron−nucleus interactions, increased practically linearly for the first four points in Figure 23, reached a maximum, and decreased at higher nickel contents. Even in the absence of knowledge

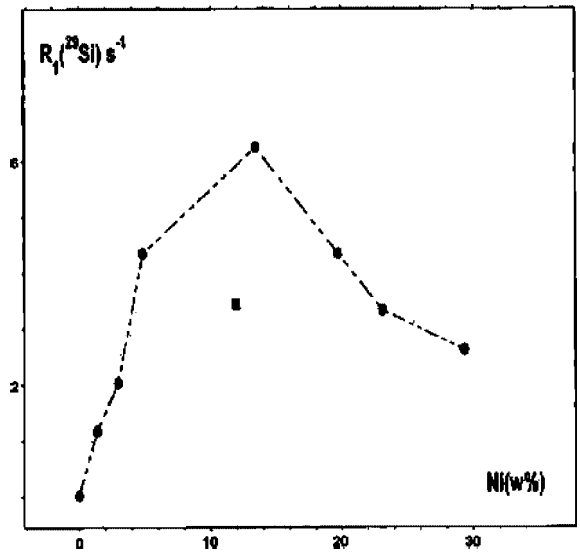

Figure 23. ^{29}Si spin−lattice relaxation rates as a function of the nickel loading in calcined supermicroporous materials $SiO_2Al_2O_3NiO$. Reprinted with permission from ref 81. Copyright 2009 Elsevier B.V.

on relaxation mechanisms, such dependences can be a good criterion for changing the nature of paramagnetic ions. The authors[81] have suggested a partial reduction of Ni^{2+} by template organic molecules to give a nonparamagnetic state, for example, Ni^0. This transformation has been independently confirmed by variable-temperature magnetic susceptibility measurements: the Ni species were identified as NiO and Ni^0 observed at high nickel loadings and aggregated into nanoparticles. The Ni^0 nanoparticles were responsible for the room-temperature ferromagnetic behavior of the materials prepared with high nickel loadings, whereas the low-temperature ferromagnetism observed in the materials with lower nickel loadings was caused by NiO nanoparticles. At the same time, it is obvious that these simple ^{29}Si T_1 measurements did not provide valuable conclusions on the structure of the matrix and the locations of paramagnetic species. However, some conclusions can be made by additional relaxation experiments involving other nuclei.

6.3.3. ^{29}Si T_1 and T_2 Relaxation in Static and Spinning Porous Amorphous Paramagnetic Silica-Based Materials

Among the numerous factors changing relaxation behavior of nuclei, which interact with unpaired electrons in amorphous porous solids, a single fact is obvious: paramagnetic metal ions shorten remarkably the T_1 and T_2 times of target nuclei.[114]

However, then, interpretations of NMR relaxation data in structural terms, where incorporation of metal ions into the matrix is most important, are not simple. Canesson and co-workers[93] have emphasized that "*a decrease in both T_1 and T_2 relaxation times cannot be regarded as characteristics of the presence of framework paramagnetic species*." This is particularly valid when relaxation mechanism is not recognized. This section shows the ^{29}Si NMR experiments performed in static and spinning paramagnetic systems and directed to discrimination in relaxation mechanisms.

When target nuclei are not quadrupolar, for example, ^{29}Si or ^{13}C, a priori their T_1, T_2 NMR relaxation is a sum of contributions due to direct electron−nucleus dipolar interaction (DD) and spin diffusion (SD) to paramagnetic impurities:

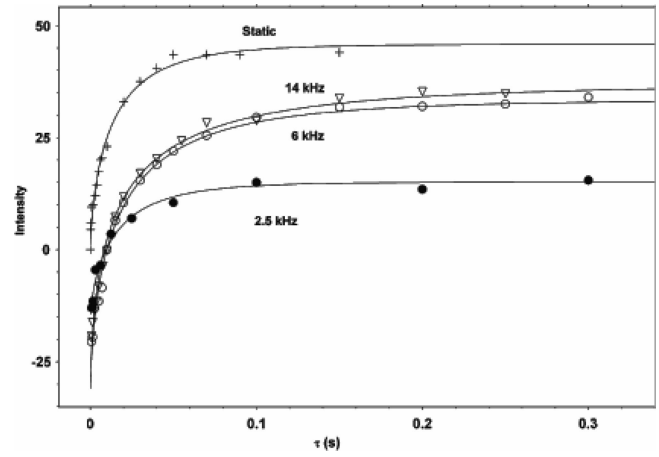

Figure 24. ^{29}Si T_1 relaxation curves obtained for static and spinning material $SiO_2Al_2O_3MnO$ (Si/Mn = 3.5, Si/Al = 21). Intensities are measured in arbitrary units and scaled to avoid the curve overlaps. The measurements at MAS are performed for isotropic resonances. Reprinted with permission from ref 208. Copyright 2008 Elsevier Inc.

$1/T_{1,2} = 1/T^{DD}{}_{1,2} + 1/T^{SD}{}_{1,2}$. Mortuza and co-workers[243] have noted that, due to the relatively low natural abundance of ^{29}Si nuclei (4.7%), their homonuclear dipolar interaction is attenuated and ^{29}Si spin-diffusion coefficient D is small ($\sim 10^{-19}$ m^2 s^{-1}). In other words, the ^{29}Si spin-diffusion mechanism can be effective in solids, where ^{29}Si relaxation times are very long (20 s and more) and amounts of paramagnetic centers are very small. Because the probability of mutual ^{29}Si spin flips remains low and increase in concentrations of paramagnetic centers shortens the ^{29}Si T_1 times, the ^{29}Si spin-diffusion cannot dominate. Maiti and McGarvey[244] have confirmed this common statement and shown that spin-diffusion contributions to the T_1 NMR relaxation of ^{13}C nuclei in some organic solids are practically negligible even at their enrichment up to 30% or higher.

At the same time, Alaimo and Roberts[205] have performed ^{29}Si T_1 measurements for silica gels with the surface functionalized by aromatic sulfonic acid and ions Cu^{2+}. The data have been interpreted in terms of the diffusion-limited mechanism because NMR decays treated with a stretched exponential have resulted in relatively high β-values (Figure 15). This conclusion, however, was not verified by experiments at different spinning rates.[209,212]

Recently, such experiments have been carried out for the supermicroporous silica-based material $SiO_2Al_2O_3MnO$,[208] synthesized by Clearfield, Shpeizer, and co-workers at Si/Mn and Si/Al ratios of 3.5 and 21, respectively. The inversion-recovery and saturation-recovery experiments performed in a static sample and a sample spinning at 2.5−14 kHz have resulted in ^{29}Si T_1 stretched exponential data with the β-parameters between 0.6 and 0.7 and absolutely *independent* of spinning rates (Figure 24). There is no doubt that ^{29}Si spin-diffusion is ineffective; the ^{29}Si spin−lattice relaxation is completely governed by direct dipolar coupling between electrons and nuclei, and thus, the relaxation data can be treated quantitatively in the structural terms.

Importance of NMR relaxation experiments at different spinning rates for interpretations of relaxation data can be additionally illustrated by NMR behavior of the diamagnetic manganese-free material $SiO_2Al_2O_3$.[208] The material has shown the ^{29}Si T_1 stretched-exponential relaxation well treated with the β-parameter of 0.80. This magnitude is very close to that corresponding to an exponential function, and

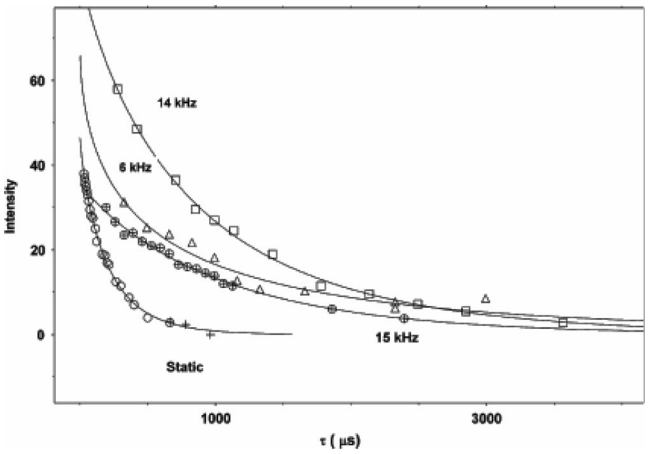

Figure 25. ^{29}Si T_2 relaxation curves obtained for static and spinning material $SiO_2Al_2O_3MnO$ (Si/Mn = 3.5, Si/Al = 21). Intensities are measured in arbitrary units and scaled to avoid curve overlaps. The measurements at MAS are performed for isotropic resonances. Reprinted with permission from ref 208. Copyright 2008 Elsevier Inc.

hence, a long ^{29}Si T_1 time of 25 s could be attributed to spin diffusion. However, again, the ^{29}Si T_1 time has been *independent* of spinning rates, and thus, ^{29}Si spin-diffusion has been negligible. In other words, discussion of the T_1 and β-parameters in the absence of the variable-spinning measurements will be unreliable.

Since spin−spin relaxation times are often applied for characterizations of different materials, T_2 experiments in static and spinning solids are also of great interest. The ^{29}Si T_2 times in the diamagnetic material $SiO_2Al_2O_3$ have been short, independent of spinning rates, and measured between 0.61 and 0.79 ms.[208] Assuming the $^{29}Si-^{29}Si$ dipolar relaxation mechanism or relaxation by direct dipolar interaction between ^{29}Si nuclei and uncontrolled paramagnetic impurities (O_2, for example) has resulted in estimation of correlation times τ of $2-4 \times 10^{-7}$ s. According to eq 12, such magnitudes are too small to provide a ^{29}Si T_2 dependence on spinning rates, in full agreement with the experiments.

In contrast, the paramagnetic materials $SiO_2Al_2O_3MnO$ have shown the ^{29}Si T_2 curves that depend on spinning rate in Figure 25. It has been found that the ^{29}Si T_2 time values increase linearly with increasing spinning rates. Moreover, it has been emphasized that the dependences observed have been surprisingly similar to those predicted in terms of spin-diffusion in eq 11 under conditions $\nu_R/\Delta\nu \gg 1$ and observed experimentally for ^{31}P and ^{27}Al nuclei in rigid solids by Kessemeier and Norberg[209] and Schmitt et al.[232] Careful analysis of these ^{29}Si T_2 effects, observed for the materials $SiO_2-Al_2O_3-MnO$ and SiO_2-MnO containing different manganese concentrations, has revealed their nature: in the absence of spin-diffusion, spinning rates can affect the ^{29}Si T_2 times due to large BMS contributions, which can reach 55−63% in static systems.[246] Because these BMS contributions will complicate quantitative analysis of nuclear relaxation, the authors have suggested their minimization by high spinning.

6.3.4. T_1 Criteria for Locations of Paramagnetic Ions: Relaxation of Isotropic Resonances

In general, nuclear relaxation in paramagnetic materials can be a tool for structural studies, if relaxation times are completely dominated by direct dipolar interactions between target nuclei and paramagnetic centers and the spin-diffusion mechanism is negligible. In practice, this situation is often realized for rare nuclei relaxing non-exponentially. Table 2 illustrates the T_1 relaxation times, measured for isotropic resonances in some spinning solids, studied at consequent variations in concentrations of paramagnetic centers. As seen, dramatic reduction of the T_1 times is observed on going from diamagnetic solids to paramagnetic systems. For example, the ^{29}Si T_1 time decreases by a factor of 45 or 64 in the kaolinites or the porous systems $SiO_2-Al_2O_3-NiO$, respectively. Then, however, the T_1 dependences look nontrivial. In spite of this fact, if the natures of paramagnetic particles and electron relaxation times are known, for example, from variable-temperature magnetic susceptibility measurements, showing the spin-states of the magnetic centers,[247] or from EPR spectroscopy,[181] there is a unique opportunity to determine contents of paramagnetic centers expressed as N_p in eq 14 assuming their homogeneous distributions though the volume of materials. This relatively simple approach is especially valuable for probing the natural molecular systems.[181]

Another strategy should be used for characterization of synthetic porous paramagnetic materials, where concentrations of paramagnetic metal ions are already determined

Table 2. T_1 Times Measured for Isotropic Resonances in Paramagnetic Solids, Where Nuclear Relaxations Are Governed by Dipole−Dipole Nucleus−Electron Interactions

material/ion	T_1 (s)/nucleus	content of paramagnetic ions (wt %)	reference
Pr_3N-CoAPO5/Co^{2+}	9/^{31}P	0	245
	0.5/^{31}P	0.05[a]	
	0.23/^{31}P	0.10[a]	
	0.13/^{31}P	0.13[a]	
	0.04/^{31}P	0.22[a]	
Co-SAPO-34/Co^{2+}	1.8/^{31}P	0.38[b]	243
	1.8/^{31}P	0.59[b]	
	0.043/^{31}P	1.6[b]	
$SiO_2-Al_2O_3-NiO/Ni^{2+}/Ni^0$	55/^{29}Si	0	81
	0.86/^{29}Si	1.35	
	0.50/^{29}Si	2.95	
	0.23/^{29}Si	4.80	
	0.16/^{29}Si	13.4	
	0.40/^{29}Si	29.3	
$SiO_2-Al_2O_3-MnO/Mn^{2+}$			
$SiO_2-Al_2O_3-MnO$	23.5/^{29}Si	0	246
$SiO_2-Al_2O_3-MnO$	0.066/^{29}Si	1.2	
$SiO_2-Al_2O_3-MnO$	0.027/^{29}Si	2.5	
	0.019/^{29}Si	19.8	
aromatic sulfonic acid silica gel/Cu^{2+}			
	23.1/^{29}Si	0	205
	22.3/^{29}Si	1[c]	
	3.2/^{29}Si	3[c]	
	3.17/^{29}Si	5[c]	
	2.49/^{29}Si	10[c]	
kaolinites/Fe^{3+}	2300/^{29}Si	<0.01	181
	17.5/^{27}Al		
	2.5/^{27}Al		
	51/^{29}Si	0.46	
	5.7/^{27}Al[d]		
	0.8/^{27}Al[d]		
	3.3/^{29}Si	1.15	
	1.9/^{27}Al[d]		
	0.25/^{27}Al[d]		
	5.3/^{29}Si	1.25	
	2.0/^{27}Al[d]		
	0.30/^{27}Al[d]		

[a] Co/P ratio. [b] Cobalt concentrations as N^p (nm^{-3}). [c] Surface coverage by Cu^{2+} in %. [d] Biexponential behavior.

Scheme 1

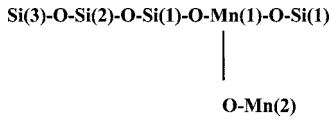

independently, whereas their locations relatively to the matrix of materials remain unknown. This task has been formulated for a series of the supermicroporous silica-based materials $SiO_2-Al_2O_3-NiO$ prepared at nickel loadings between 0 and 30 wt %.[81] These systems have shown TEM micrographs similar to those in Figure 2 revealing the nickel particles distributed homogenously through the volumes of materials. It has been demonstrated that the localization of the nickel ions can be successful by comparing the relaxation behavior of two target nuclei, one of which belongs to sites situated in pores. The T_1 MAS NMR relaxation measurements have been performed for ^{1}H and ^{29}Si resonances, characterizing water molecules located in pores and the silica matrix, respectively. It has been found that spin−lattice NMR relaxation of ^{1}H and ^{29}Si nuclei is nonexponential and completely governed by direct dipolar interactions with paramagnetic centers. The validity of the statement on the dipolar relaxation mechanism, operating for both nuclei, has been additionally supported by a linear correlation between the ^{1}H and ^{29}Si T_1 relaxation rates in eq 15:

$$R_1(^1\mathrm{H})(\mathrm{s}^{-1}) = 1170R_1(^{29}\mathrm{Si})(\mathrm{s}^{-1}) - 720 \qquad (15)$$

Then, the authors[81] have used $R_1(^1\mathrm{H})/R_1(^{29}\mathrm{Si})$ ratios determined in the materials $SiO_2-Al_2O_3-NiO$ containing different nickel concentrations. These ratios were significantly larger than those expected theoretically at equal internuclear distances $r(\mathrm{Si}\cdots\mathrm{Ni})$ and $r(\mathrm{H}\cdots\mathrm{Ni})$, revealing, thus, accumulation of the nickel centers within pores. It is obvious that the same approach can be applied for other nuclei relaxing by the dipolar mechanism.

6.3.5. T_1 Criteria Based on Relaxation of Sideband Patterns in MAS Spectra of Porous Paramagnetic Materials

Theoretically, incorporation of paramagnetic metal ions into the matrix of porous materials or their extraframework nature can be determined by quantitative analysis of T_1 relaxation times measured experimentally in terms of the distances "target nucleus−unpaired electron". Scheme 1 represents a silica-based material doped with ions Mn^{2+}, where Si(1), Si(2), and Si(3) symbolize the silica matrix whereas $Mn^{2+}(1)$ and $Mn^{2+}(2)$ correspond to ions incorporated into the matrix and accumulated in pores, respectively. It is obvious that ^{29}Si(1) nuclei are spectroscopically "invisible" because of the strong paramagnetic effects, particularly at low concentrations of the manganese. Nuclei ^{29}Si(2) and ^{29}Si(3) (or more remote nuclei) will show a very wide line in a static ^{29}Si NMR spectrum (schematically in Figure 26) due to various Si···Mn distances and the angle-dependent term $(3\cos^2\theta - 1)$, important for dipole−dipole electron−nucleus interaction in eq 1. At spinning,[44] this wide line transforms to a broad sideband pattern, where the central line in Figure 26 is isotropic resonance.

Accurate T_1 NMR measurements, performed in different spinning solids, have revealed a very interesting experimental fact: T_1 times of isotropic resonances were remarkably longer than those measured for sidebands. The effect observed for

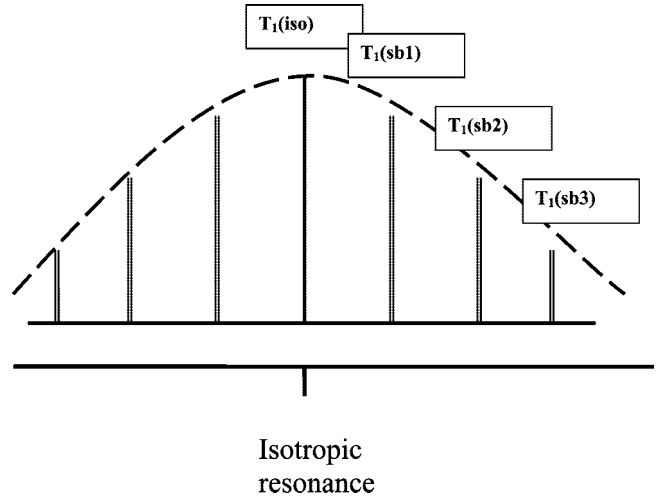

Figure 26. Static ^{29}Si NMR spectrum (dashed line) of a silica-based material doped with ions Mn^{2+} (schematically), transforming to the pattern at spinning with different T_1 times measured for the isotropic resonance and its sidebands.

^{1}H nuclei has been explained by Hayashi[212] in terms of the presence of T_1 distributions. Suttler and co-workers have reported on similar T_1 differences observed for isotropic resonances and sidebands of ^{31}P nuclei.[248]

Physically, such a T_1 behavior is reasonable. In fact, according to the authors,[249] ^{29}Si nuclei in paramagnetic silica-based materials are differently distanced from paramagnetic ions, and the lines remote from the isotropic signal in Figure 26 will belong to nuclei undergoing stronger dipolar nuclear-electron interaction and relaxing, therefore, faster. This latter will be used for quantitative T_1 analysis.

Following the Solomon's theory of nucleus−electron dipolar interaction (eqs 5 and 6),[181] the spin−spin and spin−lattice relaxation times of target nuclei in paramagnetic solids can be quantitatively analyzed in terms of distances r, *if the τ_e parameter is accurately determined*. It has been noted that the relatively long electron relaxation times τ_e can be measured by advanced EPR techniques, developed and applied in the works of Atsarkin et al.[250] and Tanaka et al.[251] In general, however, these EPR experiments are difficult and strongly limited by τ_e magnitudes. Another approach can be based on accurate T_1 and T_2 NMR determinations and exclusion of unknown distances r from eqs 5 and 6.[252] This method has recently been applied for the supermicroporous materials $SiO_2-Al_2O_3-MnO$ and SiO_2-MnO prepared at large variations in contents of Mn^{2+} ions, the nature of which has been independently studied by variable-temperature magnetic susceptibility measurements.[246] The relaxation times of electrons in Mn^{2+} ions have been determined between 0.6 and 0.8 $\times$ 10^{-8} s by the ^{29}Si R_1, R_2 NMR relaxation rates via eq 16:[208]

$$R^{\mathrm{D}}{}_2/R^{\mathrm{D}}{}_1 = 2\pi_{1\mathrm{e}}{}^2\omega_{\mathrm{I}}{}^2 + 1.5 \qquad (16)$$

where ω_I is the Larmor' frequency of ^{29}Si nuclei. Equation 17, where T_1 and $r(\mathrm{Si}\cdots\mathrm{Mn})$ are measured in s and Å, respectively, can be easily deduced from Solomon's eq 5 by addition of the well-known factor $(\mu_0/4\pi)^2$, a Mn^{2+} electron spin of 5/2, $\tau_{1e} = 1 \times 10^{-8}$ s, and the ^{29}Si resonance frequency of 79.46 MHz:

$$1/T_1 = 43.5/(0.1r(\mathrm{Si}\cdots\mathrm{Mn}))^6 \qquad (17)$$

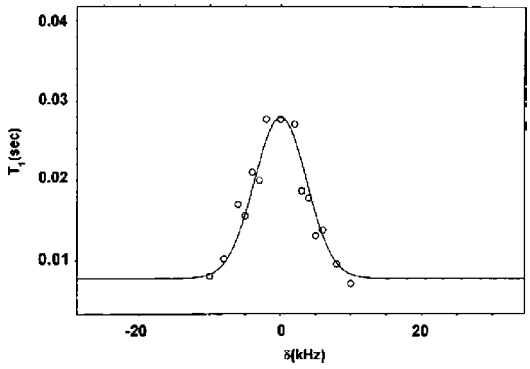

Figure 27. ^{29}Si T_1 times measured for the isotopic (central) resonance, taken as 0 kHz, and for its sidebands. The experiments were performed for material $SiO_2-Al_2O_3-MnO$ (2.5 wt % of Mn and 2 wt % of Al) spinning at different rates. Solid line corresponds to a Gaussian distribution. Reprinted with permission from ref 246. Copyright 2009 Elsevier Inc.

Finally, the expression can be applied for calculations of distances Mn···Si. On the other hand, the available X-ray data can be applied to predict ^{29}Si T_1 times for the different Mn^{2+}(1) coordination spheres in Scheme 1. In addition, ^{29}Si T_1 values can be simulated by variations in numbers of dipolar contact Mn···Si. Influence of the Mn(2) accumulated in pores and distanced from the silica lattice also can be estimated. Similar expressions also can be deduced for other target nuclei.

The criterion in the quantitative analysis of relaxation data is simple: ions Mn^{2+} will be incorporated into the silica matrix if ^{29}Si T_1 times measured for isotropic resonances in ^{29}Si MAS NMR spectra will correspond to distances Mn···Si of 7−8 Å, typical of the second manganese coordination sphere (see Si(2) in Scheme 1).

Obviously this criterion is particularly reliable if the collected NMR relaxation data are biexponential.[249] These data provide accurate determinations of short and long ^{29}Si T_1 time components where the shortest times can be involved into quantitative treatments. However, the biexponential relaxation is not typical of silica-based materials. In fact, ^{29}Si nuclei in the silica matrix in Scheme 1, which are differently distanced from Mn^{2+} paramagnetic centers, will relax differently even at relatively long distances Si···Mn. For example, a distance Si(1)···Mn(1) of 20 Å predicts the ^{29}Si T_1 values of 1.5, 3.5, and 7.3 s for Si(1), Si(2), and Si(3) nuclei, respectively.[246] In a combination with very similar chemical shifts of such remote nuclei in ^{29}Si MAS NMR spectra, the ^{29}Si relaxation process becomes theoretically multiexponential.[253] In practice, however, the relaxation curves are well treated with a stretched-exponential function. Here, a resulting T_1 time is a representative value of whole spins, and T_1 relaxation times, measured in MAS NMR experiments for isotropic resonances and their sidebands, can differ due to the presence of T_1 distributions.[212,249]

In the case of porous silica-based materials, it has been assumed that ^{29}Si T_1 distributions can be wider when paramagnetic centers are incorporated into the silica matrix. The pattern in Figure 27 obtained at different spinning rates for the supermicroporous material $SiO_2-Al_2O_3-MnO$ (2.5 wt % of Mn^{2+})[246] illustrates well this statement. As seen, the ^{29}Si T_1 time reduces from the isotropic resonance, taken as 0 kHz, to sidebands, shifted to a low- and high-field. It has been noted that the data correspond to a Gaussian distribution (solid line), and thus, the pattern in Figure 27 is a ^{29}Si T_1 image of the ^{29}Si static resonance in the static regime (compare with Figure 26).

Since the ^{29}Si T_1 data exhibit shorter T_1 times and electron relaxation time τ_e is determined as 1×10^{-8} s, the shortest T_1 components can be analyzed quantitatively, for example, in terms of eq 14, where N_p ($(4/3)\pi r_{AV}^3 N_p = 1$) is the number of paramagnetic centers, distributed homogeneously through the materials and r_{AV} is the radius of the sphere around the paramagnetic center.[242] This approach applied for the systems $SiO_2-Al_2O_3-MnO$ with 2.5 and 4.8 wt % of the manganese gave the r_{AV} parameter of 8.1 and 7.6 Å, respectively, i.e., very close to a structural situation, where Si atoms are located in the second coordination sphere of Mn^{2+}.

The treatments of short ^{29}Si T_1 components seem to be quite accurate, but they cannot be performed in the absence of independent data on the nature of paramagnetic centers. In fact, electron relaxation times depend on oxidation states of metal ions and their environments.[246] Good examples are the Al-free mixed oxides SiO_2-MnO, which at preparation by the sol/gel method and calcination are contaminated by oxide M_3O_4.[246] It is obvious that, in the presence of ions Mn^{2+} and Mn^{3+}, the above T_1/T_2 method for determinations of electron relaxation times and the T_1 analysis will be incorrect. Nevertheless, it has been shown that, at minimal contaminations of M_3O_4 (for example, 0.21 wt % of M_3O_4 versus 2 wt % of Mn^{2+}), the ^{29}Si T_1 time analysis is valid, leading to a value in the range of 13−14 Å for the closest Mn···Si distances. In other words, only extraframework manganese has been identified. Finally, to avoid misunderstandings, it should be emphasized that the presence of T_1 distributions, in itself, is not a criterion for incorporation of paramagnetic ions into the matrix of materials, whereas their quantitative analysis, based on the well-determined electron relaxation times, can provide such a criterion.

6.3.6. NMR Relaxation of Sideband Patterns in MAS Spectra of Porous Paramagnetic Materials and BMS Effects

Numerous NMR relaxation experiments performed for the supermicroporous paramagnetic materials $SiO_2-Al_2O_3$, $SiO_2-Al_2O_3-MnO$, SiO_2-MnO, and $SiO_2-Al_2O_3-NiO$[78,221,230,246,249] have demonstrated that ^{29}Si T_1 time distributions and different T_1 values measured for isotropic ^{29}Si resonances and their sidebands in MAS NMR experiments are a common phenomenon in NMR of paramagnetic solids. It has been found that this phenomenon is observed especially well for systems with relatively low concentrations of paramagnetic metal ions. In contrast, the porous material $SiO_2-Al_2O_3-MnO$ containing up to 20 wt % of Mn^{2+} shows ^{29}Si T_1 data where relaxation times of the isotropic resonance (0.019 s) and the sidebands (14 kHz, 0.012−0.013 s) are practically equal.[208,246]

The occurrence of these virtually identical ^{29}Si T_1 times, important in the methodical context, requires an explanation. Recently, the explanation has been found due to the careful measurements of ^{29}Si T_1 and T_2 times in spinning (at different rates) and static samples: *a ^{29}Si T_1 distribution can be masked by the strong BMS effects*. The masking mechanism has been simulated quantitatively.[246] It has been shown that, in systems where T_1 distributions exist, a 63% BMS contribution to sideband intensities obtained in the inversion-recovery experiments leads to practically equal T_1 times measured for all the lines in the sideband pattern. It is

obvious that these strongly paramagnetic systems restrict application of T_1 relaxation investigations. In such cases, however, direct detections of nuclei located in the first coordination spheres of metal ions by the Hahn-echo MAS NMR experiments at different frequencies are more preferable.

7. Concluding Remarks

The present review shows that chemistry of porous materials, modified by paramagnetic metal ions, is an area of increasing activity and requires development of new reliable approaches to a structural analysis of synthesized systems. The available literature illustrates how a protocol of solid-state NMR studies changes in going from diamagnetic to paramagnetic solids, when distribution of metal ions is in focus of an experimentalist. Using porous silica-based materials doped with paramagnetic ions as practical examples, we demonstrated that incorporation of ions into the matrix or their accumulation within the cavities of materials can be discriminated by the following experiments:

(i) Observation of "invisible" target nuclei by the Hahn-echo NMR experiments (static and MAS), performed at different carrier frequencies.

(ii) Editing of the Hahn-echo MAS NMR experiments.

(iii) Measurement of T_1 and T_2 NMR relaxation measurements in static and spinning paramagnetic materials.

On the basis of relaxation studies, performed by different authors, it has been shown that NMR relaxation data often show T_1 time distributions, which are observed as different T_1 values obtained in MAS NMR experiments for isotropic resonances and their sidebands. Such T_1 distributions, being a common phenomenon in paramagnetic solids, can be masked by the bulk magnetic susceptibility (BMS) effects increasing with concentrations of paramagnetic centers. The presence of T_1 distributions, in itself, is not a criterion for incorporation of paramagnetic ions into the matrix or its surface. However, a quantitative analysis of the experimentally observed short T_1 components, based on the well-determined electron relaxation times, can provide such a criterion.

8. Acknowledgments

The author thanks Prof. Vladimir V. Grushin for useful discussions.

9. References

(1) Ferey, G. *Chem. Soc. Rev.* **2008**, *37*, 191.
(2) Kim, H. C.; Park, S. M.; Hinsberg, W. D. *Chem. Rev.* **2010**, *110*, 146.
(3) Cleafield, A. In *Progress in Inorganic Chemistry*; Karlin, K. D., Ed.; Wiley & Sons: Oxford, U.K., 1998; Vol. 47, pp 371−510.
(4) Walawalkar, M. G. *Synthesis and Structural Studies of Model Compounds for Zeolite and Phosphate Materials*; Cuvillier: Gottingen, Germany, 1997.
(5) Alberti, G. *Comprehensive Supramolecular Chemistry*; Lehn, J. M., Ed.; Elsevier: New York, 1996; Vol. 7, pp 151−187.
(6) Thompson, M. E. *Chem. Mater.* **1994**, *6*, 1168.
(7) Cao, G.; Hong, H.-G.; Mallouk, T. E. *Acc. Chem. Res.* **1992**, *25*, 420.
(8) Chandrasekhar, V.; Kingsley, S.; Rhatigan, B.; Lam, M. K.; Rheingold, A. L. *Inorg. Chem.* **2002**, *41*, 1030.
(9) Clearfield, A. *Inorganic Ion Exchange Materials*; CRC Press: Boca Raton, FL, 1998; Vol. 47, p 371.
(10) Cao, G.; Lynch, V. M.; Yacullo, L. N. *Chem. Mater.* **1993**, *5*, 583.
(11) Deniaud, D.; Schollorn, B.; Mansuy, D.; Rouxel, J.; Bujoli, B. *Chem. Mater.* **1995**, *7*, 995.
(12) Alberti, G.; Casciola, M.; Polombari, R. *Solid State Ionics* **1992**, *52*, 291.
(13) Ungashe, S. B.; Wilson, W. L.; Katz, H. E.; Scheller, G. R.; Putvinski, T. M. *J. Am. Chem. Soc.* **1992**, *114*, 8717.
(14) Sokol, J. J.; Shores, M. P.; Long, J. R. *Angew. Chem., Int. Ed. Engl.* **2001**, *40*, 236.
(15) Zhang, S.-W.; Fu, D.-G.; Sun, W.-Y.; Hu, Z.; Yu, K.-B.; Tang, W.-X. *Inorg. Chem.* **2000**, *39*, 1142.
(16) Vaucher, S.; Dujardin, E.; Lebeau, B.; Hall, S. R.; Mann, S. *Chem. Mater.* **2001**, *13*, 4408.
(17) Bignozzi, C. A.; Argazzi, R.; Bortolini, O.; Scandola, F.; Harriman, A. *New J. Chem.* **1996**, *20*, 731.
(18) Chesnut, D. J.; Plewak, D.; Zubieta, J. *J. Chem. Soc., Dalton Trans.* **2001**, 2567.
(19) Haiduc, I.; Edelmann, F. T. *Supramolecular Organometallic Chemistry*; Wiley-VCH: Weinheim, Germany, 1999; Chapter 4.
(20) Iwamoto, T. In *Comprehensive Supramolecular Chemistry*; MacNicol, D. D., Toda, F., Bishop, R., Eds.; Permagon Press: Oxford, U.K., 1996; Vol. 6, Chapter 19.
(21) Shores, M. P.; Beauvais, L. G.; Long, J. R. *J. Am. Chem. Soc.* **1999**, *121*, 775.
(22) Yuan, A.; Zou, J.; Li, B.; Zha, Z.; Duan, C.; Liu, Y.; Xu, Z.; Keizer, S. *Chem. Commun.* **2000**, 1297.
(23) Olga Trofymluk, O.; Levchenko, A. A.; Tolbert, S. H.; Navrotsky, A. *Chem. Mater.* **2005**, *17*, 3772.
(24) Davis, M. E. *Nature* **2002**, *417*, 813.
(25) Tanev, P. T.; Pinnavaia, T. J. *Chem. Mater.* **1996**, *8*, 2068.
(26) Bruinsma, P. J.; Kim, A. Y.; Liu, J.; Baskaran, S. *Chem. Mater.* **1997**, *9* (11), 2507.
(27) Vietze, U.; Krauss, O.; Laeri, F.; Ihlein, G.; Schuth, F.; Limburg, B.; Abraham, M. *Phys. Rev. Lett.* **1998**, *81*, 4628.
(28) Ihlein, G.; Schuth, F.; Krauss, O.; Vietze, U.; Laeri, F. *Adv. Mater.* **1998**, *10*, 1117.
(29) Hansen, E. W.; Fonnum, G.; Weng, E. *J. Phys. Chem. B* **2005**, *109*, 24295.
(30) Hagslatt, H.; Jonsson, B.; Nyden, M.; Soderman, O. *J. Magn. Reson.* **2003**, *161*, 138.
(31) Frunza, L.; Kosslick, H.; Pitsch, I.; Frunza, S.; Schoenhals, A. *J. Phys. Chem. B* **2005**, *109*, 9154.
(32) Sahimi, M.; Tsotsis, T. J. *Catalysis* **1985**, *96*, 552.
(33) Qiao, Y.; Schoenhoff, M.; Findenegg, G. H. *Langmuir* **2003**, *19*, 6160.
(34) Sahasrabudhe, A.; Mitra, S.; Tripathi, A. K.; Mukhopadhyay, R.; Gupta, N. M. *Phys. Chem. Chem. Phys.* **2003**, *5*, 3066.
(35) Ishimaru, S.; Ikeda, R. *Recent Res. Dev. Mol. Struct.* **2002**, *1*, 143.
(36) Flodstrom, K.; Wennerstrom, H.; Alfredsson, V. *Langmuir* **2004**, *20*, 680.
(37) Zholobenko, V. L.; Khodakov, A. Y.; Durand, D. *Microporous Mesoporous Mater.* **2003**, *66*, 297.
(38) Haddad, E.; Nossov, A.; Guenneau, F.; Gedeon, A. *C. R. Chim.* **2004**, *7*, 305.
(39) Shi, L.; Zou, Y.; He, H. Y. *Chem. Lett.* **2001**, *11*, 1164.
(40) Morey, M. S.; O'Brien, S.; Schwarz, S.; Stucky, G. D. *Chem. Mater.* **2000**, *12*, 898.
(41) Janssen, A. H.; Van Der Voort, P.; Koster, A. J.; de Jong, K. P. *Chem. Commun.* **2002**, 1632.
(42) Petrovic, I.; Navrotsky, A.; Davis, M. E.; Zones, S. I. *Chem. Mater.* **1993**, *5*, 1805.
(43) Navrotsky, A.; Petrovic, I.; Hu, Y.; Chen, C. Y.; Davis, M. E. *J. Non-Cryst. Solids* **1995**, *193*, 474.
(44) Duer, M. J. *Solid-State NMR Spectroscopy: Principles and Applications*; Blackwell Science: Oxford, U.K., 2002.
(45) Fitzgerald, J. J. *Solid-State NMR Spectroscopy of Inorganic Materials*; ACS Symposium Series; American Chemical Society: Washington, DC, 1999.
(46) Zwijnenburg, M. A.; Bromley, S. T.; Foster, M. D.; Bell, R. G.; Delgado-Friedrichs, O.; Jansen, J. C.; Maschmeyer, T. *Chem. Mater.* **2004**, *16*, 3809.
(47) Zwijnenburg, M. A.; Bromley, S. T.; Jansen, J. C.; Maschmeyer, T. *Chem. Mater.* **2004**, *16*, 12.
(48) Auerbach, S. M., Carrado, K. A., Dutta, P. K., Eds.; *Handbook of Zeolite Science and Technology*; Marcel Dekker, Inc.: New York, 2003.
(49) Corma, A.; Diaz-Cabanas, M.; Martinez-Trigiero, J.; Rey, F.; Rius, J. *Nature* **2002**, *418*, 514.
(50) Shpeizer, B. G.; Bakhmutov, V. I.; Clearfield, A. *Microporous Mesoporous Mater.* **2006**, *90*, 81.
(51) Davis, M. E. *Acc. Chem. Res.* **1993**, *26*, 111.
(52) Corma, A.; Davis, M. E. *Chem. Phys. Chem.* **2004**, *5*, 304.
(53) Yanagiwawa, T.; Shimizu, T.; Kuroda, K.; Kato, C. *Bull. Chem. Soc. Jpn.* **1990**, *63*, 988.
(54) Kresge, C. T.; Leonowicz, M. E.; Roth, W. J.; Vartuli, J. C.; Beck, J. S. *Nature* **1992**, *359*, 710.

(55) Beck, J. S.; Vartuli, J. C.; Roth, W. J.; Leonowicz, M. E.; Kresge, C. T.; Schmitt, K. D.; Chu, C. T. W.; Olsen, D. H.; Sheppard, W. W.; McCullen, S. B.; Higgins, J. B.; Schlenker, J. L. *J. Am. Chem. Soc.* **1992**, *114*, 10834.
(56) Huo, Q.; Petroff, P.; Schuth, F.; Stucky, G. D. *Nature* **1994**, *368*, 317.
(57) Ciesla, U.; Schuth, F. *Microporous Mesoporous Mater.* **1999**, *27*, 131.
(58) Ying, J. Y.; Mehnert, C. P.; Wong, M. S. *Angew. Chem., Int. Ed.* **1999**, *38*, 56.
(59) Schuth, F. *Chem. Mater.* **2001**, *13*, 3184.
(60) Speizer, B. G.; Clearfield, A.; Heising, J. M. *Chem. Commun.* **2005**, 2396.
(61) Bonhomme, C.; Coelho, C.; Baccile, N.; Gervais, A. T.; Babonneau, F. *Acc. Chem. Res.* **2007**, *40*, 738.
(62) Antonelli, D. M. *Micoporous Mesoporous Mater.* **1999**, *33*, 209.
(63) Shah, P.; Ramaswamy, A. V.; Lazar, K.; Ramaswamy, V. *Microporous Mesoporous Mater.* **2007**, *100*, 210.
(64) Maxim, N.; Magusin, P. C. M.; Kooyman, J.; Wolput, J. H. M. C.; Santen, R. A.; Abbenhuis, H. C. L. *Chem. Mater.* **2001**, *13*, 2958.
(65) Shah. P. Ramaswamy, A. V.; Ramaswamy, V. *Stud. Surf. Sci. Catal.* **2005**, *158*, 565.
(66) Sun, Y.; Tao, Z.; Chen, J.; Herricks, T.; Xia, Y. *J. Am. Chem. Soc.* **2004**, *126*, 5940.
(67) Kirumakki, S. R.; Shpeizer B, G.; Sagar, G. V.; Chary, K. V. R.; Clearfield, A. *J. Catal.* **2006**, *242*, 319.
(68) Haouas, M.; Ge'rardin, C.; Taulelle, F.; Estournes, C.; Loiseau, T.; Ferey, G. *J. Chim. Phys. Phys.-Chim. Biol.* **1998**, *95*, 302.
(69) Taulelle, F.; Haouas, M.; Ge'rardin, C.; Estournes, C.; Loiseau, T.; Ferey, G. *Colloids Surf., A* **1999**, *158*, 299.
(70) Francis, R. J.; O'Brien, S.; Fogg, A. M.; Halasyamani, P. S.; O'Hare, D.; Loiseau, T.; Ferey, G. *J. Am. Chem. Soc.* **1999**, *121*, 1002.
(71) Arieli, D.; Vaughan, D. E. W.; Strohmaier, K. G.; Goldfarb, D. *J. Am. Chem. Soc.* **1999**, *121*, 6028.
(72) Corma, A.; Díaz-Cabañas, M. J.; Martínez-Triguero, J.; Rey, F.; Rius, J. *Nature* **2002**, *418*, 514.
(73) Freyhardt, C. C.; Tsapatsis, M.; Lobo, R. F.; Balkus, K. J.; Davis, M. E. *Nature* **1996**, *381*, 295.
(74) Burton, A. W. *Z. Kristallogr.* **2004**, *219*, 866.
(75) Brouwer, D. H.; Darton, R. J.; Morris, R. E.; Levitt, M. H. *J. Am. Chem. Soc.* **2005**, *127*, 10365.
(76) Huo, Q. S.; Margolese, D. I.; Ciesla, U.; Demuth, D. G.; Feng, P. Y.; Gier, T. E.; Sieger, P.; Firouzi, A.; Chmelka, B. F.; Schuth, F.; Stucky, G. D. *Chem. Mater.* **1994**, *6*, 1176.
(77) Mokaya, R.; Zhou, W.; Jones, W. *J. Mater. Chem.* **2000**, *10*, 1139.
(78) Shpeizer, B. G.; Bakhmoutov, V. I.; Zhang, P.; Prosvirin, A. V.; Dunbar, K. R.; Thommes, M.; Clearfield, A. *Colloids Surf., A* **2010**, *357*, 105.
(79) Nery, J. G.; Giotto, M. V.; Mascarenhas, Y. P.; Cardoso, D.; Zotin, F. M. Z.; Sousa-Aguiar, E. F. *Microporous Mesoporous Mater.* **2000**, *41*, 281.
(80) Shames, A.; Lev, O.; Iozefron-Khuyavskaya, B. *J. Non-Cryst. Solids* **1993**, *163*, 105.
(81) Bakhmutov, V. I.; Shpeizer, B. G.; Prosvirin, A. V.; Dunbar, K. M.; Clearfield, A. *Microporous Mesoporous Mater.* **2009**, *118*, 78.
(82) Yang, Y.; Lim, S. Y.; Du, G. A.; Chen., Y.; Ciuparu, D.; Haller, G. L. *J. Phys. Chem. B.* **2005**, *109*, 13237.
(83) Chang, Z.; Zhu, Z.; Kevan, L. *J. Phys. Chem. B* **1999**, *103*, 9442.
(84) Chen, Y.; Ciuparu, D.; Yang, Y. H.; Lim, S.; Wang, C.; Haller, G. L.; Pfefferle, L. D. *Nanotechnology* **2005**, *16*, S476.
(85) Selvaraj, M.; Lee, T. G. *J. Phys. Chem. B* **2006**, *110*, 21793.
(86) Misra, S. K.; Milan, M.; Pelikan, P.; Liska, M. *Physica B* **1995**, *210*, 55.
(87) Lim, S. S.; Ciuparu, D.; Chen, Y.; Yang, Y.; Pfefferle, L. D.; Haller, G. L. *J. Phys. Chem. B* **2005**, *109*, 2285.
(88) Lim, S. S.; Ciuparu, D.; Pak, C.; Dobek, F.; Chen, Y.; Harding, D.; Pfefferle, L. D.; Haller, G. L. *J. Phys. Chem. B* **2003**, *107*, 11048.
(89) Pak, C.; Haller, G. L. *Microporous Mesiporous Mater.* **2001**, *48*, 165.
(90) Umamaheswari, V.; Böhlmann, W.; Poppl, A.; Vinu, A.; Hartmann, M. *Microporous Mesoporous Mater.* **2005**, *89*, 47.
(91) Calis, G.; Frenken, P.; de Boer, E.; Hefni, M. A. *Zeolites* **1987**, *7*, 319.
(92) Beale, A. M.; Sankar, G.; Catlow, C. R.; Anderson, P. A.; Grween, T. L. *Phys. Chem. Chem. Phys.* **2005**, *7*, 1856.
(93) Canesson, L.; Boudeville, Y.; Tuel, A. *J. Am. Chem. Soc.* **1997**, *119*, 10754.
(94) Biasi, R. S.; Simoes, A. *J. Phys.: Condens. Matter* **1989**, *1*, 5915.
(95) Peeters, M. P. J.; Van De Ven, L. J. M.; Haan, J. W.; Van Hooff, J. H. C. *Colloids Surf., A* **1993**, *72*, 87.
(96) Montes, C.; Davis, M. E.; Murray, B.; Narayana, M. *J. Phys. Chem.* **1990**, *94*, 6425.
(97) Poncelet, G.; Centeno, M. A.; Molina, R. *Appl. Catal., A* **2005**, *288*, 232.
(98) He, X.; Trudeau, M.; Antonelli, D. *Inorg. Chem.* **2001**, *40*, 6463.
(99) Shah, P.; Ramaswamy, A. V.; Pasricha, R.; Lazar, K.; Ramaswamy, V. *Stud. Surf. Sci. Catal.* **2004**, *154*, 870.
(100) Ciuparu, D.; Chen, Y.; Lim, S.; Yang, Y.; Haller, G. L.; Pfefferle, L. *J. Phys. Chem. B* **2004**, *108*, 15565.
(101) Delannay, F., Delmon, B. In *Characterization of heterogeneous Catalysts*; Marcel Dekker Inc. NT: New York,1984; p 1.
(102) Renz, M.; Blasco, T.; Corma, A.; Fornes, V.; Jensen, R.; Nemeth, L. *Chem.—Eur. J.* **2002**, *8*, 4708.
(103) Kovalchuk, T. V.; Sfini, H.; Korchev, A.; Kovalenko, S.; Ill'in., V. N.; Zaitzev, V. G.; Fraissard, J. *J. Phys. Chem. B* **2005**, *109*, 13948.
(104) Luca, V.; MacLachlan, D. J.; Morgan, K. *Chem. Mater.* **1997**, *9*, 2720.
(105) Peloquin, J. M.; Britt, R. D. *Biochim. Biophys. Acta* **2001**, *1503*, 96.
(106) Dikanov, S. A.; Tsvetkov, Y. D. *Electron Spin Echo Envelope Modulation Spectroscopy*; CRC Press: Boca Raton, FL, 1992; pp 359−389.
(107) Dybovski, C.; Bai, S. *Anal. Chem.* **2008**, *80*, 4295.
(108) Bonhomme, C.; Coelho, C.; Baccile, N.; Gervais, C.; Azais, T.; Babonneau, F. *Acc. Chem. Res.* **2007**, *40*, 738.
(109) Brown, S. P.; Spiesss, H. W. *Chem. Rev.* **2001**, *101*, 4125.
(110) Fyfe, G. A.; Feng, Y.; Grondey, H.; Kokotailo, G. T.; Gies, H. *Chem. Rev.* **1991**, *91*, 1525.
(111) Klinowski, J. *Chem. Rev.* **1991**, *91*, 1459.
(112) Lesage, A. *Phys. Chem. Chem. Phys.* **2009**, *11*, 6876.
(113) Bakhmutov, V. I. Nuclear Magnetic Resonance Spectrometry. In *Encyclopedia of Applied Spectroscopy*; Andrews, D. L., Ed.; John Wiley and Sons Ltd.: New York, 2009.
(114) Abragam, A. *Principles of Nuclear Magnetism*; Oxford University Press: Oxford, U.K., 1961.
(115) Cory, M.; Widdifield, M.; Schurko, R. W. *Concepts Magn. Reson., Part A* **2009**, *34*, 91.
(116) Amornsakchai, P.; Apperley, D. C.; Harris, R. K.; Hodgkinson, P.; Waterfield, P. C. *Solid State NMR* **2004**, *26*, 160.
(117) Harris, R. K.; Lawrence, S. E.; Oh, S. W.; Kumar Das, V. G. *J. Mol. Struct.* **1995**, *347*, 309.
(118) Austin, E. J. W.; Barrie, P. J.; Clark, R. J. H. *J. Chem. Soc. Commun.* **1993**, 1404.
(119) Skibsted, J.; Jacobsen, C. J. H.; Jakobsen, H. J. *Inorg. Chem.* **1998**, *37*, 3083.
(120) Shubin, A. A.; Lapina, O. B.; Courcot, D. *Catal. Today* **2000**, *56*, 379.
(121) Medek, A.; Frydman, V.; Frydman, L. *J. Phys. Chem. B* **1997**, *101*, 8959.
(122) Dybowski, C.; Neue, G. S. *Prog. NMR Spectrosc.* **2002**, *41*, 153.
(123) Penner, G. H.; Li, W. *Inorg. Chem.* **2004**, *43*, 5588.
(124) Kidambi, S. S.; Ramamoorthy, A. *Inorg. Chem.* **2003**, *42*, 2200.
(125) Strub, H.; Beeler, A. J.; Grant, D. M.; Michel, J.; Cutts, P. W.; Zilm, K. W. *J. Am. Chem. Soc.* **1983**, *105*, 3333.
(126) Willans, M. J.; Sears, D. N.; Wasylishen, R. E. *J. Magn. Reson.* **2008**, *191*, 31.
(127) Smith, M. E.; van Eck, E. R. H. *Prog. Nucl. Magn. Reson. Spectrosc.* **1999**, *34*, 159.
(128) Chen, F.; Ma, G.; Bernard, G. M.; Cavell, R. G.; McDonald, R.; Ferguson, M. J.; Wasylishen, R. E. *J. Am. Chem. Soc.* **2010**, *132*, 5479.
(129) Ashbrook, S. E. *Phys. Chem. Chem. Phys.* **2009**, *11*, 6892.
(130) Ernst, R. R.; Anderson, W. A. *Rev. Sci. Instrum.* **1966**, *37*, 93.
(131) Kentgens, A. P. M.; Bos, A.; Dirken, P. J. *Solid State NMR* **1994**, *3*, 315.
(132) Kolodzieski, W.; Klinowski, J. *Chem. Rev.* **2002**, *102*, 613.
(133) Hartmann, S. R.; Hahn, E. L. *Phys. Rev.* **1962**, *128*, 2042.
(134) Gerstein, B. C. *Philos. Trans. R. Soc., A* **1981**, *299*, 521.
(135) Ooms, K. J.; Feindel, K. W.; Willans, M. J.; Wasylishen, R. E.; Hanna, J. V.; Pike, K. J.; Smith, M. E. *Solid State NMR* **2005**, *28*, 125.
(136) Lupulescu, A.; Kolecha, M.; Frydman, L. *J. Am. Chem. Soc.* **2003**, *125*, 3376.
(137) Simonutti, R.; Comotti, A.; Bracco, S.; Sozzani, P. *Chem. Mater.* **2001**, *13*, 771.
(138) Davis, P. J.; Kaseman, D. C.; Parvani, S. M.; Sanders, K. J.; Grandinetti, P. J.; Massiot, D.; Florian, P. *J. Phys. Chem. A.* 2010, *114*, 5503.
(139) Luo, Q.; Yang, J.; Hu, W.; Zhang, M.; Yue, Y.; Ye, C.; Deng, F. *Solid State NMR* **2005**, *28*, 9.
(140) Ganapathy, S.; Gore, K. U.; Amoureux, J. P. *Solid State NMR* **2003**, *24*, 184.
(141) Fredoueil, F.; Massiot, D.; Poojary, D. M.; Bujoli-Doeuff, M.; Clearfield, A.; Bujoli, B. *Chem. Commun.* **1998**, 175.
(142) Lee, J. E.; Khitrin, A. K. *Concepts Magn. Reson., Part A* **2008**, *32A*, 56.

(143) Fyfe, C. A.; Lewis, A. R.; Chezeau, J. M.; Grondey, H. *J. Am. Chem. Soc.* **1997**, *119*, 12210.
(144) Xie, X.; Satozawa, M.; Kunimori, K.; Hayashi, S. *Microporous Mesoporous Mater.* **2000**, *39*, 25.
(145) Jackson, C. L.; McKenna, G. B. *J. Chem. Phys.* **1990**, *93*, 9002.
(146) Bohlmann, W.; Michel, D.; Roland, J. *Magn. Reson. Chem.* **1999**, *37*, S126.
(147) Cheah, K. Y.; Alexander, P.; Gladden, A. P. *Appl. Catal., A* **1997**, *148*, 387.
(148) Benesi, A. J.; Grutzeck, M. W.; O'Hare, B.; Phair, J. W. *J. Phys. Chem. B* **2004**, *108*, 17783.
(149) Brown, M. J.; Void, R. L.; Hoatson, G. L. *Solid State NMR* **1996**, *6*, 167.
(150) Gardiennet, C.; Tekely, P. *J. Phys. Chem. B* **2002**, *106*, 8928.
(151) Beckmann, P. A. *Phys. Rep.* **1998**, *171*, 85.
(152) Klein, P. G.; Ries, M. E. *Prog. NMR Spectrosc.* **2003**, *42*, 31.
(153) Horsewill, A. J. *Prog. NMR Spectrosc.* **1999**, *35*, 359.
(154) Gougeon, R.; Chezeau, J. M.; Meuer, B. *Solid State NMR* **1995**, *4*, 281.
(155) Korb, J. P. *Magn. Reson. Imaging* **2001**, *19*, 363.
(156) Strange, J. H.; Mithchel, J.; Webber, J. B. *Magn. Reson. Imaging* **2003**, *21*, 221.
(157) Kuethe, D. O.; Montano, R.; Pietra, T. *J. Magn. Reson.* **2007**, *186*, 243.
(158) Stupic, K. F.; Cleveland, Z. I.; Pavlovskaya, G. E.; Meersmann, T. *Solid State NMR* **2006**, *29*, 79.
(159) Caprihan, A.; Clewett, C. F. M.; Kuethe, D. O.; Fukushima, E.; Glass, S. J. *Magn. Reson. Imaging* **2001**, *19*, 311.
(160) Sharp, R.; Lohr, L.; Miller, L. *Prog. NMR Spectrosc.* **2001**, *38*, 115.
(161) Wickramasinghe, N. P.; Kotecha, M.; Samoson, A.; Past, J.; Ishii, Y. *J. Magn. Reson.* **2007**, *184*, 350.
(162) Wang, W.; Hu, J. Z.; Alderman, D. W.; Pugmire, R. J.; Grant, D. M. *Solid State NMR* **1995**, *5*, 257.
(163) Wind, R. A.; Duijvestun, M. J.; Van Der Lugt, C.; Manenschijn, A.; Vriend, J. *Prog. NMR Spectrosc.* **1985**, *17*, 33.
(164) Reynhard, E. C. *Concepts Magn. Reson.* **2003**, *19A*, 44.
(165) Woods, M.; Woessner, D. E.; Sherry, A. D. *Chem. Soc. Rev.* **2006**, *35*, 500.
(166) Wickramasinghe, N. P.; Yoshitaka Ishii, Y. *J. Magn. Reson.* **2006**, *181*, 233.
(167) Kervern, G.; Pintacuda, G.; Emsley, L. *Chem. Phys. Lett.* **2007**, *435*, 157.
(168) Peng, W. K.; Samoson, A.; Kitagawa, M. *Chem. Phys. Lett.* **2008**, *460*, 531.
(169) Poole, C. P. *Electron Spin Resonance*; Wiley: New York, 1983.
(170) McConnel, H. M.; Chesnut, D. B. *J. Chem. Phys.* **1958**, *28*, 107.
(171) Bernal, O. O.; Rodrigues, C.; Martinez, A. *Phys. Rev. Lett.* **2001**, *87*, 196402.
(172) Nowak, B.; Troc, R. *Solid State NMR* **2000**, *18*, 53.
(173) Kubo, A.; Spaniol, T. P.; Terao, T. *J. Magn. Reson.* **1998**, *133*, 330.
(174) Barbara, T. M. *J. Magn. Reson., A* **1994**, *109*, 265.
(175) Aime, S.; Bertini, I.; Luchinat, C. *Coord. Chem. Rev.* **1996**, *150*, 221.
(176) Bloembergen, N.; Purcell, E. M.; Pound, R. V. *Phys. Rev.* **1948**, *73*, 679.
(177) Forte, C.; Geppi, M.; Malvaldi, M.; Mattoli, V. *J. Phys. Chem. B* **2004**, *108*, 10832.
(178) Tse, D.; Hartmann, S. R. *Phys. Rev. Lett.* **1968**, *21*, 511.
(179) Bloembergen, N. *Physica* **1949**, *15*, 386.
(180) Hayashi, S.; Hayamizu, K.; Akiba, E. *J. Phys. Chem.* **1992**, *96*, 10928.
(181) Solomon, I. *Phys. Rev.* **1955**, *99*, 559.
(182) Bloembergen, N. *J. Chem. Phys.* **1957**, *27*, 572.
(183) Grey, C. P.; Smith, M. E.; Cheethem, A. K.; Dobson, C.; Duptreet, R. *J. Am. Chem. Soc.* **1990**, *112*, 4670.
(184) Mali, G.; Ristić, A.; Kaucic, V. *J. Phys. Chem. B* **2005**, *109*, 10711.
(185) Flambard, A.; Ruhlmann, L.; Canny, L.; Thouvenot, R. *C. R. Chim.* **2008**, *11*, 415.
(186) Blumel, J.; Herker, M.; Hiller, W.; Koehler, F. H. *Organometallics* **1996**, *15*, 3474.
(187) Heise, H.; Kohler, F. H.; Xie, X. *J. Magn. Reson.* **2001**, *150*, 198.
(188) Clayton, A. N.; Dobson, C. M.; Grey, C. P. *Chem. Commun.* **1990**, 72.
(189) Brough, A. R.; Grey, C. P.; Dobson, C. M. *J. Am. Chem. Soc.* **1993**, *115*, 7318.
(190) Siminovitch, D. J.; Rance, M.; Jeffrey, K. R.; Brown, M. F. *J. Magn. Reson.* **1984**, *58*, 62.
(191) Mizuno, M.; Itakura, N.; Endo, K. *Chem. Phys. Lett.* **2005**, *416*, 358.
(192) Feuerstein, M.; Lobo, R. F. *Chem. Mater.* **1998**, *10*, 2197.
(193) Accardi, R. J.; Lobo, R. F. *Microporous Mesoporous Mater.* **2000**, *40*, 25.
(194) Terskikh, V. V.; Ratciffe, C. I.; Ripmeester, J. A.; Reinhold, C. J.; Anderson, P. A.; Edwards, P. P. *J. Am. Chem. Soc.* **2004**, *126*, 11350.
(195) Chazel, C.; Menetrier, M.; Croguenne, L.; Delmas, C. *Magn. Reson. Chem.* **2005**, *43*, 849.
(196) Plevert, J.; Okubo, T.; Wada, Y.; O'Keefe, M.; Tatsumi, T. *Chem. Commun.* **2001**, 2112.
(197) Stebbins, J. F.; Kelsey, K. E. *Phys. Chem. Chem. Phys.* **2009**, *11*, 6906.
(198) Canesson, L.; Tuel, A. *Chem. Commun.* **1997**, 241.
(199) Tuel, A.; Canesson, L.; Volta, J. C. *Colloids Surf., A* **1999**, *158*, 97.
(200) Wilcke, S. L.; Cairns, E. J.; Reimer, J. A. *Solid State NMR* **2006**, *29*, 199.
(201) Bakhmutov, V. I. *Practical NMR Relaxation for Chemists*; Wiley: Chichester, U.K., 2005.
(202) Zhou, J.; Fu, R.; Hu, J.; Li, L.; Ye., C. *Solid State NMR* **1997**, *7*, 291.
(203) Horsewill, A. J.; Tomdah, I. B. I. *Solid State NMR* **1993**, *2*, 61.
(204) Pfleiderer, B.; Albert, K.; Bayer, E.; van den Ven, L.; de Haan, J.; Cramers, C. *J. Phys. Chem.* **1990**, *94*, 4189.
(205) Alaimo, M. H.; Roberts, J. E. *Solid State NMR* **1997**, *8*, 241.
(206) Rorschach, H. E. *Physica* **1964**, *30*, 38.
(207) Narayanan, A.; Hartman, J. S.; Bain, A. D. *J. Magn. Reson., A* **1995**, *112*, 58.
(208) Bakhmutov, V. I. *Solid State NMR* **2008**, *34*, 197.
(209) Kessemeier, H.; Norberg, R. E. *Phys. Rev.* **1967**, *155*, 321.
(210) Gil, A. M.; Alberti, E. *Solid State NMR* **1998**, *11*, 203.
(211) Jia, Z.; Zhang, L.; Chen, Q.; Hansen, E. W. *J. Phys. Chem. A* **2008**, *112*, 1228.
(212) Hayashi, S. *Solid State NMR* **1994**, *3*, 323.
(213) Haeberlen, U.; Waugh, J. S. *Phys. Rev.* **1969**, *185*, 420.
(214) Oldfield, E.; Haase, J.; Schmitt, K. D.; Schramm, S. F. *Zeolites* **1994**, *14*, 101.
(215) Romanenko, K. V.; Lapina, O. B.; Sominova, L. G.; Fraissard, J. *Phys. Chem. Chem. Phys.* **2002**, *5*, 2686.
(216) Hayashi, S.; Komori, Y. *Solid State NMR* **2009**, *36*, 167.
(217) Bakhmutov, V. I. *Solid State NMR* **2009**, *36*, 164.
(218) Dementyev, A. E.; Li, D.; MacLean, K.; Barrett, S. E. *Phys. Rev. B* **2003**, *68*, 153302.
(219) Franzoni, M. B.; Levstein, P. R. *Phys. Rev. B* **2005**, *72*, 235410.
(220) Wind, R. A.; Duijvestun, M. J.; Van Der Lugt, C.; Manenschijn, A.; Vriend, J. *Prog. NMR Spectrosc.* **1985**, *17*, 33.
(221) Bakhmutov, V. I.; Shpeizer, B. G.; Clearfield, A. *Magn. Reson. Chem.* **2006**, *44*, 861.
(222) Munoz-Aguado, M. J.; Gregokiewitz, M.; Bermejo, F. J. *J. Non-Cryst. Solids* **1995**, *189*, 90.
(223) Mokaya, R. *Microporous Mesoporous Mater.* **2001**, *44*−*45*, 119.
(224) Simonutti, R.; Comotti, A.; Bracco, S.; Sozzani, P. *Chem. Mater.* **2001**, *13*, 771.
(225) Huang, W.; Schopfer, M.; Zhang, C.; Howell, R. C.; Todaro, L.; Gee, B. A.; Francesconi, L. C.; Polenova, T. *J. Am. Chem. Soc.* **2008**, *130*, 481.
(226) Goldfarb, D. *Zeolites* **1989**, *9*, 509.
(227) Abidi, N.; Deroide, B.; Zanchetta, J. V.; Menorval, L. C.; Espinose, J. B. *J. Non-Cryst. Solids* **1998**, *231*, 49.
(228) Tucker, M. C.; Dieff, M. M.; Richardson, T. J.; Finones, R.; Reimer, J. A.; Cairns, E. J. *Electrochem. Solid-State Lett.* **2002**, *5*, A95.
(229) Grey, C. P.; Dobson, C. M.; Cheethman, A. K.; Jakeman, R. J. B. *J. Am. Chem. Soc.* **1989**, *111*, 505.
(230) Bakhmutov, V. I.; Shpeizer, B. G.; Clearfield, A. *Magn. Reson. Chem.* **2006**, *44*, 985.
(231) Bakhmutov, V. I.; Shpeizer, B. G.; Clearfield, A. *Magn. Reson. Chem.* **2007**, *45*, 118.
(232) Schmitt, K. D.; Haase, J.; Oldfield, E. *Zeolites* **1994**, *14*, 89.
(233) Berlier, G.; Prestipino, C.; Rivallan, M.; Bordiga, S.; Lamberti, C.; Zecchina, A. *J. Phys. Chem. B* **2005**, *109*, 22377.
(234) Cordoba, G.; Arroyo, R.; Fierro, J. L. G.; Viniegra, M. *J. Solid State Chem.* **1996**, *123*, 93.
(235) Sanchez, C.; Soller-Illia, G. J. A.; Ribot, F.; Lalot, T.; Mayer, C. R.; Cabuil, V. *Chem. Mater.* **2001**, *13*, 3061.
(236) Kresge, C. T.; Vartuli, J. C.; Roth, W.; Leonowicz, M. E. *Stud. Surf. Sci. Catal.* **2004**, *148*, 53.
(237) Sayari, A., Ed. *Studies in Surface Science and Catalysis: Nanoporous Materials II*, Proceedings of the 2nd Conference on Access in Nanoporous Materials; Elsevier Science: New York, 2000; Vol. 129, pp 1−889.
(238) Shunn, R. A.; Baker, R.; Cole, R. J.; Gilbert, J. D.; Madden, D. P. *Inorg. Synth.* **1974**, *15*, 5.
(239) Scholz, K.; Thomas, B. *Solid State NMR* **1995**, *4*, 309.
(240) Sen, S.; Stebbins, J. F. *Phys. Rev. B* **1994**, *50*, 822.
(241) McHenry, M. R.; Silbernagel, B. G.; Wernick, J. H. *Phys. Rev. B* **1972**, *5*, 2958.
(242) Mali, G.; Kaucic, V. *Solid State NMR* **1998**, *12*, 243.
(243) Mortuza, M.; Dupree, G. R.; Holland, D. *J. Non-Cryst. Solids* **2001**, *281*, 108.
(244) Maiti, B.; McGarvey, B. R. *J. Magn. Reson.* **1984**, *58*, 37.

(245) Chen, S. H.; Sheu, S. P.; Chao, K. *J. Chem. Commun.* **1992**, 1504.
(246) Bakhmutov, V. I.; Shpeizer, B. G.; Prosvirin, A. V.; Dunbar, K. R.; Clearfield, A. *Solid State NMR* **2009**, *36*, 129.
(247) Bourdreaux, E. A.; Mulay, L N. *Theory and application of molecular magnetism*; Wiley: New York, 1976; p 210.
(248) Suttler, B.; Taylor, R. E.; Hossner, L. R.; Ming, D. W. *Soil Sci. Soc. Am. J.* **2002**, *66*, 455.
(249) Bakhmutov, V. I.; Shpeizer, B. G.; Clearfield, A. *Magn. Reson. Chem.* **2006**, *44*, 861.
(250) Atsarkin, V. A.; Demidov, V. V.; Simon, G. F. G.; Moritomo, Y.; Conder, K.; Janossy, A.; Forro, L. *J. Magn. Magn. Mater.* **2003**, *258*−*259*, 256.
(251) Tanaka, S.; Mizushima, K.; Iida, S. *J. Phys. Soc. Jpn.* **1980**, *49*, 569.
(252) Carper, W. R. *Concepts Magn. Reson.* **1999**, *11*, 51.
(253) Chudek, J. A.; Hunter, G.; McQuire, G. W.; Rochester, C. H.; Smith, T. F. S. *J. Chem. Soc., Faraday Trans.* **1996**, *92*, 453.

CR100144R